Scaling Staged-Combustion Testing

Test Bench Architecture and Cost Analysis for 2 MN Staged-Combustion Engines

Joris de Lint

Delft University of Technology

TU Delft

Scaling Staged-Combustion Testing

Test Bench Architecture and Cost Analysis for 2 MN Staged-Combustion Engines

by

Joris de Lint

to obtain the degree of Master of Science
in Aerospace Engineering
at the Delft University of Technology,
to be defended publicly on Monday November 17, 2025 at 14:00.

Student number:	4844807	
Project duration:	February 17, 2025 – November 17, 2025	
Thesis committee:	Prof. Dr. B. L. A. Vermeersen,	TU Delft, Chair
	Dr. A. Cervone,	TU Delft, Supervisor
	Dr. A. Menicucci,	TU Delft, Examiner
	K. Underhill,	ESA, External Supervisor

Cover:	RS-88 Test Firing, by NASA Rocket Propulsion Test Program Office [79].
Style:	TU Delft Report Style, with modifications by Daan Zwaneveld and Joris de Lint

An electronic version of this thesis is available at `http://repository.tudelft.nl/`.

TU Delft

Acknowledgements

This thesis marks the completion of my Masters in Aerospace Engineering (Space Engineering track) at Delft University of Technology. The research was conducted at the European Space Agency (ESA) in Paris from February to October 2025 and brings together two years of coursework, practical engineering, and a long-standing fascination with spaceflight and spacecraft design.

This work would not exist without Kate Underhill, Upper Stage and Propulsion Demonstrators Project Manager at ESA. Kate did far more than approve a topic: she framed the problem with amazing clarity, facilitated across FLPP and the test-bench community (STS-IF), and trusted me with the autonomy to explore while insisting on rigour and transparent work. She gave me access to the right people at the right moments, asked the necessary questions when my assumptions were lazy, and repeatedly helped me translate research curiosity into decisions a programme can act on. Kate, thank you very much for your time, trust, and mentorship.

Doing a thesis would not make much sense without a university supervisor. I approached Professor Cervone because I knew he might be interested, and luckily he was. I was allowed a wide scope for the thesis, as long as I could land precisely: quantify the trade-offs, show the sensitivity, and document what changes if an assumption moves. That mentorship shaped not only this thesis, but also how I will approach complex projects ahead.

I have been fortunate to receive help from many capable people beyond my day-to-day supervisors. I am grateful to everyone at ESA who made time for my questions. In particular, Jörn Bellermann and Fehmi Mejri for their enthusiasm and patience on all things surrounding test benches; Javier Serrano Gómez, Andrea Polomini, and Edouard Gourier, the cost wizards who initiated me into the practical arts of cost engineering; and the entire FLPP team for welcoming me and challenging my work, especially STS-FP.

The young people at ESA turned headquarters into a second home. Thank you for the coffee breaks, billiard games or baby-foot (table football) sessions, football during lunch and unfailing good humour on long days.

Back in Delft, I owe a great deal to family and friends who kept me grounded throughout my time in Delft. Thank you to my parents and siblings for steady encouragement from the first page to the last; to friends and housemates for late-night dinners, early-morning rides, and making sure I also did something else than study; and to my TU Delft and Leiden University bachelor and master friends, for making my time as a student unforgettable. Your support and friendship made the hard parts lighter and the good parts better.

Joris de Lint
Delft, November 2025

Summary

Europe is entering a phase where staged-combustion (SC) engines, critical to higher performance and reusability, are moving from prototypes to regular test campaigns. Yet Europe lacks an affordable, readily available facility for full-scale SC hot-fires, creating a bottleneck for engine maturation and program cadence. This thesis responds to that gap by developing a high-level design for a modular, sea-level propulsion test bench sized for engines of 2 MN, and by coupling the technical concept with siting, cost, RAMS, and operations analyses that determine whether such a bench can be built and run sustainably in a European context.

The design work begins from first principles of engine-facility interfacing. Top-level requirements are derived around thrust capacity, chamber-pressure envelope, and cycle compatibility (FFSC/ORSC/FRSC) for methalox and hydrolox service, with horizontal installation to simplify handling and reduce cost. The bench architecture is sized from first principles of engine demand and facility constraints, with tanks and lines set by worst-case mass-flow scenarios and pressurisation strategies (N_2 for LOX/CH_4, He for LOX/H_2). A first-order EcosimPro/ESPSS model verifies stable interface dynamics: the LOX system can deliver 650 kg/s to the engine at 4 bar with a tightly regulated, constant run tank pressure of 20 bar, while control loops maintain steady supply. Differences for CH_4 and H_2 service, like helium permeation, seal requirements, and the benefit of He recovery are outlined to generalise the LOX design.

Technical design is laid out as well as programmatic feasibility. A parametric cost model lays out the cost of other benches and their scale, to assess the potential cost range of a to-be-built facility. This parametric CAPEX, identified to be around €92.2 million, combined with fixed and variable OPEX, is converted into a required day-rate via a discounted-cash-flow model under realistic utilisation, for a specified investor payback horizon (and discount rate). A multi-criteria site shortlisting compares European countries on permitting complexity, population density, logistics and workforce availability, revealing a consistent tier of viable candidates, like Bulgaria, Greece, Portugal, Poland, Spain, and Hungary, where infrastructure and operating costs align with the benchs utilisation needs. Location cost advantages translate directly into lower required day-rates at equal investor horizons. Reliability and safety are addressed via a FMECA spanning cryogenic flow, start transients, pressurisation and purge, structures, and controls. The result is a set of mitigations that reduce high-criticality risks to acceptable levels.

In sum, this work demonstrates that Europe can field a cost-effective, modular, sea-level test bench for 2 MN staged-combustion engines, and it provides the design logic, siting rationale, and operational blueprint to do so. The recommended next steps are proper tool selection for future work, instrumentation definition, EcosimPro verification expansion, and expanding the parametric cost model.

Contents

Preface i

Summary ii

Nomenclature ix

1 Introduction 1
1.1 Thesis Outline . . . 1

2 Literature Review 3
2.1 Test benches . . . 3
2.1.1 Types of Test benches: Sea-Level vs Altitude, Subscale vs Full-Scale, and Orientation . . . 4
2.1.2 Test Bench Infrastructure . . . 6
2.1.3 Historical Evolution of Test Stands . . . 7
2.1.4 State-of-the-Art Research . . . 8
2.1.5 Product Breakdown Structure . . . 9
2.2 Operations . . . 11
2.2.1 Roles and Responsibilities . . . 11
2.2.2 Planning and Preparation . . . 12
2.2.3 Information Management . . . 13
2.3 Combustion Cycles . . . 14
2.3.1 Gas Generator Cycle . . . 14
2.3.2 Expander Cycle . . . 15
2.3.3 Pressure-Fed Cycle . . . 16
2.3.4 Electric Pump-Fed Cycle . . . 16
2.3.5 Tap-Off Cycle . . . 17
2.3.6 Staged Combustion . . . 17
2.4 AI and Automation . . . 22
2.4.1 Tasks of Test Bench . . . 22
2.4.2 AI-Driven Anomaly Detection . . . 22
2.5 Conclusions . . . 23

3 Research Proposal 25
3.1 Problem Statement . . . 25
3.2 Research Questions . . . 26
3.3 Hypotheses . . . 27
3.4 Timeline . . . 27

4 Requirements 30
4.1 Customer Requirements . . . 31

5 Fluid Supply System 35
5.1 Tank Sizing . . . 35
5.1.1 Identification of Peak Operating Points . . . 35
5.1.2 Computation of Propellant Mass Flows and Worst-Case Selection . . . 39
5.2 Conversion to Liquid Volumes Using CoolProp . . . 39
5.2.1 Ullage Volume . . . 43
5.2.2 Tank Setup . . . 44
5.3 Pressurisation . . . 45
5.3.1 Thermodynamic Properties . . . 45
5.3.2 Gas Mass Flow Rate Calculation . . . 46

5.3.3 Pressurant Cylinder Sizing . . . 46
5.4 Piping . . . 47
5.4.1 Sizing . . . 47
5.4.2 Pressure Drop . . . 48
5.5 EcosimPro Simulations . . . 49
5.5.1 System Overview . . . 50
5.5.2 Ecosim Pressurisation . . . 58
5.5.3 Ecosim Engine Running . . . 60
5.5.4 Conclusions from Simulation . . . 66

6 Site Selection **69**
6.1 Labour Cost . . . 69
6.2 Ease of Doing Business . . . 70
6.3 Population Density and Logistics . . . 71
6.4 Availability of Skilled Workforce . . . 73
6.5 Final Results . . . 74
6.5.1 Shortcomings of the Selection . . . 76

7 Cost Modelling **78**
7.1 Top-Down Cost Approximation . . . 78
7.2 Bottom-up Cost Assessment . . . 81
7.3 OPEX . . . 85
7.4 Business Plan . . . 85

8 Failure Mode, Effects, and Criticality Analysis **89**

9 Conclusion **93**

10 Recommendation for Future Work **95**

References **97**

A Gantt Chart **105**

B EcosimPro Background **107**
B.1 Design Iterations . . . 107

C Adjustment Factors for Rocket Test Stands **112**
C.1 NASA A-3 (SSC) . . . 113
C.2 NASA B-2 (SSC) . . . 113
C.3 NASA A-2 (SSC) . . . 114
C.4 Stand 4670 (MSFC) . . . 115
C.5 USAF 2-A (Edwards) . . . 115
C.6 DLR P5.2 (Lampoldshausen) . . . 116
C.7 SIET (India) . . . 116

D Valuation spreadsheet: structure and formulas **117**
D.1 Core equations. . . . 117
D.2 Excel sheet layout . . . 118
D.3 Model verification . . . 118

List of Figures

2.1 B Test Complex at Stennis Space Center in Hancock County, Mississippi, United States [67] . . . 3
2.2 ESA P3.2 rocket engine test bench at DLR Lampoldshausen [30] . . . 5
2.3 Cross-section of the ESA P4.1 high-altitude simulation test bench at DLR Lampoldshausen [102] . . . 5
2.4 Hydra-Blue Steel schematic [96] . . . 8
2.5 SpaceX McGregor horizontal test stand: (left) Full test bench with LOX and CH_4 tanks clearly visible; (right) Test cell with Raptor 3 [86]. . . . 9
2.6 Standard phases for testing a rocket engine . . . 13
2.7 Gas generator engine [25] . . . 15
2.8 Expander combustion engine [23] . . . 15
2.9 Pressure-fed engine [26] . . . 16
2.10 Electric pump-fed engine [22] . . . 17
2.11 Tap-off combustion engine [21] . . . 17
2.12 Fuel-rich staged combustion engine [27] . . . 18
2.13 Oxidizer-rich staged combustion engine [11] . . . 18
2.14 Full flow staged combustion engine [24] . . . 18
2.15 Schematic of the Space Shuttle Main Engine flow logic [55] . . . 21

5.1 Sea-level specific impulse vs. mixture ratio for FRSC (hot CH_4, cold LOX) at various chamber pressures and nozzle expansion ratios. . . . 36
5.2 Sea-level specific impulse vs. mixture ratio for ORSC (cold CH_4, hot LOX) at various chamber pressures and nozzle expansion ratios. . . . 37
5.3 Sea-level specific impulse vs. mixture ratio for FRSC (hot H_2, cold LOX) at various chamber pressures and nozzle expansion ratios. . . . 39
5.4 Liquid volume based on the input parameters . . . 40
5.5 LH_2 vs LOX Liquid Volume Requirements for the FRSC Worst-Case Thrust Scenario . 41
5.6 Sea-level I_{sp} comparison between RocketCEA and Cantera at $P_c = 100\,\mathrm{bar}$ and $\varepsilon = 35$: FRSC (left; $T_f = 650\,\mathrm{K}$, $T_{\mathrm{ox}} = 90\,\mathrm{K}$) and ORSC (right; $T_f = 250\,\mathrm{K}$, $T_{\mathrm{ox}} = 650\,\mathrm{K}$). . . . 41
5.7 Vulcain 2 vacuum I_{sp} at O/F 6.1 and P_c=115 bar with CH_4 at 250 K and $\epsilon = 58.2$. . . . 42
5.8 LE-7 I_{sp} vs O/F at Sea Level & Vacuum and P_c=127 bar with CH_4 at 250 K and $\epsilon = 52$. 43
5.9 Computed friction factor f versus Reynolds number for different pipe surface roughnesses, using the Swamee-Jain approximation. Vertical dashed lines at $Re = 2300$ and $Re = 4000$ mark the laminar-turbulent transition. . . . 48
5.10 System schematic two tanks - top, tile 1 of 4. . . . 51
5.11 System schematic two tanks - top, tile 2 of 4. . . . 52
5.12 System schematic two tanks - top, tile 3 of 4. . . . 53
5.13 System schematic two tanks - top, tile 4 of 4. . . . 54
5.14 System schematic two tanks - bottom, tile 1 of 4. . . . 55
5.15 System schematic two tanks - bottom, tile 2 of 4. . . . 56
5.16 System schematic two tanks - bottom, tile 3 of 4. . . . 57
5.17 Tank pressure build-up . . . 58
5.18 N_2 tank pressure . . . 58
5.19 Mass flow of nitrogen into the tanks . . . 59
5.20 Gas mass of non-condensable gas (N_2) and boil-off in the run tanks . . . 59
5.21 Pressure at different points in the system . . . 60
5.22 Gas temperature of control volumes in the tanks . . . 60
5.23 Mass flow starting from t=2400 . . . 61
5.24 Valve position for multiple important valves . . . 61

5.25 Position of Valve_A throughout the run 62
5.26 Engine supply pressure during the run 62
5.27 Error in tank pressure 63
5.28 LOX tank pressure 63
5.29 Velocity of oxygen and nitrogen in different parts of the system 64
5.30 N_2 tank pressure 64
5.31 Fill level of Tank A and B 65
5.32 Pressure drop in Pipe_A_inlet_valve_A (15 m length, 22 cm diameter) 66

6.1 Gross Average Monthly Wages by Country 70
6.2 Population Density by Region in Portugal 71
6.3 Distribution of Suitability Score by Country under Weight Variations 73
6.4 Stability of the Country Selection based on k-Selection 73
6.5 Ranking of Countries by their Composite Score, per Scenario 76

7.1 Computed equivalent cost (in 2025 MEUR) as a function of thrust equivalent (MN), including a linear regression fit ($R^2 = 0.810$). 81
7.2 NPV vs. CAPEX and P_1 (evaluated at $r = 4\%$); zero-NPV frontier shown. 87
7.3 The cumulative NPV plotted over time, payback at 26.9 years. 88

A.1 Gantt Chart 106

B.1 Simplified model architecture for a single-tank pressurization using a bypass, and engine feed system (1 of 2). 108
B.2 Simplified model architecture for a single-tank pressurization using a bypass, and engine feed system (2 of 2). 109
B.3 Simplified model architecture for a single-tank pressurisation and engine feed system (1 of 2). 110
B.4 Simplified model architecture for a single-tank pressurisation and engine feed system (2 of 2). 110
B.5 Simplified model architecture for a multi-tank pressurisation and engine feed system. . . 111

D.1 Valuation spreadsheet: base-case inputs and year-by-year nominal cash flows with discounted series (PV_Rev$_t$, PV_Cost$_t$) and cumulative NPV (CAPEX 100 M, $P_1 = 85$k/day, $\pi = 2.5\%$, $r = 4\%$). CAPEX and cumulative NPV are marked in red. 119
D.2 Heatmap showing cumulative NPV values for different CAPEX and P_1. $P_1 = 85$k/day . 120
D.3 NPV as a function of discount rate r and base price P_1 for three CAPEX cases (90, 100, 130 M); horizon $K = 20$. 120
D.4 NPV as a function of discount rate r and base price P_1 for three CAPEX cases (90, 100, 130 M); horizon $K = 30$. 120

List of Tables

3.1 Thesis Timeline . . . 27

4.1 Customer Requirements . . . 31

5.1 Input parameters used to generate the I_{sp} vs. O/F curves . . . 36
5.2 Input parameters used to generate the H_2/LOX I_{sp} vs. O/F curves . . . 38
5.3 Worst-case scenario results for CH_4 and LOX liquid volume in the FFSC engine at P_c = 100 bar, $T = 600$ K, and $\varepsilon = 35$. . . . 40
5.4 FRSC worst-case results at $P_c = 100$ bar, $T_f = 600$ K, $\epsilon = 60$. . . . 41
5.5 Sea-level I_{sp} comparison: RocketCEA vs. Cantera at $P_c = 100$ bar and $\varepsilon = 35$. . . . 42
5.6 Sea-level I_{sp} of the BE-4 at O/F = 3.5 and P_c=140 bar with CH_4 at 250 K, for varying LOX temperatures and expansion ratios. . . . 42
5.7 Volumes of H_2 and LOX Tanks . . . 44
5.8 Pipe sizing from velocity limits for liquid propellants. . . . 47
5.9 Criteria for the pressurisation and feed system LOX tanks. . . . 50
5.10 Assessment of pressurisation and feed-system criteria. . . . 65

6.1 European countries with average monthly wages below 80% of Germany's (in PPP USD) 70
6.2 Dealing with Construction Permits: Rankings and Scores from Doing Business 2020 . . 71
6.3 Tertiary Education Attainment Rates (Age 25–64) [88] . . . 74
6.4 Weight Vectors . . . 75

7.1 Overview of Rocket Engine Test Stands by Region . . . 79
7.2 Adjustment factors and 2025-equivalent costs for rocket test stands [52][50][51] . . . 81
7.3 Comparison of Lampoldshausen vs. High-thrust bench capabilities ('yes' = available, 'no' = not available). . . . 82
7.4 PBS element cost shares. Yes = excluded from horizontal bench. [1] . . . 84
7.5 Annual OPEX as a percentage of initial CAPEX, by facility type and age[2] . . . 85
7.6 Base assumptions and dynamics . . . 86

8.1 Pressurisation/purge, instrumentation/controls, and utilities FMECA items . . . 89
8.2 Structures/mechanical, operations/human factors, and architecture-specific FMECA items 90

C.1 Performance factor criteria by type of bench. . . . 112
C.2 Construction factor criteria by scope of works. . . . 112
C.3 Assessment for NASA A-3 (SSC). Performance factor chosen per Table C.1; construction factor per Table C.2. . . . 113
C.4 Assessment for NASA B-2 (SSC). Performance factor chosen per Table C.1; construction factor per Table C.2. . . . 113
C.5 Assessment for NASA A-2 (SSC). Performance factor chosen per Table C.1; construction factor per Table C.2. . . . 114
C.6 Assessment for Stand 4670 (MSFC). Performance factor chosen per Table C.1; construction factor per Table C.2. . . . 115
C.7 Assessment for USAF 2-A (Edwards). Performance factor chosen per Table C.1; construction factor per Table C.2. . . . 115
C.8 Assessment for DLR P5.2 (Lampoldshausen). Performance factor chosen per Table C.1; construction factor per Table C.2. . . . 116
C.9 Assessment for SIET (India). Performance factor chosen per Table C.1; construction factor per Table C.2. . . . 116

D.1 Verification checks and outcomes 119
D.2 Zero-NPV frontier $u^{(C)}$ at sample CAPEX values. 119

Nomenclature

Abbreviations

Abbreviation	Definition
AI	Artificial Intelligence
BE-4	Blue Engine 4
CAPEX	Capital Expenditure
CEA	Chemical Equilibrium Applications
CI	Critical Item
CN	Criticality Number
CNN	Convolutional Neural Network
COTS	Commercial off-the-shelf
CRV	Current Replacement Value
D	Detection
DLR	Deutsches Zentrum für Luft- und Raumfahrt
EC	Economic Conditions
ELC	European Launcher Challenge
EM	Extraordinary Maintenance
ESA	European Space Agency
EU	European Union
EUR	Euro
FFSC	Full-flow staged combustion
FMECA	Failure Mode, Effects, and Criticality Analysis
FRSC	Fuel-rich staged combustion
GG	Gas-generator
GOX	Gaseous Oxygen
GPU	Graphics Processing Unit
He	Helium
HT	High-Thrust
Hydrolox	Hydrogen-liquid oxygen
ILOT	ukasiewicz Research Network - Institute of Aviation
INR	Indian Rupee
JT	Joule-Thompson
LAM	Lampoldshausen
LCH_4	Liquid methane
LH_2	Liquid hydrogen
LOX	Liquid oxygen
LSTM	Long Short-Term Memory
LUMEN	Liquid Upper Stage Demonstrator Engine
M	Mega
MCC	Measurement Command and Control System
Methalox	Methane-liquid oxygen
MSFC	Marshall Space Flight Center

Abbreviation	Definition
N_2	Nitrogen
NASA	National Aeronautics and Space Administration
NCF	Net Cash Flow
NPV	Net Present Value
NPO	Nauchno-Proizvodstvennoe Obedinenie
NUTS	Nomenclature of Territorial Units for Statistics
O/F	Oxidizer to Fuel
OM	Ordinary Maintenance
OPEX	Operational Expenditure
ORSC	Oxygen-rich staged combustion
P	Probability
PA	Product Assurance
PBS	Product Breakdown Structure
PLC	Programmable Logic Controller
PLD	Payload Aerospace
PPP	Purchasing Power Parity
PSLV	Polar Satellite Launch Vehicle
QA	Quality Assurance
Repex	Replacement Expenditure
ROM	Rough Order of Magnitude
RP-1	Rocket Propellant-1 or Refined Petroleum-1
RPA	Rocket Propulsion Analysis
S	Severity
SC	Staged Combustion
SIET	Semi-cryogenic Integrated Engine and Stage Test facility
SLS	Space Launch System
SSC	Stennis Space Center
STS-I	Space Transportation Directorate, Infrastructure and Value Chain
SVM	Support Vector Machine
TBD	To Be Determined
TR	Test Request
TRR	Test Readiness Review
TWT	Trisonic Wind Tunnel
USAF	United States Air Force
USD	United States Dollar
VAE	Variational Autoencoder

Symbols

Symbol	Definition	Unit
A	Area	m^2
Amo	Amortization	€/year
C	Capital expenditure	€
$CAPEX_0$	Capital expenditure	€

Symbol	Definition	Unit
d_r	Regional density	people/km^2
d_t	NPV factor	-
D	Diameter	m
D_t	Utilisation	days/year
$Elas$	Elastic OPEX	€/year
f	Friction factor	-
F	Factor	-
F_t	Thrust force	N
g_0	Gravity	m/s^2
h	Enthalpy	kJ/kg
I_{sp}	Specific impulse	s
I_t	Cost index	-
$Inel_1$	Inelastic OPEX	€/year
JT	Joule-Thomson	
L	Length	m
M	Molar mass	g/mol
$\dot{m}$	Mass flow	kg/s
$\dot{m}_g$	Gas mass flow	kg/s
$\dot{m}_l$	Liquid mass flow	kg/s
n	Number	-
n_{cyl}	Number of moles per cylinder	mol
N_{cyl}	Number of cylinders	-
NCF_t	Net cash flow	€/year
NPV	Net present value	€
P	Pressure	Pa
P_{in}	Inlet pressure	Pa
P_{out}	Outlet pressure	Pa
P_1	Test day price	€/day
P_r	Population	# of people
PV_C	Present value of cost	€
PV_R	Present value of revenue	€
Q	Volumetric flow rate	m^3/s
r	Discount rate	%/year
R	Regression coefficient	-
Re	Reynolds number	-
$Repex$	Replacement expenditure	€/year
R_t	Annual revenue	€/year
t	Time	s
T	Temperature	K
T_f	Fuel temperature	K
T_{ox}	Oxidizer temperature	K
T	Horizon	year
u	Flow velocity	m/s
V	Volume	m^3
V_f	Final volume	m^3
V_i	Initial volume	m^3
$V_{removed}$	Removed volume	m^3

Symbol	Definition	Unit
x	Length	m
z	Height	m
α_t	Price factor	-
Δ	Difference	-
Δp_{fric}	Friction pressure drop	Pa
Δp_{grav}	Gravitational pressure drop	Pa
ϵ	Expansion ratio	-
η	Offset	-
π	Inflation	%/year
ρ	Density	kg/m^3
ρ_g	Gas density	kg/m^3
ρ_l	Liquid density	kg/m^3

1 Introduction

High-thrust staged-combustion (SC) rocket engines are the pinnacle of rocket engine cycles. Their appeal is rooted in cycle efficiency and durability: by burning propellants in preburners before the main chamber, SC engines can operate at higher chamber pressures while keeping turbine inlet temperatures comparatively low, improving performance margins and reliability. Validating such engines requires test benches that deliver hundreds of kilograms per second of cryogenic propellant at tightly regulated pressures, manage violent transients cleanly, and return high-fidelity data suitable for design iteration. Yet the open literature offers little practical guidance. Test-bench design is rarely described because it is commercially sensitive or export-controlled; when it is discussed, it is typically at (very) small or mid-scale and isolated to subsystems rather than complete, full-thrust facilities.

European institutional and commercial programs are seeking higher test cadence at lower cost to accelerate propulsion development. Despite this demand, Europe currently lacks affordable, accessible facilities capable of routine hot-fire testing of full-scale staged-combustion engines. Existing options tend to be legacy, limited in availability, optimized for other regimes, or economically out of reach for New Space companies' test campaigns. This situation constrains independent capability, causes longer development schedules, and pushes teams toward costly workarounds such as sub-scale testing that does not fully take away risk at engine level.

These two challenges, meeting the stringent interface requirements of full-scale SC engines and achieving affordability and availability within the European context, are rarely addressed together. In practice, they often diverge: the very features that stabilize starts, throttle ramps, and aborts (large run-tanks, robust pressurization, extensive water and exhaust handling) drive civil works and operations cost. However, programs that rely on rapid iteration need both capability and low cost per hot-fire minute. In such cases, the objectives converge into a single design requirement: a modular, Europe-aware sea-level test bench that satisfies staged-combustion interfaces while being economical to build, operate, and scale.

This thesis addresses that need by developing a high-level design for a sea-level propulsion test bench dedicated to 2 MN staged-combustion engines. The work integrates an architecture tailored to SC start-up and control, first-order sizing of cryogenic and pressurization systems, and an approximation of cost with an operational model. It is conducted in collaboration with the European Space Agency (ESA) and aims to demonstrate the technical and economic viability of an affordable European facility for full-scale staged-combustion engine testing.

1.1. Thesis Outline

- **Chapter 2: Literature Review** dives into sea-level versus altitude test benches, the required infrastructure and logistics behind the operations of a test facility, possible applications of automation and AI in a test bench, staged-combustion engine fundamentals, and the state-of-the-art information on rocket engine test facilities.

- **Chapter 3: Research Proposal** presents the main research question as well as different sub questions that guided the work performed.
- **Chapter 4: Requirements** consolidates customer requirements into test-capability, safety, modularity, schedule, and cost targets that drive the bench architecture.
- **Chapter 5: Fluid Supply System** sizes tanks, pressurisation and piping from worst-case mass flows and verifies stable interface conditions with EcosimPro/ESPSS.
- **Chapter 6: Site Selection** evaluates European locations on labour cost, permitting, remoteness and logistics, and workforce, producing a shortlist of viable countries.
- **Chapter 7: Cost Modelling** determines CAPEX and OPEX with top-down and bottom-up approaches and maps them to required day-rates via discounted-cash-flow analysis.
- **Chapter 8: Failure Mode, Effects, and Criticality Analysis** identifies critical risks across cryogenic flow, pressurisation and purge, structures, controls, and operations with targeted mitigations.
- **Chapter 9: Conclusion** summarises technical feasibility, siting and economic viability, and the operational blueprint for a modular European bench for $\geq$ 2 MN SC engines.
- **Chapter 10: Recommendations for Future Work** proposes concrete next steps on software use, multi-propellant configuration finalisation, and cost-model expansion.

2

Literature Review

This literature review aims to provide a solid background on rocket engine test facilities, their operations, what they consist of, rocket engine cycles, and possible applications of automation and AI.

2.1. Test benches

Rocket engine test facilities (or test benches) are specialized installations where liquid-propellant rocket engines and stages are fired on the ground under controlled conditions prior to flight. These facilities enable engineers to validate performance, study phenomena like ignition and shutdown transients, and ensure safety by uncovering issues on the ground rather than in flight. Ground testing is significantly less costly and risky than inflight testing, making it the foundation of propulsion development. This section reviews the types and capabilities of rocket engine test benches, the required facility infrastructure, the historical evolution of these facilities from early rocketry to the present and the state-of-the-art.

Figure 2.1 shows NASA's B Test Complex at Stennis Space Center. This large dual-position vertical test stand was originally built in the 1960s for static-firing the Saturn V first stage. It was later used for Space Shuttle Main Propulsion System tests and recently for the SLS core stage Green Run [69]. The structure includes massive concrete foundations, flame deflectors, water deluge systems, and cranes for handling large test articles.

Figure 2.1: B Test Complex at Stennis Space Center in Hancock County, Mississippi, United States [67]

2.1.1. Types of Test benches: Sea-Level vs Altitude, Subscale vs Full-Scale, and Orientation

Rocket engine test stands are often categorized by the environmental conditions they simulate and the scale of the article that is being tested. The theory discussed in this section only refers to test stands for engines with a thrust of more than 100 kN. The primary distinction is between sea-level test stands and altitude test stands:

- Sea-Level Test Stands: These facilities operate at ambient atmospheric pressure. They are commonly used for booster engines or stages that ignite at or near ground level. Sea-level stands can directly measure sea-level thrust and assess startup transients in an environment similar to launch. However, sea-level testing does not replicate high-altitude vacuum conditions, so engine flow expansion and performance differ from in-space operation. Sea-level stands typically have a massive foundation to restrain the engine, and a flame bucket or trench to deflect exhaust plumes horizontally or vertically away, with water deluge for cooling and sound suppression. Engines may be mounted vertically, which is preferred for most liquid engines to mimic the flight orientation and ensure proper turbopump suction head, or horizontally, which is often used for solid motors or small engines. Vertical test stands must account for the engine's weight component along the thrust axis (which can slightly affect thrust measurements), whereas horizontal stands avoid that but have other challenges in exhaust handling. All sea-level stands require robust blast protection and remote operation due to the explosive risk of engine failure. [80]
- Altitude Simulation Test Stands: These are designed to test engines under reduced ambient pressure conditions, simulating (high-) altitude or near-space operation. The term altitude simulation is often used as an umbrella for both vacuum and (high-) altitude test environments, although in practice, most facilities simulate partial vacuum in the range of 10 to 100 mbar. Vacuum simulation, which is used for in-space propulsion testing, requires pressures well below 1 mbar and is achieved in fully enclosed vacuum chambers with cryopumps and molecular drag pumps. These facilities, such as ESA's EPL at ESTEC, are typically limited to microthrusters or subscale engines due to exhaust handling constraints and chamber size. The boundary between vacuum and high-altitude simulation is not a strict one, as the term vacuum is often used in literature to describe high-altitude simulation, as shown in [103] and [80]. ESA, DLR, and CNES documents follow the same naming pattern[1]. Altitude test facilities use vacuum chambers to lower ambient pressure prior to and during the firing. Engines are typically enclosed in a sealed test cell connected to steam-ejector vacuum systems or high-capacity pumps that maintain low pressure while exhausting the hot gases. This allows measurement of vacuum thrust and evaluation of engine start, steady-state and shutdown in conditions similar to upper-stage flight. Altitude stands are far more complex and costly than sea-level stands due to the vacuum systems, large flame ducts, and refrigeration or gas injection needed to avoid damage to the vacuum equipment. For instance, DLR's P4.1 altitude test stand in Lampoldshausen (Germany) can simulate high-altitude backpressure for upper-stage engines like Vinci by using a dual-bell nozzle and vacuum chamber. It has a water deluge system with a centre body diffuser that requires 4000 litres per second to keep cool. Altitude test benches enable testing of ignition at high altitude and expansion nozzles at proper pressure ratios, which cannot be done at sea level. [102]

Figure 2.2 and Figure 2.3 show a horizontal sea-level test bench and a vertical altitude simulation test bench, respectively. As can be seen, a high-altitude simulation test bench is significantly more complex than a sea-level bench.

[1] Personal correspondence with Fehmi Mejri

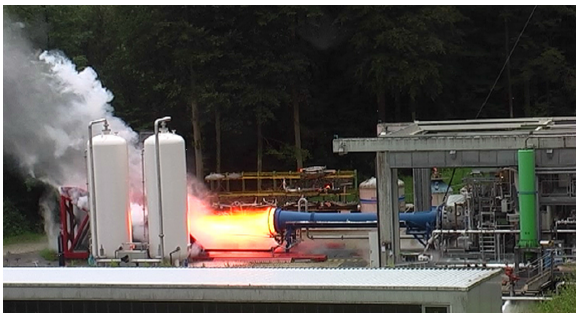

Figure 2.2: ESA P3.2 rocket engine test bench at DLR Lampoldshausen [30]

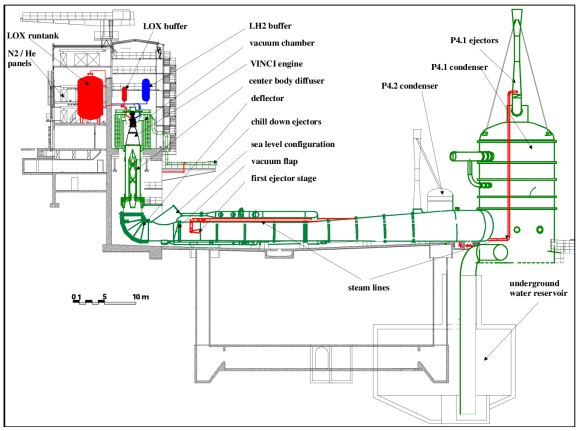

Figure 2.3: Cross-section of the ESA P4.1 high-altitude simulation test bench at DLR Lampoldshausen [102]

Another distinction is the scale of the test article. Facilities range from subscale component test rigs to full-scale stage test stands:

- Component/Subscale Test benches: These are smaller stands dedicated to testing individual components, like injectors, turbopumps, thrust chambers or subscale combustion devices. For example, the European P8 test facility at DLR Lampoldshausen has been used to test subscale thrust chamber assemblies and preburners for technology development [95]. Component test rigs often allow frequent testing and easier instrumentation. They are crucial for assessing combustion stability or injector performance before committing to full-scale hardware.
- Engine and Stage Test Stands: Full-scale engine test stands hold complete engines or even entire stages. A vertical engine test stand usually supports a single engine (or a pair) firing into a flame trench. A stage test stand can mount an entire rocket stage (with multiple engines) for integrated firing. For example, the B-2 stand at NASA Stennis Space Center was built to static-fire the Saturn V first stage (S-IC) with five F-1 engines, requiring an enormous concrete foundation to absorb 7.5 million pounds of thrust (33.4 MN). Stage test stands are among the largest and most capable, often featuring multiple positions. They provide system-level verification. The Saturn V S-IC stage, Shuttle Main Propulsion Test Article with three RS-25 engines, and SLS core stage Green Run were all tested in such facilities. [116]

Finally, orientation is either vertical or horizontal firing. Vertical stands position the engine/stage upright, which closely mimics flight orientation and ensures propellants settle similarly to flight. Horizontal stands orient the motor sideways; these simplify some structural aspects and eliminate the hydrostatic pressure head effect on thrust measurement, but they require effective flame deflection and can have higher acoustic impact on surroundings. Horizontal firing is more common for solid rocket motors and small engines. For solid rockets, this is because of their immense weight, making vertical positioning very difficult, not to mention the additional required infrastructure for a large vertical solid rocket motor (flame trench, foundation to keep the engine on the ground). As the combustion behaviour is largely insensitive to gravity, and solid motors have no turbopumps or sloshing, it is mostly cost that is a driver for horizontal solid motor testing. Horizontal setups are cheaper, give easier access, and simplify post-test grain and nozzle inspection. For small engines, horizontal orientation is typically preferred because of cost constraints. These are primarily used in microgravity environments, and because of that their ground test orientation is generally not critical. In space, these engines operate in conditions where gravity is absent, and thrust vectoring is decoupled from gravitational alignment. Most ground tests use externally pressurised feed systems and do not replicate flight tanks, making gravitational effects irrelevant. Both orientations require extensive hold-down structures: vertical stands use hold-down posts or cages, and horizontal stands use saddles and reaction frames to contain the thrust. For a realistic and precise recording of thrust and moments, the vertical installation of the rocket engine is usually better suited due to the orientation of the thrust. Vertical tests direct the thrust in the real direction of flight, which simulates the actual load case during rocket launch. This allows axial thrust forces

and the resulting bending moments and torsional forces to be measured precisely, just as they occur in flight. Another reason for the vertical position is to minimize lateral interference factors. In a horizontal setup, lateral forces have a stronger effect, which can distort the measurement results. Engines that are tested horizontally have to be able to sustain their own weight in such a position, and their subsystems still have to function. Furthermore, a support in a horizontal position can generate additional friction or side forces that affect the accuracy of the load cells. The last reason is fuel behaviour and fluid dynamics. With liquid engines, the position of the tanks and the behaviour of the propellants under gravity play a major role. A vertical test allows realistic conditions for fuel delivery, and thus more precise data on thrust control and turbopump performance. Vertical tests are therefore considered technically superior for the precise measurement of thrust and torque, as they simulate realistic load cases, minimize disturbances and reproduce the engine structure and dynamics as in real flight.[2]

2.1.2. Test Bench Infrastructure

Testing a rocket engine requires a vast support infrastructure. The basics of this infrastructure are listed below in detail. At the end of the section, a Product Breakdown Structure of a high-thrust test bench is provided.

- Propellant Storage and Handling: Large storage tanks for liquid propellants, like LOX and RP-1, are located a safe distance from the stand, often behind berms. Tanks containing cryogens, propellants with a temperature below 123 K, are vacuum-insulated, often spherical, vessels. These so called *run tanks* feed the test stand via insulated piping, with redundant pumps and vaporizers. The propellant feed system includes fast-acting emergency shutoff valves to terminate flow instantly if required. In case of flameout or abort, dump systems safely drain propellants from feed lines. Ground facilities use GN_2 purges to inert lines and engine cavities before and after tests. All storage is designed per pressure vessel codes and has multiple relief valves leading to flare stacks or vent ponds. For example, hydrogen flare stacks at Stennis safely burn off H boil-off or dump gas far above ground.
- High-Pressure Gas and Power: Large high-pressure gas bottles supply gaseous Nitrogen (GN_2) for purging and sometimes Gaseous Helium (GHe) for tank pressurisation, in case the propellant liquifies nitrogen. These gases are distributed through control manifolds to actuate valves and pressurise engine tanks. The site also requires significant electrical power for pumps, instrumentation, and potential cryogenic refrigeration systems. Backup power ensures data acquisition and safing can continue even if primary power is lost during a test, so data of a failure event is not lost.
- Cooling and Water Deluge: To protect the test article and stand structure from heat and acoustics, cooling systems are essential. A water deluge system dumps large quantities of water into the flame trench or flame diverter just as the engine fires. This water absorbs heat and damps acoustic waves, preventing excessive reverberation that could damage the engine or bench. The sound suppression water system at large stands can flow on the order of tens of thousands of litres per minute. The water deluge system for the SLS testing at the B Complex of Stennis supplies 21000 litres per second [15]. Additionally, some stands have flame duct water curtains and cooled flame deflectors. At altitude stands, instead of open flame trenches, the engine's exhaust is diffused into vacuum systems and often quenched with water or liquid oxygen to cool the gas.
- Structural Mounts and Thrust Measurement Systems: The stand structure itself must withstand and redirect the forces. Reinforced concrete foundations and steel superstructures anchored deep in bedrock are common. For example, the B-2 stand's foundation is a 39-ft thick concrete slab for the hold-down arms [80]. Embedded within the mount are the thrust measurement load cells which output to the data system. These must be calibrated and compensated for thermal and other effects (some stands calibrate by hanging known weights or using hydraulic jacks prior to tests). Stands often have a movable crane on top for lifting engines or stages into place.
- Control Centre and Instrumentation: A blockhouse or control bunker is located at a safe distance. It houses the test conductor and engineers who monitor readouts. Modern control centres are computer-equipped, but also maintain manual engine cutoff switches and emergency abort triggers. Communications systems link the control centre to all personnel and range safety. Data from

[2]Personal correspondence with Andreas Haberzettl

sensors is sent via hardened cables or fibre optics from the stand to the control room in real time, which realises a high bandwidth. [91]

- Safety Systems: Safety is paramount, as engine tests involve explosive propellants. Facilities maintain rigorous safety zones: typically a large cleared radius where no uninvolved personnel are allowed during tests. Explosive Safety Reviews are done to calculate hazard distances for overpressure and where fragments might end up. For example, NASA requires that overpressures at the fence line remain below a threshold for engine test stand siting. Stands themselves have blast deflectors and shields. These thick concrete walls or earthen berms protect nearby equipment and personnel shelters. An inert gas purge system is used to prevent accumulation of flammable mixtures in confined volumes. Hydrogen in particular needs to be carefully purge because it can pool in pockets. That is why many stands use continuous GN_2 purges around the engine interface and a hydrogen sniffer system to detect any leakage. Before a test, the facility is put in secured mode: all personnel evacuate the stand, going to the control bunker or beyond. Automated checklists and a countdown procedure ensure all valves and systems are in the correct configuration. If any condition is detected that is not within the tolerated bounds, an automatic safing sequence will abort the test. Post-test, a stand fire suppression system can be activated if any residual fire is detected. Lightning protection is provided by tall masts and catenary wires to avoid strikes on the bench. The facilities also maintain on-site fire and rescue crews during tests.
- Environmental Protection: Rocket tests can produce noise and release chemicals into the atmosphere. Test centres are usually in remote areas to mitigate noise impact on the public. Water residual from the deluge and cooling, and residual propellants can be collected to prevent pollution. Before hypergolic tests, special containment is set up since those fuels are toxic. The facilities must comply with environmental regulations, which is another driver for isolated locations.

2.1.3. Historical Evolution of Test Stands

Rocket engine test stands have evolved in scale and sophistication since the beginning of rocketry. During the Second World War, Germany established one of the first large engine test complexes at Peenemünde, where the V-2 missile's engines were fired in fortified vertical stands (Prüfstände in German) [82]. These early test benches validated the V-2's design but also revealed critical issues, like combustion instability. The Peenemünde facilities were the birthplace of a lot of post-war rocketry programs, not only because the German rocket scientists were sought after by the Americans (operation Paperclip), but also because it served as a lesson for the rest of the world on how to design rockets.

By the 1960s, the US and USSR constructed far larger test stands to support human spaceflight. NASA's MSFC 4670 was built in 1965 to static-fire the Saturn V first stage, which used a cluster of five F-1 engines, with a 33 MN total thrust. This steel and concrete stand, 90 m tall, enabled full-duration stage burns on the ground. Later, Stennis B-2 was used for this. These Apollo-era stands proved their worth by uncovering issues like pogo vibrations in the F-1, which were solved through exhaustive testing and redesign before flight.

After Apollo, many stands were repurposed for new programs. NASA's Stand 4670, for example, was later modified to test the Space Shuttle Main Engine (SSME) in the 1970s and the Shuttle's External Tank systems. At NASA Stennis, the Apollo-era vertical stages, the A-1/A-2 stands, were converted for single-engine SSME testing. Engineers added a gimbal mount and high-speed instrumentation, and even installed a diffuser on A-2 to simulate altitudes up to 18 km for the hydrogen-fuelled SSME. Over 3,000 SSME tests were conducted at Stennis from 1975 to 2009, totalling more than 820,000 seconds of firing and contributing to 135 Shuttle flights. This era established best practices in test operations and demonstrated the value of extensive ground firing to ensure reliability of reusable engines. [71]

In recent years, the landscape of test facilities has further grown with commercial players. Old stands have found new life through public-private partnerships. An example of this is Blue Origin refurbishing MSFC 4670 to support its modern methane-fuelled engines, exemplifying how old infrastructure can be adapted to new propulsion technologies [78]. Meanwhile, SpaceX has built extensive private test facilities in McGregor, Texas for rapid engine development, and other firms also operate their own test stands or share national facilities. This commercialization of test stands is accelerating innovation by increasing test cadence and diversifying approaches, all while standing on the shoulders of the proven principles developed over decades.

2.1.4. State-of-the-Art Research

When it comes to the state-of-the-art research on high-thrust liquid rocket engine test facilities, resources are very sparse. [111] is the most expansive source of information on test benches, but does not go deeper than the basics on any topics besides operations. Complementing this, a small set of peer-reviewed and agency sources focus specifically on test infrastructure: [44] documents Europe's P-series benches at DLR Lampoldshausen and how capability upgrades could be orchestrated to support a program like SCORE-D. On the U.S. side, [90] provides a detailed look at mid-scale R&D infrastructure (NASA SSC E-3), and provides an in-depth overview of data acquisition. However, the rest of this paper does not contain any information that is missing from [80], where capabilities of all benches on Stennis premises are listed. [57] characterises an altitude hot-fire environment (NASA's In-Space Propulsion Facility) where upper stage vehicles are tested in a space environment. It contains information on the full-scale bench, but it is not a sea-level bench, and the information is concerning the vacuum, hence not relevant.

For sea-level benches, the state-of-the-art does not cover high-thrust benches. This has multiple reasons: work surrounding high-thrust rocket propulsion is almost always confidential, and if it is not confidential, it covers a very small part, like the ideal angle of a flame trench. Diving deeper when it comes to the actual design of a rocket engine test bench, the following sources are the most relevant: [96], [6], and [113] are student-built test stands consisting of a liquid stand with integrated feed system, a trailer-mounted mobile stand, and a lab-scale hybrid stand respectively. The maximum thrust rating for these projects is 5 kN, or $\frac{1}{400}$ of the thrust relevant in this project. [18] is a thesis performed in collaboration with ISAR Aerospace, where a bi-propellant rocket engine test stand with two test cells is discussed, for a thrust of up to 35 kN. The dynamics that play with an engine that is 57 times smaller than the engines to be considered here are different, since results at much smaller scale often do not transfer to full scale without care. They do however show some elements that might be necessary for the large scale bench, like a very detailed feed system, visible in Figure 2.4, that even though it lacks the scale of a big facility and is non-cryogenic, provides valuable information on valve sequencing and instrumentation.

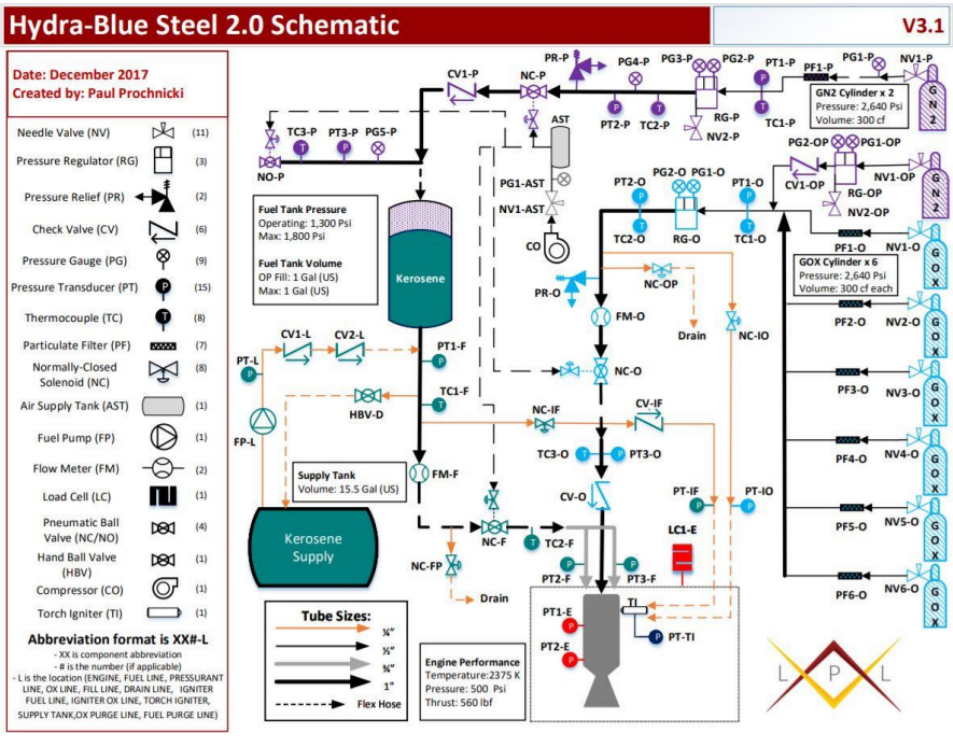

Figure 2.4: Hydra-Blue Steel schematic [96]

Thus, for large test facilities, the knowledge mostly relies on industry professionals. A lot of the findings in this thesis are achieved with insights obtained in consultation with practising test-stand engineers and other industry professionals. A final, less formal but highly informative source are images of SpaceXs

McGregor site in Texas, which offers a contemporary reference for horizontal engine test benches. It is the only horizontal bench of similar scale (Raptor thrust is currently around 2.75 MN) that has been photographed. It can be seen in Figure 2.5.

Figure 2.5: SpaceX McGregor horizontal test stand: (left) Full test bench with LOX and CH_4 tanks clearly visible; (right) Test cell with Raptor 3 [86].

The LOX tank and methane tank, both suspended in a steel structure (to accurately measure I_{sp}), are clearly visible. It can test for 460 seconds, with an unknown throttling profile [86]. The accompanying LOX and LCH_4 mass flows, if the engine was at 100% for full duration, are 510 kg/s, 0.5 m^3/s and 140 kg/s, 0.333 m^3/s [56, 11]. This seems impossible considering the size of the tanks, so it can be assumed the engine was throttled. The infrastructure is clearly visible, as is the plume of the non-diverted exhaust. The debris plume of the stand is 75 meters wide and 350 meters long, and there was no water deluge until recently. The bench is the ideal example of a modular, easy to build and maintain test facility. [61]

2.1.5. Product Breakdown Structure

A high-level Product Breakdown Structure (PBS) of a test bench is provided in this subsection.

1. **Test Cell**
   - Engine installation structure
   - Vacuum chamber (if high-altitude simulation required)
   - Propane burners at the end of the engine nozzle to avoid the spread of unburned propellants into the test cell
   - Microphones for high noise levels in case of acoustic anomalies during tests
   - Camera system
   - Crane and support tools
2. **Exhaust Gas Guiding System**
   (a) **Diffuser**
      - Traditional diffuser or centre body diffuser
      - Water cooling system

   (b) **Guide Tube**
      - Water cooling system

   (c) **Flame Deflector**
      - Redirect exhaust flow
      - Optional water-cooling system

   (d) **Exhaust Duct (if applicable)**
3. **Engine Propellant Supply System**
   (a) **Propellant Storage Tanks**

- Cryogenic tanks (for LH2, LOX, LCH_4)
- Semi-cryogenic tanks (LOX with RP1)
- Non-cryogenic tanks (ambient temperature fluids)

(b) **Buffer Tanks (optional, simulate operational conditions)**

(c) **Pipe Subsystem**

- Vacuum-insulated pipes (for cryogenic fluids)
- Standard pipes (non-cryogenic fluids)
- Valves and control elements
- Filters for cryogenic fluid supply
- Chill-down systems (cryogenic)

4. **Gaseous Supply System**

(a) **Gas Storage & pressurisation Tanks**

- Nitrogen (GN2)
- Hydrogen (GH2)
- Helium (GHe)
- Oxygen (GOX)
- Methane and Propane

(b) **pressurisation Subsystem**

- Tank pressurisation lines
- Line pressurisation and purge lines

(c) **Ignition Gas Supply**

- Gaseous hydrogen and oxygen to igniters
- Ignition system valves and regulators

(d) **Venting System**

- Neutral gas (helium, nitrogen) venting lines

5. **Water Supply System**

- Water storage tank
- Refrigeration system (cooling to $\sim 7°C$)
- Pumping system
- Distribution pipe network
- **Water-cooled subsystems (if applicable):**
  - Diffuser cooling system
  - Guide tube cooling
  - Flame deflector cooling system
  - Condenser and steam generator cooling lines
- Fire extinguish system

6. **High-Altitude Simulation System (if applicable)**

(a) **Steam Generation System**

- Liquid oxygen (LOX) and alcohol storage
- Steam generator combustion chamber
- Gas (GN2) pressurisation and venting system

(b) **Steam Storage Tank**

(c) **Steam Injection System**

- Main steam ejectors
- Auxiliary nozzle (optional)
- Chill-down ejectors (if applicable)

(d) **Exhaust Handling System**

- Multi-stage ejectors (first and second stage)
- Auxiliary nozzle (optional)

(e) **Condenser**

- Cooling water spray system
- Exhaust gas condensation chamber

7. **Vacuum Pump System (if applicable)**
   - Water-ring rotary pumps
   - Sliding-vane rotary vacuum pumps
   - Pressure monitoring & control systems
8. **Measurement, Command and Control (MCC) System**
   - Centralized real-time monitoring and control
   - Data acquisition (low and high-frequency channels)
   - Data processing and storage infrastructure
   - Safety and emergency shutdown system
   - Control room infrastructure (remote monitoring)
9. **Flare Stack**
   - Gas combustion chamber
   - Ignition device
   - Exhaust gas dispersion nozzle

This PBS was created using [37], [111], [101], [3], and [4].

2.2. Operations

The way a *commercial* test bench operates is an established, and universal procedure. For completeness, the differences compared to a test bench owned by a company that tests their own engines will be mentioned at the relevant points in this section. This section describes the typical logic flow of when industry asks a commercial test bench operator if they can test their engine.

2.2.1. Roles and Responsibilities

For the overall test campaign, three roles are established:

- Test Engineer: Responsible for the preparation of the test article and defining which tests the bench must execute.
- Test Bench Operator: Responsible for designing and running the test bench so that it carries out the Test Engineer's prescribed procedures.
- Independent Safety Responsible: Responsible for assurance of safety, independently of the Test Bench Operator and Test Engineer.

[3] Personal correspondence with Dirk Schneider
[4] Personal correspondence with Jörn Bellermann

The Test Engineer, Test Bench Operator and Independent Safety Responsible are not individuals, but teams. Within these teams, there are more detailed definitions of roles and responsibilities. At the Test Readiness Review (TRR), the responsibilities are assigned to individual persons, to define the team that will conduct the test campaign.

2.2.2. Planning and Preparation

An engine test usually begins with the customer, represented by the previously mentioned test engineer, submitting a test plan to the test bench operator, a few months before the intended test(s). This plan outlines what the engine developer wants to test, like thrust levels, chamber pressure, and throttling sequences. It provides the operator with some 'redlines': a sensor value limits that should not be exceeded, and if exceeded, should lead to an automatic abort of the test [33]. Furthermore, it includes details on the engine hardware (mass, dimensions, type), propellants, and necessary capabilities provided by the test facility (mass flow, measurements).

This plan is then reviewed by the test facility engineering team. In the current testing landscape in Europe, the capabilities of commercial test benches are known at companies that develop rockets. It is thus unlikely that they would request to test an engine at a bench where it cannot be tested. However, if something were to be requested outside of the normal operating envelope of the bench, the facilitator can assess whether modifications are possible. This applies to all areas of the test facility, including process engineering, MCC and specimen. Besides the technical feasibility, the test plan is also evaluated for safety concerns, for example regarding the pressures in the preburners, or the thrust level with respect to the structural limits of the stand. The customer and the operator iterate on the plan until both are satisfied that the test(s) can be done safely *and* meet the objectives.

The contract that is set up between a test operator and a customer contains the roles and responsibilities. A very important note in the contract with a commercial test bench operator is that the facility operator controls all facility systems and thus that the customer does not interfere with the test. This means that the customer is condemned to watch the test being carried out. If any crucial errors were made in the test plan, this could mean catastrophic failure. After the contract is signed, the main responsibility of the customer is delivering the engine in test-ready configuration. The operator is responsible for the propellants, data acquisition systems, control hardware and the personnel that should run the test. In some cases, like for example with the Airborne Engineering Ltd test bench in Westcott, using a customers own propellant tanks is possible if properly discussed with the operator.

Once the contract is signed and the test plan is accepted, the facilitators prepare the bench for the test. The sensor locations and measurement channels have been planned, the sampling rates agreed upon and now the bench needs to be made ready for testing. As all relevant parameters of the engine are known, the propellant feed lines can be adjusted, the connectors put in place to mate with the engine, and the support systems (fire suppression, water deluge or ignition source) are in place and ready to be used. Leak and pressure tests are performed to see if the pressurised propellant feed lines have leaks and if the valves operate correctly. A cryogenic chilldown, where gaseous nitrogen or helium is used to pre-cool the propellant feed lines and valves to avoid temperature shock when the propellants flow to the engine, has to be performed to see if the system works properly. After the bench checkout is completed, a formal *TRR* is convened. In the TRR the operator and customer jointly verify that:

- All mechanical, electrical and instrumentation tasks are closed out.
- Safety analyses and redline limits are correctly implemented in the control logic.
- Emergency procedures, communication protocols and abort scenarios are understood by all parties.

During the test, the operators execute the test according to the aforementioned test plan. As stated before, the customer cannot intervene in the test: it can only watch the data and potentially the test through cameras. If the engine performs nominally, the test is run for the planned duration and then shutdown is initiated. This is a pre-programmed sequence, if the rocket has its own ramp-down controller, where the propellant flow is stopped. The facility now triggers safing actions, which are actions

to put the test article and the bench in a safe state. The feed lines are purged, as well as the engine. Once the test operator has established that the stand is safe, the test is complete. If it was an anomaly that triggered an abort of the test, the safing is done very quickly. Emergency valves will close, and the engine is safed in as little time as possible, to prevent any damage to the test object. Once the test is done and the site is considered safe, after venting any remaining gases and establishing the stand safe to approach by personnel, the operator and customer can look at the stand and engine respectively to assess any damage done during the test.

The last step of the normal operations of a test bench is the post-processing of the acquired raw data. For a commercial test bench, the raw data is supplied to the customer, who will use that to identify possible new 'redlines' to be set and tests to be performed. Not only does the operator provide the measured data, but also the data from the bench itself is shared. The information regarding the supply of propellant to the engine is crucial information for the customer, as the exact numbers give insight on the performance of the engine. If the test was part of a series of tests, the test plan might be adjusted to incorporate the lessons learnt.

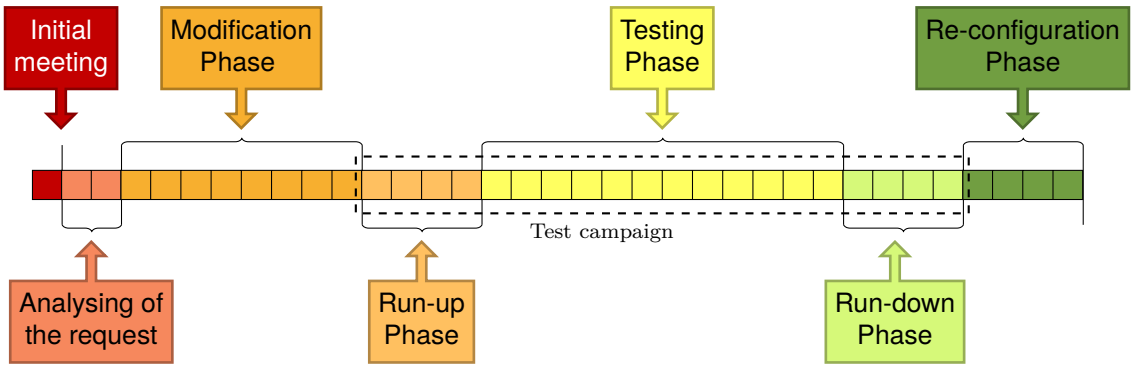

Figure 2.6: Standard phases for testing a rocket engine

2.2.3. Information Management

To provide a better overview of the documentation that is typically provided by the test engineer and the test operator, this subsection sums up the most relevant documents and what kind of information they contain.[5]

- Test Plan: Mentioned in detail in subsection 2.2.2. Describes the tests to be run, including the number of tests, the test configuration, main and passenger objectives, and test details such as hot-run durations and operating points.
- Product Assurance (PA) Requirements: Specifies the customer-required norms or standards against which product assurance must be carried out.
- Measurement Request/ Instrumentation Plan: For each test this plan comprises a table and accompanying narrative that lists every sensor and measurement channel installed on the test article. Each channel is identified by a unique sensor name and described by its general type (static pressure, temperature, strain gauge, etc.), its specific model, full-scale measurement range, and the archiving rate defined per test phase (for instance, 1 kHz during ignition, 100 Hz during steady-state, 10 Hz during shutdown). For each sensor, it also specifies any required filter settings (low-pass, high-pass, or band-pass), identifies whether it is acquired by the Test Bench MCC or an external measurement system, and enumerates which test sequences the channel is active in. Channels designated for automatic redline logic, that feed the MCC's safety system, are clearly flagged. In addition, any special or non-standard measurement systems, such as high-speed cameras or spectrometers, are described in detail, including equipment models, mounting and line-of-sight requirements, synchronization and trigger arrangements with the main data acquisition system, and any ancillary needs for fluid supplies or power so that installation and operation during the test campaign are fully supported.

[5]Personal correspondence with Kate Underhill and Andreas Haberzettl

- Test Specimen Risk Analysis: Identifies all risks posed by the test specimen and the required mitigation actions. The objective is to identify possible failure modes and define mitigation actions to be implemented to reach an acceptable risk status for each identified failure mode. This document is updated before each test.
- Test Request: Prescribes the complete facility configuration (control-valve manifold layout, orifice diameters, piping and instrumentation schematics), initial conditions (fluid type, fill levels, pressures and temperatures in all vessels), the full test sequence (chill-down profile, interface verification, start-up ignition and propellant flow schedule, steady-state hot-run thrust-hold, controlled shut-down and reconditioning protocols), and all control-loop setpoints (open-loop valve timings and stroke values, closed-loop mass-flow, pressure and temperature targets with PID tuning). In addition, the TR defines the automatic abort thresholds (overpressure, overtemperature, vibration limits), emergency shutdown logic and manual redline criteria enforced by the MCC. As the overarching document for the campaign, the TR establishes the common framework of configuration, sequence architecture, control logic and safety limits that every complementary, test-specific request will inherit.
- Specifications of Operational Procedures: Serves as a user manual for the test article, detailing for each test the precise mechanical and functional steps required to install the specimen in the test frame and verify its condition both before and after firing. It prescribes the operations for mounting the hardware; the pre-test inspections (visual checks, leak tests, sensor verification and dimensional surveys); the conditioning routines needed to prepare the article for ignition (purges, pressurisation, thermal soak); and the post-test activities (controlled depressurisation, demounting, cleaning and hardware conditioning). Where a designer's user manual exists, it is referenced; otherwise, the Operational Procedures fully substitute as the definitive guide. By consolidating all installation, inspection, conditioning and control-check sequences into a single document, the plan guarantees that every test follows a consistent, verifiable workflow.
- Test Specimen Documentation: Includes technical interface details (mechanical and electrical) with drawings, a sensor-layout and cabling plan (positions, connections, pin assignments) and calibration data files for all specimen sensors.
- Summary of Results: Prepared after each test to compile and publish the measured outcomes and key observations from the test day.

2.3. Combustion Cycles

In this section, the working principle of rocket combustion engines is explained. Before diving in-depth in staged combustion engines, a basic overview of other combustion cycles is provided, along with their respective advantages and disadvantages compared to staged combustion. After that, a full-flow staged combustion cycle is explained in detail. At the end of the section, the differences between full-flow, oxidizer-rich and fuel-rich is touched upon.

2.3.1. Gas Generator Cycle

The gas generator (GG) cycle uses a small combustion chamber to burn a fraction of the propellants, producing hot gas to drive the turbopump turbines, after which the exhaust is expelled rather than fed into the main chamber [111]. This design is relatively simple and has been widely used in many launch vehicles, owing to fewer complex components compared to closed cycles and a large base of operational experience [111]. The simplicity of the GG cycle contributes to reliable and robust operation, and it allows independent testing of the turbopump assembly, called powerpack tests, before full engine integration. However, discarding the turbine exhaust comes at the cost of efficiency: gas-generator engines lose some propellant mass flow that does not contribute to thrust, yielding a lower specific impulse than staged-combustion or expander cycles [58]. Moreover, the turbine inlet conditions in GG engines are often made extremely energetic: high-temperature, fuel-rich gases, to extract sufficient work with minimal mass flow, which imposes thermal stress on components and still results in performance below that of more closed cycles. This high temperature through the turbine is also one of the main reasons why GG engines are typically not reusable, and if they are, either their performance is hurt, or the amount of possible reuses is low. Figure 2.7 shows a schematic representation of a GG engine.

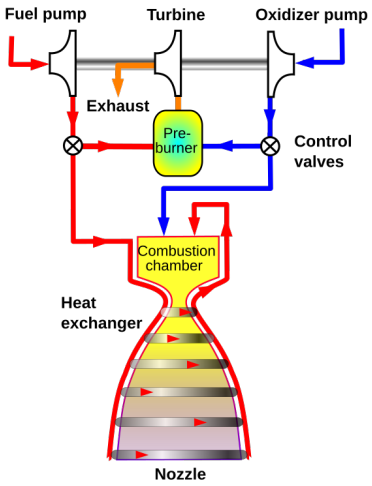

Figure 2.7: Gas generator engine [25]

2.3.2. Expander Cycle

In the expander cycle, the fuel or sometimes oxidizer is first circulated through the engines cooling jackets, where it absorbs heat from the chamber and nozzle, and is thus vaporized into a high-pressure gas that drives the turbine before being injected into the main combustion chamber and burned [111]. Because this cycle eliminates the need for a separate gas generator or preburner, it contains fewer high-temperature components and plumbing lines, which leads to lower mechanical complexity and generally lower turbine temperatures during operation [111]. These features make expander-cycle engines highly robust and dependable. Expander engines have extensive flight experience, often achieve high specific impulse, and can be designed for multiple restarts in space. The principal drawback is that the expander cycle is inherently limited by the amount of heat available for vaporizing propellant. As the engine thrust increases, the chamber/nozzle surface area (heat source) does not scale sufficiently fast to gasify the larger propellant flow required, imposing an upper thrust limit on practical expander engines. This is approximately 3 MN [93]. Consequently, expander cycles are typically restricted to relatively low-thrust, cryogenic-fueled engines, usually hydrogen-fueled upper-stage applications, where the thermal energy is adequate for pump-driving, and they run at lower chamber pressures than pump-fed open cycles since no combustion energy (preburner/gas generator) is added for power extraction [58]. A schematic of an expander engine can be seen in Figure 2.8.

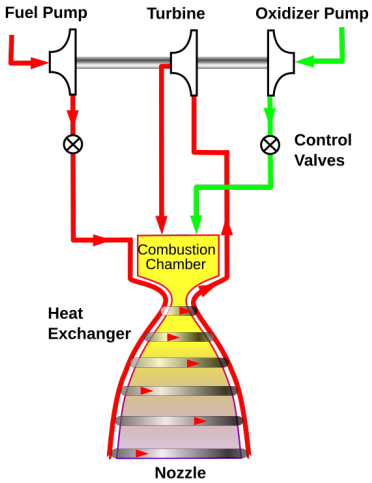

Figure 2.8: Expander combustion engine [23]

2.3.3. Pressure-Fed Cycle

A pressure-fed engine has no turbopumps at all. The propellants are forced into the combustion chamber by high pressure in the propellant tanks (maintained by pressurant gas or ultra-strong tank structures) [58]. The obvious advantage of this feed cycle is its simplicity. The elimination of turbomachinery yields a propulsion system with far fewer parts and failure modes, which tends to enhance reliability and ease of operation and maintenance [58]. Pressure-fed engines can be advantageous for moderate-thrust stages or reaction control thrusters where simplicity and storability outweigh performance concerns. The major disadvantages are the significant weight and performance penalties incurred: the propellant tanks must withstand high pressurisation and thus become heavy, and additional pressurant gas and plumbing are required, all of which increases the dry mass of the vehicle [58]. Furthermore, without pumps the achievable chamber pressure, and as a result the thrust-to-weight and impulse, is much lower than in pump-fed cycles, so pressure-fed designs generally deliver lower overall performance and are impractical for very high-thrust applications [58]. Figure 2.9 shows a pressure-fed engine cross-section.

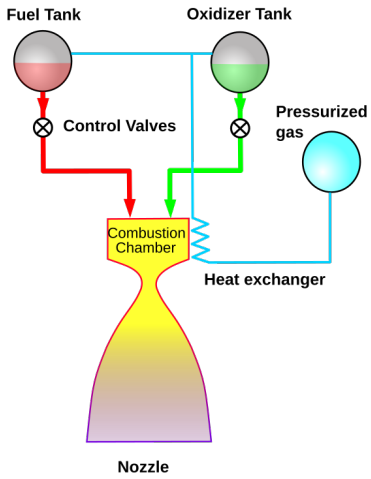

Figure 2.9: Pressure-fed engine [26]

2.3.4. Electric Pump-Fed Cycle

In an electric pump-fed engine, electrically driven motors drive the propellant pumps in place of a gas turbine, thereby decoupling the pump power source from the propellant combustion process [62]. This approach enables a high degree of throttleability and operational control and it removes the need for gas generators, preburners, and their associated plumbing, potentially simplifying the engine layout and improving reliability. An electric pump-fed cycle can achieve high chamber pressures and performance comparable to turbopump-fed engines while avoiding the thermal stresses of hot gas drive, and it has a fast development turnaround for small engines [58, 62]. However, the most important drawback is the added mass of the electrical power system: batteries, electric motors, and control electronics are dead weight that does not contribute to thrust, which severely limits the practicality of this cycle for larger engines or long-duration burns [62]. The energy density of current batteries constrains electrically driven pumps mainly to relatively small-scale launch vehicles or upper stages. For higher power requirements, the weight of the required batteries and motors grows dramatically and can negate the performance gains [59]. An electric pump-fed system is visible in Figure 2.10.

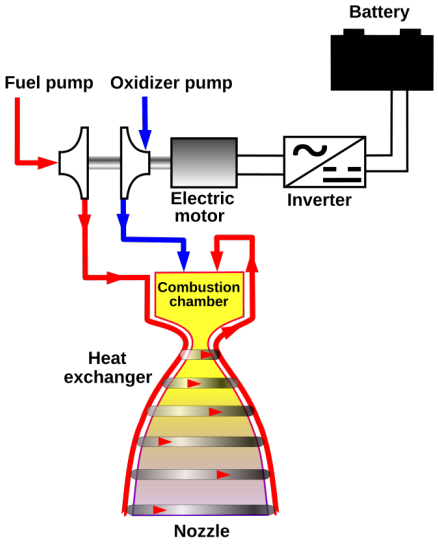

Figure 2.10: Electric pump-fed engine [22]

2.3.5. Tap-Off Cycle

The tap-off cycle draws off a portion of the hot gases from the main combustion chamber to power the turbopump turbines, instead of using a separate preburner or gas generator. In essence, the main chamber itself acts as the gas generator [58]. By eliminating the stand-alone gas generator and its feed lines, the tap-off configuration can simplify the engine and reduce part count, as demonstrated in the BE-3 engine of Blue Origin. The cycle can be seen in Figure 2.11.

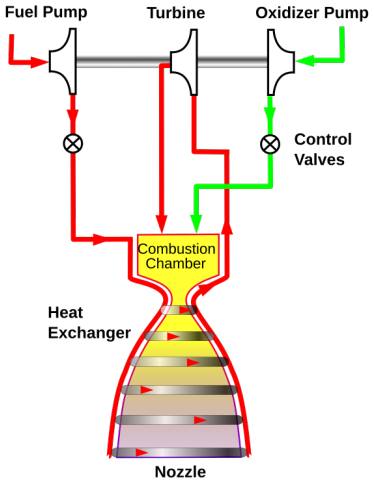

Figure 2.11: Tap-off combustion engine [21]

2.3.6. Staged Combustion

The combustion cycles mentioned above are divided in *closed* and *open* cycles. In open cycles, turbine exhaust is dumped overboard or injected only downstream of the throat, adding little thrust. In closed cycles, all turbine exhaust returns to the main chamber and expands through the nozzle, yielding somewhat higher performance at the cost of higher pressures and complexity [111]. The expander cycle and staged combustion cycle are the typical closed combustion cycles (except the expander-bleed cycle), with the electric pump-fed being a non-traditional closed cycle. In staged-combustion engines, the heat of fuel used for regenerative cooling is not a limiting factor for the turbine power. Therefore, higher pressures and thrust is possible for these engines.

This subsection dives deep into the working of a full-flow staged combustion engine, as this type of staged

combustion engine combines the working of a fuel-rich staged combustion engine and an oxidizer-rich staged combustion engine in one. Illustrative images, showing the different types of staged combustion engines, are shown in Figure 2.12, Figure 2.13, and Figure 2.14.

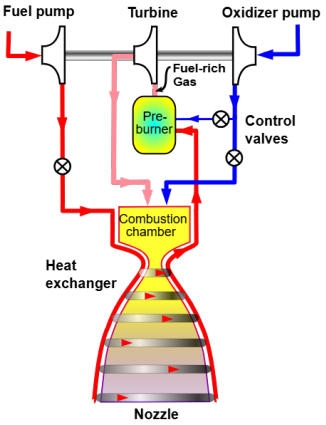

Figure 2.12: Fuel-rich staged combustion engine [27]

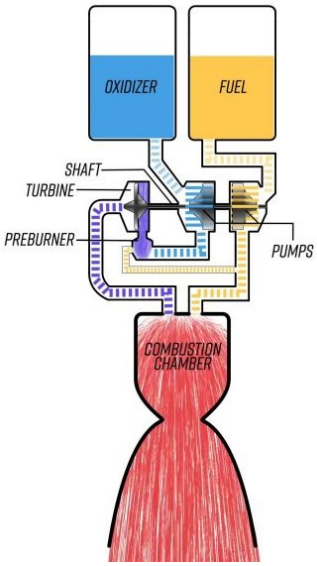

Figure 2.13: Oxidizer-rich staged combustion engine [11]

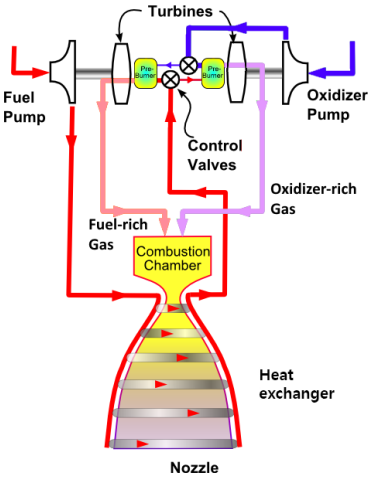

Figure 2.14: Full flow staged combustion engine [24]

It must be noted that these are the basic forms of this combustion cycle. The diagrams are schematic and do not represent engineering subtleties such as the number of shafts, start systems, and turbopump arrangements, which can differ substantially across specific engine implementations.

In fuel-rich staged combustion (FRSC) and oxidizer-rich staged combustion (ORSC), a preburner partially burns the propellants to create hot turbine drive gas, after which the exhaust is routed to the main chamber (closed cycle). In FRSC, most of the *fuel* and a small amount of oxidizer enter the preburner, producing a fuel-rich gas that eases oxygen-compatibility demands on hot turbomachinery but, with hydrocarbons, can promote soot formation and coking unless temperature is controlled. In ORSC, most of the *oxidizer* and a small amount of fuel are used, yielding an oxidizing gas that mitigates hydrocarbon coking yet imposes stringent oxygen-materials compatibility and transient-control requirements. In both cases, mixtures are highly off-stoichiometric so that the turbine inlet temperature is limited while still providing sufficient shaft power. FRSC is best suited to hydrogen engines, where coking is not an issue and a fuel-rich turbine environment is benign. ORSC is favoured for kerosene, to avoid soot and/or coking in turbines, while still reaching very high chamber pressures and compact pumps. It is increasingly used for methane as well. The main benefit of FRSC over ORSC is that the turbine does not have to handle a very oxygen-rich environment. This is very corroding for the turbine blades. An advantage of ORSC is that a higher mass flow through the turbine can be achieved, pushing up the turbine power available.

In a full-flow staged combustion cycle, all the propellant (both fuel and oxidizer) is fed through preburners and turbines before reaching the main chamber. This means the oxidizer and fuel are each split into two paths: one path goes into a fuel-rich preburner and the other into an oxygen-rich preburner. Only a small fraction of each propellant is diverted to the opposite preburner to allow partial combustion:

- Fuel-Rich Preburner: Almost all the fuel and a small portion of the oxidizer combine here. The oxidizer supplied is just enough to burn a small fraction of the fuel, making the mixture extremely fuel-rich. Essentially all the oxygen that enters this preburner is consumed, but most of the fuel remains unburned. This produces hot, fuel-rich gases.
- Oxygen-Rich Preburner: Almost all the oxidizer and a small portion of the fuel combine in this preburner. All the fuel in this preburner is consumed, while most of the oxygen stays unreacted

(an oxygen-rich hot gas results).

Because each preburners mixture ratio is extreme (one very fuel-rich, the other very oxygen-rich), only a few percent of the total propellant gets burned in the preburners. The rest remains as hot gaseous propellant to be fully burned later in the main chamber. Mass is conserved at every junction: the total fuel flow is the sum of what goes into the fuel preburner and the small amount going into the oxygen preburner, and similarly for the oxidizer. After the preburners, the two streams pass through their respective turbines and then reunite in the main combustion chamber. There, the remaining fuel and oxygen finally mix and burn completely to produce high-pressure combustion products for thrust. In summary, all propellant end up as gas in the main chamber, which is the defining feature of the staged combustion design.

Pump efficiency increases with volume flow rate, and is between 58-76% for existing engines [121], for which the information is public, with a maximum of 90% for very large flows ($0.05 m^3/s$) [111]. Because the oxidizer turbopump has a significantly higher mass flow than the fuel turbopump, the oxidizer turbopump typically has a higher efficiency.

Pressure Staging and Injector Pressure Drops

To move propellant through the engine and ensure stable combustion, the cycle has a series of different pressure levels. Each step of the flow, from tanks, through pumps, preburners, turbines, and into the main chamber, has carefully managed pressures to overcome losses and drive flow. A key principle is that propellants must be injected from a higher pressure environment into a lower pressure combustion chamber. The injectors cause a deliberate pressure drop to atomize and mix propellants. The pressure upstream of an injector must be a certain factor higher than the pressure in the combustion space it feeds, the pressure drop is present"with the aim to establish sufficient decoupling between oscillations in the combustion chamber pressure and the propellant supply pressures in the feed lines to the injector head." [6] For staged-combustion, a high injector pressure drop imposes a more stringent requirement on the turbomachinery, as there is a need for a higher supply pressure. A typical injector pressure drop is between 15-30%, and higher mass flow and pressure allow for a lower injector pressure drop. [7][48, 49, 121]

Starting from the propellant tanks, heres how pressures rise and fall through the system:

- Propellant Tanks: Both the oxidizer and fuel have a storage pressure that is sufficient to supply the engine with a pressure of around 4 bar. This is far below the operating pressure of the engine, so each propellant needs significant pumping.
- Pump Discharge: Each turbopump boosts the propellant to a high pressure to meet the needs of the cycle. Both turbopumps might raise the pressure to the high hundreds of bar. These high pressures are required to overcome downstream drops.
- Fuel Regenerative Cooling: Before entering the fuel preburner, the fuel is often sent through a cooling jacket around the main chamber and nozzle. This cooling circuit causes a substantial pressure drop in the fuel line.
- Preburner Injector Pressure Drop: The propellants flow into the preburners through injectors, which require a higher supply pressure equal to the preburner pressure times the percentual injector pressure drop.
- Preburner Combustion Chambers: Inside each preburner, partial combustion raises the temperature. The pressures in the fuel preburner and oxidizer preburner are designed to be high because they feed the turbines and ultimately must supply the main chamber. After the preburners, the hot gases expand through turbines, causing another pressure drop. [104]
- Turbine Outlet Pressure: After doing work in the turbines, the gases exhaust at a lower pressure which is set to feed the main combustion chamber injectors. This pressure is thus equal to the

[6] Personal correspondence with Dirk Greuel
[7] personal correspondence with Dirk Greuel

chamber pressure times the drop factor of the injectors, minus some small losses in-between turbine exit and injector inlet. Example: if the injector pressure drop is the same for both the oxidizer-rich gas and the fuel-rich gas, the turbine outlet pressures are the same, not considering any losses inbetween the outlet and injector.

- Main Chamber Injector Drop: Finally, the mixed fuel-rich and oxygen-rich gases are injected into the main combustion chamber. In the chamber, the remaining propellants react completely at a defined pressure, generating high-temperature, high-pressure combustion products that then expand out of the nozzle to produce thrust.

Pump Outlet Pressure and Power Requirements

Achieving the high pressures in this cycle requires very powerful pumps. The pump outlet pressure must be high enough to supply the preburners after accounting for all losses (injector drops and, for the fuel, cooling losses). Raising a fluids pressure to such high levels requires a large energy input per unit mass. This is usually shown via a pressure head (ΔH) or equivalently the pump specific work. For example, using the guesstimates of SpaceX's Raptor performance provided by [107] and [56], pumping liquid oxygen from 3 bar to 633 bar corresponds to a pressure increase of 630 bar. In terms of energy per kilogram, that is enormous. For LOX, the required head is in the order of 5.6×10^3 m. In other words, the pump must impart enough energy on each kg of LOX as if lifting it 5+ kilometres upward. For the methane, using the numbers of LOX, the pressure rise is even larger (an 640 bar increase), and liquid methane is less dense, resulting in a head of about 1.55×10^4 m (over 15 km). These figures illustrate just how much work the pumps must impart on the propellants. [64]

Turbine Pressure Ratios and Expansion

After the preburners, the hot propellant gases expand through turbine wheels, converting pressure and thermal energy into mechanical work. A critical parameter here is the turbine pressure ratio (TPR), which describes how much the gas pressure drops across the turbine. Because the inlet pressure is much higher than the exhaust, this ratio is a number less than 1 (P_{exit} / P_{inlet}). Sometimes engineers refer to the inverse as the expansion ratio; but in any case, the concept is how aggressively the turbine expands.[8]

In the example that is being covered, both turbines need to expand their gas from the preburner pressure to the post-turbine pressure, both of which are equal to each other if the injector pressure drops into the main combustion chamber are the same. The result is that the fuel-side turbine pressure ratio (TPR_f) and oxidizer-side turbine pressure ratio (TPR_o) are equal in this case. This is an interesting consequence: if all injector pressure ratios are identical, the two turbine pressure ratios will track one another closely or even match. Its important to note that the oxidizer pumps required outlet pressure is actually dictated by the fuel side of the cycle. The oxidizer pump must feed both the oxidizer-rich preburner and supply oxidizer to the fuel-rich preburner. In practice, this means the oxidizer pump outlet pressure is set to equal the fuel line pressure after cooling, if the injector pressure drops are equal for fuel and oxidizer, so that oxidizer can be injected into the fuel preburner at the same pressure. As a consequence, the oxygen-rich preburners inlet pressure is tied to the fuel turbines pressure ratio solution. [46]

Turbine Inlet Temperatures and Thermal Balance

Once the hot gases enter the turbine, some of their energy is extracted as work. The drop in gas enthalpy across the turbine equals the mechanical work required by the pump (plus allowances for efficiency). In practical terms, the gas cools down by a certain amount as it expands through the turbine. How much it cools depends on how much energy must be taken out, and on the gass heat capacity.

For the oxidizer turbine, the gas has a relatively lower heat capacity. To supply the massive amount of power needed by the oxidizer pump, the oxygen-rich gas has to surrender a certain amount of energy per kilogram. This translates to a temperature drop, which corresponds to the required enthalpy extraction (when multiplied by the mass flow and specific heat of the gas). The fact that the turbine has an efficiency of less than 1 means the ideal isentropic drop would be a bit larger, but in reality the gas

[8] Personal correspondence with Dirk Greuel

doesnt cool quite as much because not all heat is converted to shaft work. Some remains as additional entropy/thermal energy in the exhaust.

On the fuel turbine side, the situation differs because the gas has a much higher heat capacity. The fuel-rich preburner gas contains a lot of unburned fuel and partially burned species, which can absorb and release a lot of heat for a given temperature change. This high c_p means that to extract the power needed for the fuel pump, the required temperature drop is smaller (if c_p is 4x bigger and the mass flow is less than 4x smaller, this is the case). The energy associated with this temperature drop is enough to drive the pump. The turbine efficiency is accounted for as well, meaning the actual drop is a bit more than the ideal needed.

Lastly, a fundamental requirement of any staged combustion engine is that the power extracted by the turbines equals the power needed by the pumps, keeping into account any efficiencies. Its crucial that these balances close, otherwise the engine wouldnt operate in a steady state: if a turbine produced too little power, the pump couldnt maintain pressure, or if it produced too much, the shaft would overspeed.

The architecture and flow logic presented above is simplified. There are a lot of different architectures possible for staged combustion engines, ranging from a dual-turbopump structure (first low-pressure and then high-pressure, so a staged pressure rise) to multiple combustion chambers, a dual-shaft system with two fuel-rich or two oxygen-rich preburners, and single shaft systems like typical oxidizer-rich and fuel-rich staged combustion engines. The SSME shown in Figure 2.15 for example has two fuel-rich preburners, driving the turbopumps with two turbines, thus both turbines drive one turbopump (dual-shaft). This is different from Figure 2.12, where a single turbine runs both turbopumps.

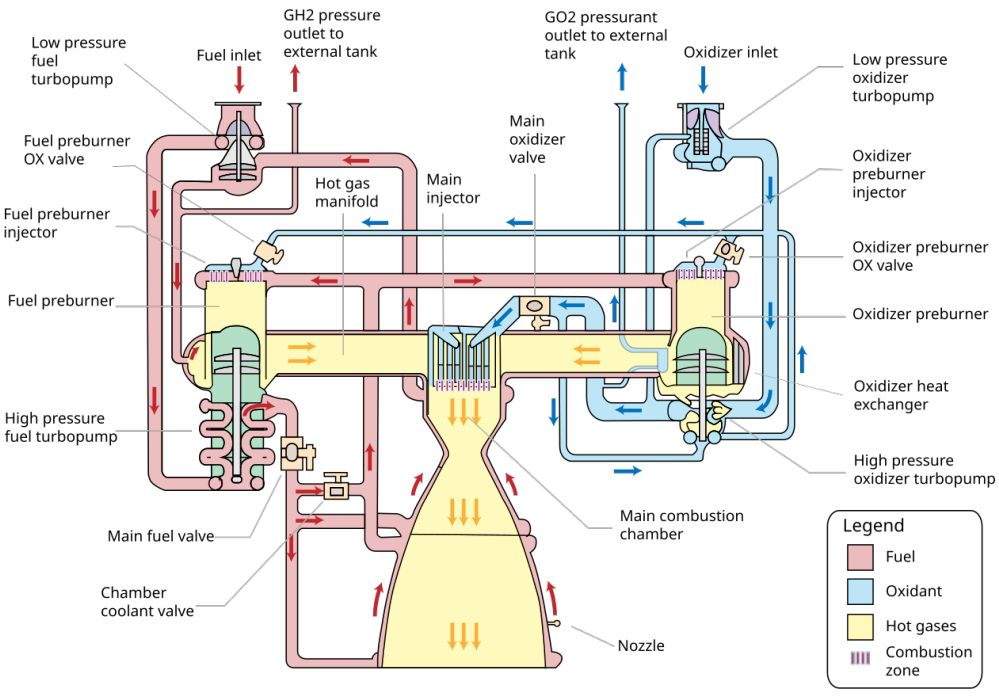

Figure 2.15: Schematic of the Space Shuttle Main Engine flow logic [55]

The engines considered in this thesis are fuel-rich or oxidizer-rich staged combustion engines, with a single preburner, single turbine and thus also a single shaft. This means, as also shown in Figure 2.12 and Figure 2.13, there is cross flow of the propellants, but this is limited to either the regeneratively cooled fuel (fuel that was used for regenerative cooling) being injected into the main chamber directly, with a small fraction going to the oxidizer-rich preburner, or most oxidizer is directly injected in the

main combustion chamber with the regeneratively cooled fuel partially combusted by the cross flown oxidizer.

2.4. AI and Automation

If there's one incontrovertible truth, it's that rocket testing remains, even in a world where AI and computers can make life significantly simpler, fundamentally an empirical endeavour. It's always the engineer with some twenty years of experience who defines a rocket engine's true limits, not the computer. Just because this has been the way to do it for the past 99 years, when Goddard launched the first liquid-fuelled rocket on March 16th 1926, does not mean that it should stay that way. The fact that redlines are set based on experience, and not by combining experience with computer models, just means the models are not good enough. There is significant improvement to be made in this respect, especially on the side of the engine developer. From the test bench perspective, a lot of effort is already being but in automation of testing. Most of the logic regarding valve sequencing, pressurisation and automatic aborts have been controlled routines for years. Countdowns, chill-down sequences and shutdown when a redline violation occurs are all handled without the test controller having to push a button. In this section, possible improvements to a test bench with regard to automation and applications of artificial intelligence are discussed.

2.4.1. Tasks of Test Bench

Within the automation and AI applications that can be used on a test rig, it is important to divide the tasks between operator and customer. Anything happening on the engine development side is part of the responsibilities of the customer, while the operator is responsible for the rig configuration, propellant supply and data delivery. Within the data delivery, there is the possibility to deliver raw data, or sometimes the customer doesn't know how to handle the raw data, and ask the test provider to process the raw data before delivery. Applications of AI and automation, considering a test bench that should be cheap, are limited to automating the bench operations, thus not including any post-processing of the data, as this would imply extra costs on the workforce. Within this space, the LUMEN project of DLR is the absolute best in Europe at implementing novel techniques around monitoring and control systems for engines. The demonstrator is designed for optimised operations on a test bench without restrictions on installation space or weight. Because of the design, LUMEN can offer a more in-depth view of the operating behaviour of a rocket engine than would be possible in real rocket engines. [16][114]

This is a point where it is very important to distinguish between a commercially operated bench, and an in-house bench of a company developing a propulsion system. As a company establishes redlines for components for a test bench operator, the incentive to innovate on advanced monitoring software that can predict anomalies rather than observe them is taken away. This is because commercial test providers operate within fixed service-level agreements that prioritize uninterrupted throughput and strict adherence to customer-defined redlines. Any predictive monitoring that might abort a test or trigger additional hardware inspections translates directly into schedule delays. By contrast, a company-owned development bench treats unscheduled shutdowns as valuable data for model refinement and anomaly characterization. In that context, early warning and adaptive control are embraced as mechanisms to accelerate learning and reduce overall development risk, rather than avoided to protect revenue. Consequently, commercial benches tend to default to reactive, threshold-based alarms, while in-house benches would deploy proactive, AI-driven prognostics. This is something that could easily be changed if the rocket engine testing market was a competitive market, *or* if a bench comes on the market that is significantly cheaper than competitors.

2.4.2. AI-Driven Anomaly Detection

A commercial bench has a unique advantage over a bench owned by a company developing an engine: the opportunity to test different engines created by different manufacturers. By using AI, unforeseen evolutions in vibrations or any other area can be spotted before a redline is crossed, allowing for a shutdown. This could result in the avoidance of possible prolonging of the test campaign because of a failure. To be able to detect this, the AI can be trained on previous test data. Different models that could be used for this are listed below. It is important to note that to optimise detection, they should be used in conjunction. [117]

A **LSTM-Autoencoder** learns to reconstruct fixed-length sequences of multivariate sensor readings. Anomaly scores derive from reconstruction error exceeding a predefined threshold [63][17]. **Variational Autoencoder (VAE)** maps high-frequency multivariate inputs, like vibrations, to a Gaussian latent distribution of healthy operation. During a burn, each window's approximate posterior likelihood is evaluated on an edge GPU; likelihoods below a preset percentile indicate off-nominal behaviour. The control logic then records a high-resolution pre-abort buffer and commands safe-state transition, preserving data for analysis after the burn [89][100]. **Isolation Forest & One-Class SVM** are unsupervised methods operating on engineered features to isolate outliers [105]. A **CNN-LSTM Hybrid** has 1D convolutional layers that extract local spectral or vibrational patterns, feeding into LSTM units for long-range temporal context [122]. Lastly, a **Transformer-Based Anomaly Detector** analyses multivariate time-series data to produce anomaly scores, and is able to detect both local and long range dependencies in the data [32]. This allows for early and subtle detection of anomalies in a high-noise environment.

Implications

Implementing AI models on either the engine side, the bench side, or both, can have significant implications on the setup of future test campaigns. A simulation model of a bench can be used to generate synthetic data, which can in turn be used to train neural networks. These can serve as a baseline that can be iterated on, where complex effects can be added later on [20]. The application of the aforementioned models is not only meant to make testing safe. By early detection of anomalies in the operations, or by being able to predict behaviour before even testing (synthetic data and old data), test campaigns can be adapted and possibly shortened. The test campaign becomes a feedback-driven process rather than a fixed sequence of burns, for which the redlines have been established in a very long and labour-intensive process.

In an ideal scenario, each burn's outcome informs not only the immediate next test point, but also dynamically adjusts the underlying virtual model. As anomalies are flagged, the digital twin is recalibrated using both the fresh hot-fire data and targeted synthetic adjustments. This means that subsequent synthetic datasets more closely mirror the real engine behaviour. Such a system can enforce a dual-loop control: an inner loop that reacts in milliseconds to preserve hardware health, and an outer loop that retunes both the AI thresholds and the campaign plan. Rather than pre-defining a dozen intermediary thrust levels, the operator lets the AI optimize the intermediate steps. The result is fewer burns, each more information-rich, and an overall campaign timeline shortened. Not only does it shorten the test campaign, it also makes it cheaper, as fewer test days and propellants are needed. [9] This, in turn, affects the rigour of rocket engine testing campaigns. As mentioned in chapter 2, a test campaign is usually predefined, the duration contractually fixed, and the operator has other companies waiting to test after the campaign is finished. In order for these dynamic redlines to shorten testing campaigns, it is necessary to reassess the processes surrounding these test campaigns. Otherwise, rapid iteration does not pay off.

2.5. Conclusions

This review narrows the problem to a European, sea-level bench for 2 MN staged-combustion engines and makes two things explicit. Firstly, the public record is thin precisely where feasibility and cost cross each other: propellant supply, pressurisation, exhaust handling, water systems, and MCC. Secondly 'state-of-the-art' sources skew to sub-scale (student) rigs and are therefore poor design templates for a high-cadence, high-thrust, low-cost bench. Since the literature does not provide concrete know-how, contemporary practice and industry professional input are used as architectural references, with McGregor's horizontal test bench serving to illustrate modular horizontal installation, fast turnaround, and very cheap infrastructure. The PBS and operations sections fix the work breakdown and information flows that a commercial bench must support, and the combustion-cycle discussion provides insight into the engine-side interfaces that drive facility pressures and flows. These findings now translate directly into the next phase: a requirements set that prioritises SC-compatibility, high-thrust fluid supply, and economic viability. A fluid-supply architecture sized from engine demand with regulated run-tanks;

[9] Personal correspondence with Daniel Chipping

a cost-model framework mapped to key PBS items; and a RAMS/FMECA baseline that targets the high-criticality items first. The thesis plan that follows maps these into sizing, siting, and cost.

3

Research Proposal

This chapter describes the research proposal for this thesis. First, the problem statement is laid out, after which the objectives of the thesis are stated. From these objectives, research questions are drafted, for which hypotheses are stated. Finally, the initial thesis timeline is presented.

3.1. Problem Statement

Europe currently lacks an affordable, high-capacity sea-level facility for full-scale staged-combustion engine testing. Existing benches in Europe are either not configured for high-thrust staged-combustion or are financially unattractive for programmes of New Space companies. Adaptions of legacy infrastructure for new engines, like the implementation of a new propellant capability at an existing large test bench at DLR Lampoldshausen, are in themselves heavy projects, illustrating the schedule and cost penalties that arise when facilities are not designed for this purpose from the beginning.

In the public domain, there is little design-level guidance for large test benches. Cost and availability figures are confidential, and the most consequential subsystems for feasibility, like propellant supply, pressurisation, exhaust and water systems, are rarely treated with engineering detail. As a result, agencies and companies cannot trace design choices to performance, cadence and cost with confidence in a European context.

This thesis therefore addresses the concrete need for a cheap, high-thrust propulsion test bench in Europe. The benchmark is a commercially operated facility where industry requirements lead. In practice, this means:

- capability for long test durations with stable engine-interface conditions across the staged-combustion envelope;
- low cost per hot-fire minute through simple civil works, modular utilities and site selection that favours affordable operations;
- high test cadence supported by infrastructure decisions.

The problem addressed in this work is to define a Europe-aware, high-level design for such a facility and to show, with quantified trade-offs, how the proposed architecture can meet the capability targets in chapter 4 while reducing expected cost and time to operate at scale. In order to achieve this objective, this thesis involves:

- Discussion with ESA experts and where appropriate industry specialists on the requirements (key characteristics) of a potential high-thrust test stand - both technical (propellant type, mass flow rate, thrust rating) and programmatic (capital expenditure, running costs).
- Scouting for innovative technologies of interest along with potential providers.

- Initial concept of the test bench (components, lay-out, etc.), including where applicable innovative technologies (AI and Automation) to reduce production and operation costs.
- Initial safety / RAMS analysis of operation, identification of critical items (After layout is defined).
- If relevant, and as a second option compared to a new test bench, identification of adaptions to an existing test bench.
- Scout for possible bench locations.
- Initial operations plan including estimate of work force.
- Initial cost estimate for (1) Bench Development; (2) Bench operation (cost for customers); (3) Yearly costs. Identification of the main bench requirements that drive the cost of development and operation.
- Outline of a potential 'business plan' for a bench operator.

3.2. Research Questions

The research questions are divided in two categories. One is the questions that were already posed before the literature review and have been answered by the literature review, and the other is the questions that the literature review and the problem statement together result in. As can be seen, some research questions have been struck through. These were research questions posed by ESA that have been discarded. A rationale is provided. First, the main research question is the following:

> *What high-level architecture and configuration of a sea-level propulsion test bench best enables routine hot-fire testing of 2 MN staged-combustion engines in Europe, while remaining economically viable under realistic utilisation?*

The subquestions used to answer this question are the following, divided over the two categories that were mentioned in the introduction of the section.

1. What innovative technologies (AI, automation, smart sensors, materials) are relevant to test bench efficiency or safety?
    - This is answered in section 2.4.
2. How can innovative technologies reduce production costs and operational costs?
    - This is answered in section 2.4.
3. What are the workforce and operational logistics required for routine testing?
    - This is answered in section 2.2.

These are the research questions that will be addressed in the rest of the thesis:

1. How do the specific characteristics of high-thrust staged combustion engines influence the design?
2. What location for a bench is both feasible and cost-effective?
3. What are the critical technical and programmatic requirements for a 2 MN staged combustion engine test bench?
4. What are the RAMS and safety implications of testing high-chamber-pressure engines?
5. What are the key cost drivers of test bench development and operation?
6. What are benchmark costs from similar facilities globally, and how would this bench compare?
7. What could a viable business model for operating the bench look like?
8. ~~Which existing ESA or commercial facilities could be adapted to support such tests?~~
    - This is confidential.
9. ~~What component layout best supports safety, accessibility, and measurement accuracy?~~
    - As measurements are not something that is investigated in this thesis, nor is the structure, the layout of the components is outside of the scope.
10. ~~Who are the potential suppliers and technology partners?~~

- This is a question that is answered internally, but it does not provide any value for the thesis.

3.3. Hypotheses

1. High-thrust staged combustion engines (2 MN) have extreme chamber pressures and thermal loads. The test cell or clearance (if no test cell is used) will have to account for this. Furthermore, the high thrust imposes an extreme requirement on the mass flow, and thus the storage capability and piping of the test facility.
2. Eastern European countries have lower wages than the countries where rocket engines are being developed. Countries in this area with relatively low population density areas and good infrastructure are possibly good contenders.
3. Besides customer requirements, that still have to be refined based on the initial research done, the requirements that follow from the thrust level and type of engine are critical for the design. Programmatically, the site selection is probably of the largest influence, as well as typical propulsion test bench operations.
4. A rigorous RAMS strategy, using real-time monitoring and fault detection, is essential to manage the risks of high chamber pressure, high mass flow testing.
5. Structural reinforcements, advanced cryogenic systems, and staff cost will be the primary cost drivers.
6. The bench should be significantly cheaper than benches that are currently capable of testing engines of that thrust level.
7. The bench can be used for purposes of the company that funded it, offering the possibility for other companies to test on the bench as well (if said company is an industry player). The financial gain to be made by the funding party can be focused on earning back the original investment, or a scheme can be thought of that saves on the own testing costs of the funding company.

3.4. Timeline

Table 3.1: Thesis Timeline

Time Period	Tasks
Weeks 7–10 (Early April – Early May)	**Requirement Refinement & Site Selection Trade-Off** • Refine technical and programmatic requirements in collaboration with ESA/industry experts. • Perform a trade-off for site selection, following system engineering principles **Preliminary Safety & RAMS Considerations** • Begin a high-level safety analysis focusing on high-chamber-pressure operation. • Identify critical items for deeper study in later weeks. **Initial System Architecture** • Sketch major subsystems (propellant feed, thrust frame, measurement layout, etc.). • Identify potential integration of innovative technologies (automation, AI-driven data analysis).

Table 3.1 – Continued from previous page

Time Period	Tasks
Weeks 11–15 (Early May – Early June)	**Preliminary Conceptual Design** • Develop a first-pass layout for the test bench, including major components, piping, and instrumentation. • Incorporate design decisions (e.g., modular construction, dedicated safety systems). **Cost and Operational Analysis (Initial)** • Identify main cost drivers (propellant logistics, staff cost, cooling capacity). • Draft an outline of the business model, including potential revenue streams and target market segments. **Prepare for Mid-Term Review** • Compile progress: highlight design concepts, preliminary safety findings, and updated cost estimates.
Mid-Term Review (04 June, Week 16)	• Present the design concept, preliminary cost and safety findings, and updated research plan to the committee. • Gather feedback and agree on adjustments or additional analyses.
Weeks 17–25 (June – Late July)	**Refinement of Design & Safety Analysis** • Incorporate feedback on design aspects, safety, and cost assumptions. • Expand the RAMS analysis (Reliability, Availability, Maintainability, Safety), focusing on test operations at 2 MN thrust. **Technology Scouting** • Investigate feasibility of integrating advanced diagnostics, automation tools, and data-driven control systems. **Operations Plan & Workforce Considerations** • Detail operational flow. • Define any specific training or skill sets needed.
Weeks 26–28 (06 Aug – 27 Aug)	**Holidays (3 weeks).** Minimal or no thesis work unless specifically arranged.
Weeks 29–30 (Late Aug – Early Sep)	**Pre-Finalisation Sprint** • Re-check final details before the Green Light Review. • Complete any outstanding design or feasibility tasks paused during the holiday. • Finalise draft chapters for design, cost analysis, and safety.
Green Light Review (10 Oct, Week 30)	• Present near-final concept, safety analysis, cost model, and operations/business plan. • If approved, proceed to finalise the thesis document.
Weeks 34–37 (Mid to Late Oct)	**Final Thesis Preparation and Hand-In** • Incorporate last feedback from the Green Light Review. • Polish all chapters (summary, technical details, cost/operations, references, consistency). • Submit thesis by the expected hand-in date (03/11/2025).
Weeks 38–39 (Early to Mid Nov)	**Thesis Defence Preparation** • Prepare presentation materials, rehearse defence, address final remarks from the committee. • Officially present and defend the thesis results (17/11/2025).

The Gantt chart presented in Appendix A shows the detailed project planning.

4

Requirements

From the problem statement, a clear objective is to specify, at system level, the capability envelope and programme constraints of a commercially operated, sea-level test bench for full-scale staged-combustion engines.

The requirements were compiled and refined from three complementary sources:

1. Stakeholder input from prospective users and facility operators, gathered via correspondence [1].
2. A literature and benchmarking review of public information on engine cycles, facility capabilities, and operating constraints.
3. Business-case drivers developed in this thesis, like capital cost targets and utilisation.

Because detailed facility data in Europe are often confidential, stakeholder inputs were normalised to public, checkable quantities and ranges of values. This chapter summarises all top-level customer requirements. Their labels will be used throughout this report for reference purposes. Each requirement includes a short rationale, notes on related challenges, and an intended verification method (*Analysis*, *Review*, or *Demonstration*).

[1] Personal correspondence with Kate Underhill

4.1. Customer Requirements

Table 4.1: Customer Requirements

ID	Type	Requirement
CR-1	Thrust capacity	The test stand shall accommodate rocket engines providing a nominal thrust of 2 MN at sea-level.
CR-2	Engine cycle compatibility	The test stand shall support FFSC, ORSC, and FRSC rocket engine cycles.
CR-2.1	Propellant storage	The test stand shall incorporate low-pressure propellant tanks, with nominal tank pressures between 5 - 20 bar.
CR-2.2	Propellants	The test stand shall support testing of methalox and hydrolox engines.
CR-3	Cost	The test stand capital expenditure cost shall not exceed €150 million.
CR-3.1	Orientation	The test stand shall allow for safe installation and operation of test articles in horizontal configurations.
CR-4	Modular	The test stand shall be designed so that it can be used by different engines with minimal adaptations.
CR-5	Test duration	The test stand shall enable continuous hot-fire test durations of at least 600 s.
CR-6	Combustion pressure rating	The test stand shall safely support rocket engine operation at chamber pressures ranging from 150 bar up to 300 bar.
CR-7	Full-engine testing	The test stand shall accommodate full-scale liquid rocket engine tests without requiring partial or sub-scale hardware.
CR-8	Schedule	The test stand shall be fully operational no later than 36 months from the start of the creation of the design.

Detailed Description of Customer Requirements

ID	Type	Requirement
CR-1	Thrust capacity	The test stand shall accommodate rocket engines providing a nominal thrust of 2 MN at sea-level.

Rationale for CR-1

A 2 MN capability ensures compatibility with the staged-combustion engines that will be developed in the coming decade(s) in Europe.

Comments on related challenges

The fluid system needs to be compatible with a range of engines with different thrust levels and efficiency.

Validation method

Analysis

ID	Type	Requirement
CR-2	Engine cycle compatibility	The test stand shall support FFSC, ORSC, and FRSC rocket engine cycles.

Rationale for CR-2

Ensures the stand can test full-flow, oxidizer-rich and fuel-rich staged-combustion cycles, which will be the dominant configuration in next-generation engines.

Comments on related challenges

Safety considerations should take into account that staged combustion, and especially full-flow, involves very high pressures. Furthermore, as these engine cycles have high temperature gas flowing through the turbine(s), catastrophic failure of the turbines is a risk. Instrumentation should be placed and adjusted according to this higher complexity. The fluid supply system has to be sized for a reasonable range of possible engines.

Validation method

Analysis

ID	Type	Requirement
CR-2.1	Propellant storage	The test stand shall incorporate low-pressure propellant tanks, with nominal tank pressures between 5 - 20 bar.

Rationale for CR-2.1

As the cycles being tested on the bench are pump-fed, rather than pressure-fed, and the bench tests only full engines (CR-8), the pressure of the propellant should be between 5 and 20 bar, as the typical pressure being fed into the engine is 4 bar.

Comments on related challenges

Sizing the tanks to provide required run time while maintaining the pressure limit. The pressurisation infrastructure has to maintain the pressure when running, and the pressure has to be sufficiently high to maintain the mass flow.

Validation method

Analysis

ID	Type	Requirement
CR-2.2	Propellants	The test stand shall support testing of methalox and hydrolox engines.

Rationale for CR-2.2

CH_4/LOX and H_2/LOX are the main propellants considered for staged combustion engines, keeping in mind reusability of the engine. Methalox is more common, because hydrolox is more difficult to handle.

Comments on related challenges

Cryogenic handling (insulation, boil-off management) is required for both LOX/CH_4 and LOX/H_2 systems. Different pressurisation infrastructure is required for both, as well as different venting systems.

Validation method

Ideally, demonstration of boil-off control and temperature maintenance during the run. Within the scope of this thesis, demonstration by designing for it. Analysis

ID	Type	Requirement
CR-3	Cost	The test stand capital expenditure cost shall not exceed €150 million.

Rationale for CR-3

This is the most important requirement by the customer. The solution should be cheap to build, because current estimates on what high-thrust benches would cost are (too) expensive [2]. The cost of benches across the world is laid out in Table 7.1. The cost should not be too high, because it should be an interesting investment. What is being investigated here is a *commercial* test bench, thus the investors have to earn their money back within a reasonable horizon.

[2]Personal correspondence with Jean-Noel Caruana

Comments on related challenges

Selecting a country to build the bench, and finding public data to build a cost model from.

Validation method

Review/Analysis

ID	Type	Requirement
CR-3.1	Orientation	The test stand shall allow for safe installation and operation of test articles in horizontal configurations.

Rationale for CR-3.1

Horizontal mounting simplifies plumbing and exhaust management for large engines. It is also significantly cheaper than vertical testing, when the scale is considered. That is why it is a child of CR-3.

Comments on related challenges

Ensuring proper support for different engine geometries when mounted horizontally.

Validation method

Review/Analysis

ID	Type	Requirement
CR-4	Modular	The test stand shall be designed so that it can be used by different engines with minimal adaptations.

Rationale for CR-4

Reduces downtime and tooling cost when switching between engine types. The adaptations of current test benches is a costly and time-intensive endeavour.

Comments on related challenges

Requires a flexible mounting interface and quick-change connectors.

Validation method

Review/Analysis

ID	Type	Requirement
CR-5	Test duration	The test stand shall enable continuous hot-fire test durations of 600 s.

Rationale for CR-5

Long burns are required to characterise thermal and performance stability under steady-state conditions. Some current engines burn for such a long duration. As an example, Vulcain burns for 605 seconds when it is fired on Ariane 5 or 6 [9]. Industry wants to be able to test their engines for that duration, even though it might be fired for less time when launching their rockets.

Comments on related challenges

Thermal protection and cooling systems must handle prolonged heat loads without degradation. The propellant tanks must be designed to hold enough propellant to support a burn time of this magnitude, and the pressurisation system should be designed to manage this.

Validation method

Review/Analysis

ID	Type	Requirement
CR-6	Combustion pressure rating	The test stand shall safely support rocket engine operation at chamber pressures ranging from 100 bar up to 300 bar.

Rationale for CR-6

These combustion pressures are not achieved in European (staged combustion) engines yet, but are within a range of values that is to be expected of staged combustion engines in development. Chamber pressure is an engine-internal parameter. The bench must accommodate the *consequences* of operating in this envelope: thrust-reaction loads, exhaust thermal and acoustic loads, and instrumentation/data-handling ranges.

Comments on related challenges

Sizing the thrust structure and load distribution.

Validation method

Analysis and review

ID	Type	Requirement
CR-7	Full-engine testing	The test stand shall accommodate full-scale liquid rocket engine tests without requiring partial or sub-scale hardware.

Rationale for CR-7

Avoids the complexity and cost of designing separate sub-scale test rigs.

Comments on related challenges

The envelope, thrust structure, and support systems must be sized for the largest engine expected.

Validation method

Analysis

ID	Type	Requirement
CR-8	Schedule	The test stand shall be fully operational no later than 36 months from the start of the creation of the design.

Rationale for CR-8

Aligns final commissioning with programmatic timelines and engine development schedules.

Comments on related challenges

Requires strict project management, early risk mitigation, and phased procurement.

Validation method

Review

5

Fluid Supply System

To test an engine with a thrust of 2 MN for ten minutes, the volume of a little bit less than half an Olympic swimming pool of liquid hydrogen is necessary in the tanks[1]. This provides an insight in the extreme needs of rocket engine testing. The comparison is instructive: the fluid supply system is a primary driver of bench layout, safety zoning, cost, and operability.

The fluid supply system determines whether the bench can run representative tests safely and repeatably. In this chapter, the run tanks, pressurisation, and feed lines are sized for engines in the 2 MN class, with an explicit focus on mass flows and stable engine-interface pressure. The analysis is limited to sea-level testing and considers both methalox and hydrolox operation. First, performance points are generated with NASA CEA (via RocketCEA) to obtain specific impulse as a function of mixture ratio and chamber pressure. These results are translated into total, fuel, and oxidiser mass flows for a 600 s run, and then into liquid volumes using real-fluid densities from CoolProp. Ullage, stratification, and end-of-test residuals are added to derive tank geometric volumes. Next, pressurisation requirements (N_2 is used to pressurise LOX, He is used for LH_2 and LCH_4) are computed. Finally, pipe diameters are set by velocity limits, and a complete setup is built and simulated in EcosimPro. The result is a bench layout that can accommodate rocket engines, delivers $650\,\mathrm{kg\,s^{-1}}$ LOX at approximately 4 bar to the engine interface, and provides a clear basis for propellant operation and dual pressurisation.

5.1. Tank Sizing

To size the run tank, and assess the necessary capacity of the storage tanks, a method was established. Tanks are sized to the *worst credible mass-flow case*, which is the lowest plausible I_{sp} at the required thrust and sea-level pressure. In practice, this may occur with a conservatively tuned staged-combustion engine, like an ORSC engine at sea level with a non-optimal expansion ratio, rather than an FFSC operating at its typical higher P_c. According to the thrust equation,

$$F_t = \dot{m}\, I_{\mathrm{sp}}\, g_0,$$

an engine with higher I_{sp} produces the same thrust with less propellant mass flow. Therefore, the tanks are sized using the lowest I_{sp} scenario within the design envelope, ensuring the bench remains adequate for any staged-combustion variant without any works having to be performed.

5.1.1. Identification of Peak Operating Points

For each combination of chamber pressure P_c, mixture ratio O/F, nozzle expansion ratio ε, and propellant inlet temperatures (hot fuel/cold LOX for FRSC; cold fuel/hot LOX for ORSC), the NASA CEA (Chemical Equilibrium with Applications) program is used via the RocketCEA Python interface to compute the sea-level I_{sp} curve as a function of mixture ratio. CEA determines the equilibrium composition and thermodynamic properties of the combustion products by solving the chemical equilibrium

[1] Personal correspondence with Jörn Bellermann

and energy conservation equations. The peak I_{sp} and corresponding mixture ratio are extracted from the computed curve for each scenario. These curves are shown for a specific set of conditions, that is summed up in Table 5.1.

Table 5.1: Input parameters used to generate the I_{sp} vs. O/F curves

Parameter	Value(s)
Chamber pressure, P_c	100 bar, 150 bar, 200 bar
Nozzle expansion ratio, ε	20, 25, 30, 35, 40
CH_4 inlet temperature (FRSC, hot)	650 K, 700 K,750 K
LOX inlet temperature (FRSC, cold after pump)	90 K
CH_4 inlet temperature (ORSC, cold after regen)	250 K
LOX inlet temperature (ORSC, hot)	650 K, 700 K, 750 K
Mixture-ratio sweep, O/F	1.5 - 5.0
Typical NASA CEA offset, η	0.95
Ambient pressure for sea-level I_{sp}	1.01325 bar

The curves for cold LOX and hot CH_4 can be seen in Figure 5.1, and those for hot lox and cold CH_4 in Figure 5.2. The lowest inlet fuel temperature and the lowest pressure result in the lowest peak I_{sp}. An increase in temperature of the fuel and/or oxidizer, as well as an increase in pressure, results in a curve that is shifted upwards.

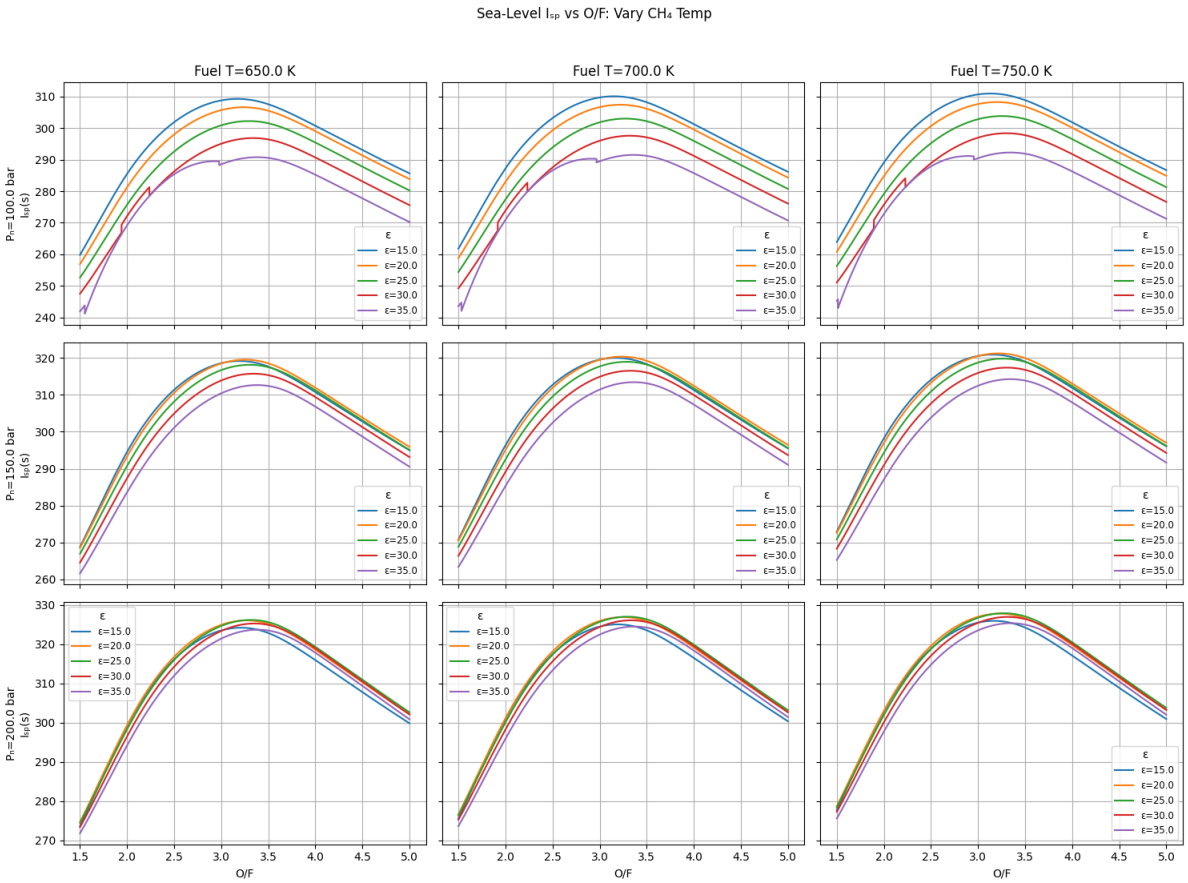

Figure 5.1: Sea-level specific impulse vs. mixture ratio for FRSC (hot CH_4, cold LOX) at various chamber pressures and nozzle expansion ratios.

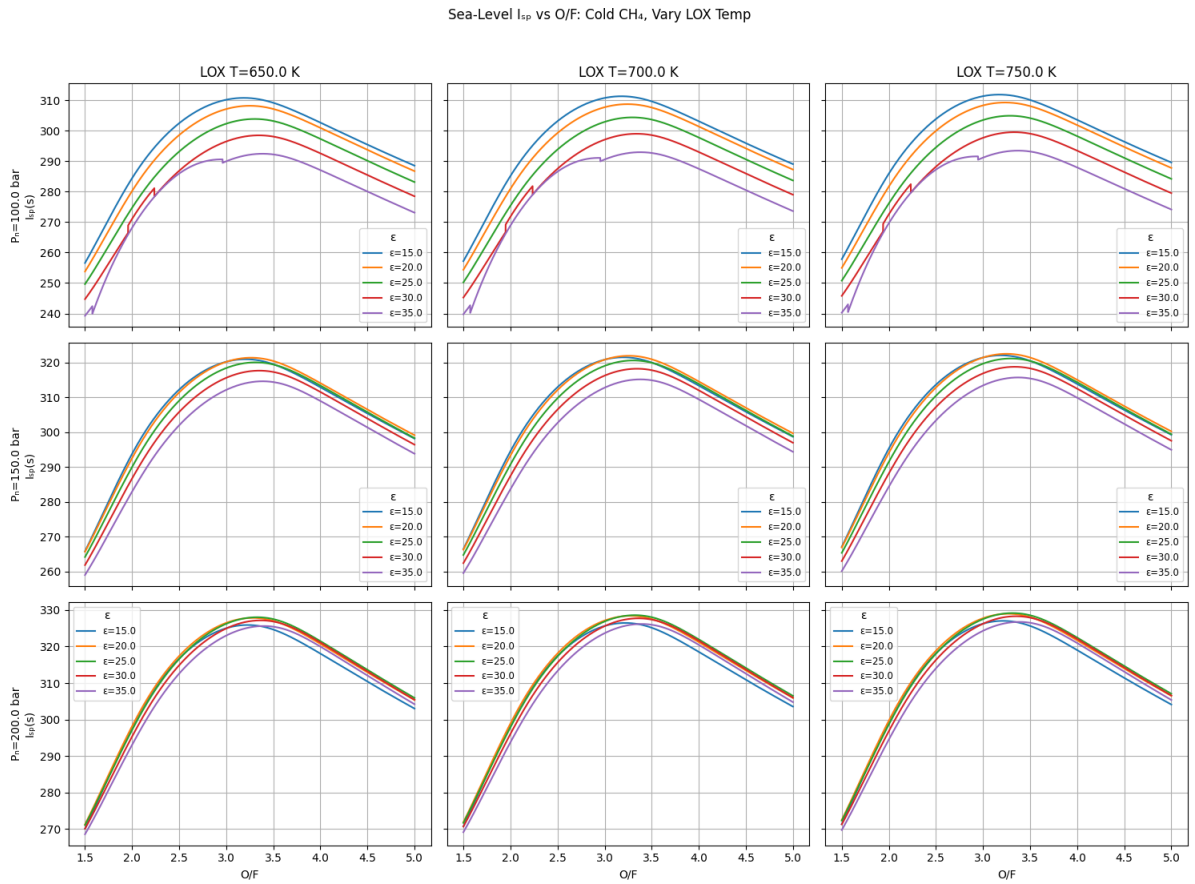

Figure 5.2: Sea-level specific impulse vs. mixture ratio for ORSC (cold CH_4, hot LOX) at various chamber pressures and nozzle expansion ratios.

There are a few considerations at play that have to be addressed:

- Firstly, the 'worst-case scenario' that is being considered here is testing an engine that is designed to deliver a thrust of 2.5 MN at *sea-level*, but that is not necessarily optimised for sea-level. The nozzle expansion ratio is bigger than ideal, because it should also perform well at higher altitudes. In Figure 5.1, it is clearly visible that an expansion ratio of 35 has the lowest I_{sp} peak. Because the mixture ratio used in current methalox engines is not public information, but rather based on guesstimates, the governing assumption in this analysis is that the engines are designed for the maximum I_{sp} they can achieve for their respective expansion ratios. An expansion ratio of 35 is, for a LOX/CH_4 engine, a reasonable worst-case estimate [11, 8, 73, 72]. For LOX/H_2, the range of engine expansion ratios is different, because hydrogen-oxygen combustion products have a much lower molecular weight and higher characteristic velocity than methane-oxygen. Their exhaust expands more rapidly and to a higher velocity, which means higher optimal expansion ratios.
- The code cannot model the fuel-rich, partially combusted mixture, or oxygen-rich mixture, that comes into the combustion chamber, nor the uneven propellant mixing by injectors. Instead, it assumes all propellants are burnt in the combustion chamber. As it assumes complete combustion, the modelling of the mixtures is not of importance. Since the engines considered are only staged combustion engines, in which all propellant that flows in also flows out, using this assumption is not very far from reality. As explained in [19], CEA's deviation from reality tends to decrease with increasing engine size, and to make sure that the engine is accurately represented, an efficiency factor of 0.95 was included, which covers the 5% overstatement of I_{sp} by CEA.
- The nozzle expansion ratios used result in small bumps that can be seen in Figure 5.1, in the 100 bar-case for an expansion ratio of 35. This means CEA reaches a certain state in which it switches polynomial to solve for the I_{sp} curve, later correcting itself. As the peak is still in the expected place, this behaviour is ignored.

- As the focus of future engines will be on reliability and re-use, the temperature range chosen was between 650 and 750 Kelvin. This was done, because limiting the temperature of the preburner exhaust benefits the lifetime of the turbine blades. Running a very fuel-rich LOX/CH_4 mixture, or a very oxygen-rich mixture, through the preburner ensures the temperature of the partially combusted end product is not too high for the turbine.

For LH_2/LOX, ambient pressure and the limited nozzle area ratio at sea level cause a proportionally larger reduction from vacuum I_{sp} than for methalox. While sea-level LH_2/LOX engines are viable and widely used, designs optimised solely for sea-level operation accept a relatively larger efficiency trade-off. This explains the use of moderate expansion at lift-off and very high expansion in upper-stage applications. Moreover, LH_2 significantly less dense than CH_4 (70 vs 422 kg/m^2), meaning very large storage tanks are required on the spacecraft. That is why rocket engines using hydrolox are not designed for the mixture ratio that maximises the specific impulse, which would be in the proximity of O/F = 3.3 - 4. Rather, the O/F-ratio is a trade-off between performance and storage volume, snowballing into vehicle mass and drag. For the sake of this thesis, a 2-MN sea-level engine for hydrolox will be considered. The input parameters are shown in Table 5.2. The logic for this is different from the LCH_4/LOX engine. Here, 'worst case' for tank and feed sizing is defined as the lowest plausible sea-level I_{sp} within the operating band. A broad sweep of $O/F = 3$–7 is used to map the trend, but modern hydrolox engines typically operate near $O/F \approx 6.0$ (about 5.9-6.1). For clarity, the maximum LH_2 mass flow would occur at the lower bound of this range $O/F = 5.9$. That case is not selected, because the current selection method with a range of high expansion ratio options is considered to be enough of a buffer to deal with any deviations. [112]

Table 5.2: Input parameters used to generate the H_2/LOX I_{sp} vs. O/F curves

Parameter	Value(s)
Chamber pressure, P_c	100 bar, 150 bar, 200 bar
Nozzle expansion ratio, ε	50, 55, 60, 65, 70
H_2 inlet temperature (FRSC, hot)	600 K, 650 K, 700 K
H_2 inlet temperature (FRSC, cold after regen)	250 K
LOX inlet temperature	90 K
Mixture-ratio sweep, O/F	3.0 - 7.0
Typical NASA CEA offset, η	0.95
Ambient pressure for sea-level I_{sp}	1.01325 bar

The results from this analysis are shown in Figure 5.3.

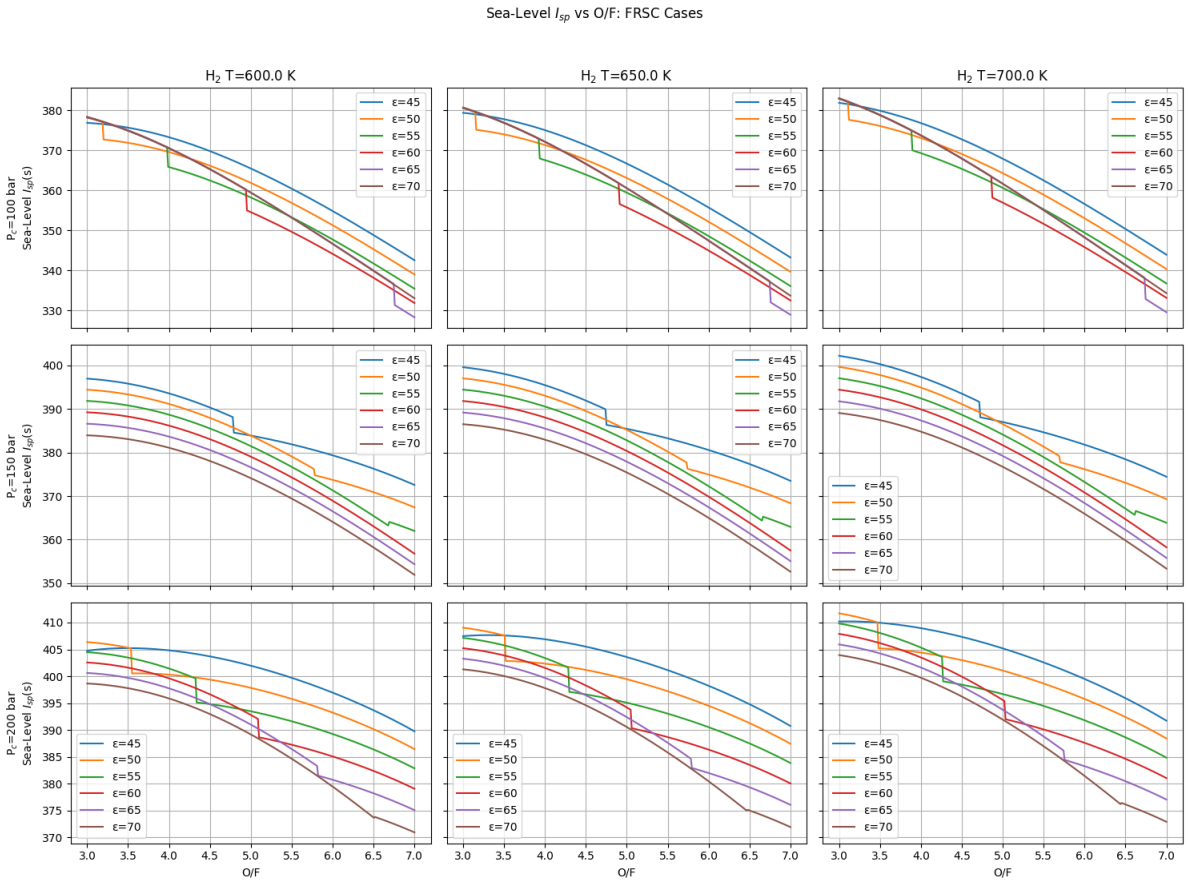

Figure 5.3: Sea-level specific impulse vs. mixture ratio for FRSC (hot H_2, cold LOX) at various chamber pressures and nozzle expansion ratios.

In the H_2/LOX ambient-I_{sp} sweeps a constant nozzle expansion ratio is specified, ϵ, but RocketCEA sometimes changes polynomial to solve for the I_{sp}, which was also seen in Figure 5.1 and Figure 5.2. This switch produces a small jump in a lot of I_{sp} vs O/F curves. [112]

5.1.2. Computation of Propellant Mass Flows and Worst-Case Selection

Once the peak performance point is known, the total propellant mass flow

$$\dot{m}_{\text{tot}} = \frac{F_t}{I_{\text{sp}}\, g_0}$$

is split into oxidizer and fuel flows according to the mixture ratio O/F:

$$\dot{m}_{\text{fuel}} = \frac{\dot{m}_{\text{tot}}}{1 + (\text{O/F})}, \quad \dot{m}_{\text{ox}} = \dot{m}_{\text{tot}} \frac{(\text{O/F})}{1 + (\text{O/F})}.$$

The scenario yielding the maximum $\dot{m}_{\text{fuel}}$ defines the worst-case CH_4 tank requirement, while the scenario with maximum $\dot{m}_{\text{ox}}$ defines the worst-case LOX tank requirement. Integration over the burn duration Δt_{burn} produces total propellant masses:

$$m_{\text{prop}} = \dot{m}_{\text{prop}}\, \Delta t_{\text{burn}}.$$

5.2. Conversion to Liquid Volumes Using CoolProp

The CoolProp library is used to obtain accurate liquid densities of methane and oxygen at typical tank conditions. CoolProp computes real-fluid properties from fundamental equations of state [5]. At 111

K and 4 bar, liquid CH_4 density is approximately 422 kg/m^3; at 90 K and 4 bar, liquid O_2 density is approximately 1140 kg/m^3. Propellant masses are converted to liquid volumes via

$$V_{\text{prop}} = \frac{m_{\text{prop}}}{\rho_{\text{prop}}}.$$

For the simulations using the parameters as laid out in Table 5.1, the graph is presented in Figure 5.4. Figure 5.4a shows the peak I_{sp} for each run, and the associated O/F ratio. Using the mass flow formulas presented in the previous section, this can be transformed into a graph showing the necessary volume per propellant. This is Figure 5.4b. This volume does not correspond to the volume of the tank, because it does not yet include the ullage volume, which is discussed in the next subsection.

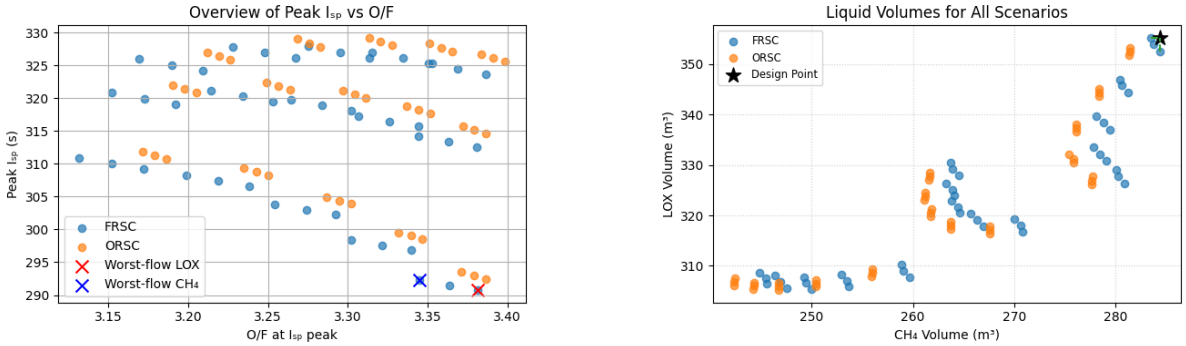

(a) Peak I_{sp} vs O/F ratio for all combinations

(b) Liquid volumes for LOX and CH_4

Figure 5.4: Liquid volume based on the input parameters

Table 5.3 presents the worst-flow scenarios for both CH_4 and LOX.

Table 5.3: Worst-case scenario results for CH_4 and LOX liquid volume in the FFSC engine at $P_c = 100$ bar, $T = 600$ K, and $\varepsilon = 35$.

Scenario	O/F	I_{sp} [s]	$\dot{m}_{CH_4}$ [kg/s]	$\dot{m}_{O_2}$ [kg/s]	Δt_{burn} [s]	V_{liquid} [m^3]
CH_4 worst-flow (FRSC)	3.345	292.27	200.75	-	600	284.36 (CH_4)
LOX worst-flow (FRSC)	3.381	290.78	-	676.60	600	355.21 (O_2)

The mass flow that can be seen in Table 5.3 for LOX is a reasonable estimate. Current industry wishes for LOX flow for high-thrust engines are centred around a LOX flow of approximately 650 kg/s. Moreover, rocket engine manufacturers would not fly an engine with an I_{sp} this low, but since there is no estimation available as to the minimum they would consider designing, the I_{sp} in the table is used. Lastly, the O/F ratio is on the low side, considering that methalox engines mixture ratios are usually in a range of 3.5 to 3.8. Once again, because the margin on the I_{sp} is considerable, this is ignored. The results for H_2 liquid volume are shown in Figure 5.5, with Table 5.4 showing the worst-case flow results for a hydrolox engine.

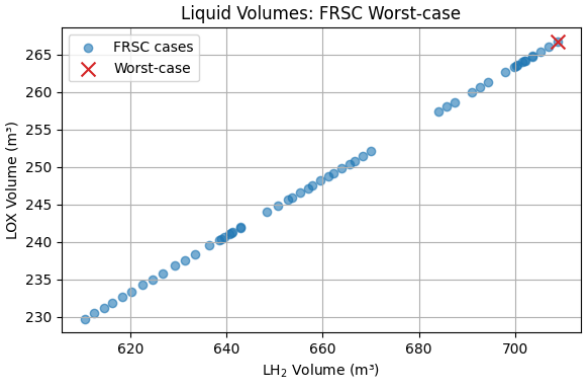

Figure 5.5: LH_2 vs LOX Liquid Volume Requirements for the FRSC Worst-Case Thrust Scenario

Table 5.4: FRSC worst-case results at $P_c = 100$ bar, $T_f = 600$ K, $\epsilon = 60$.

Scenario	O/F	I_{sp} [s]	$\dot{m}_{LH_2}$ [kg/s]	$\dot{m}_{LOX}$ [kg/s]	Δt_{burn} [s]	V_{liquid} [m^3]
Worst-flow (FRSC)	6.00	344.15	84.66	507.94	600	708.74 (LH_2) 266.69 (LOX)

Verification

To cross-check the CEA-based results, an independent equilibrium analysis was performed in Cantera using the same input sets (P_c, ε, O/F) and inlet temperatures as in Table 5.1 [41]. The chamber state is obtained via an enthalpy-pressure equilibrium ('HP') solve that accounts for the sensible enthalpy of the inlets by treating CH_4 as a hot gas and LOX either as a cold liquid, with the thermophysical properties coming from a fluid database, for the FRSC cases, or as a hot gas for the ORSC cases [85]. The nozzle expansion is modelled as isentropic, shifting equilibrium down to sea level, from which the thrust coefficient and I_{sp} are computed including the $(p_e - p_a)A_e$ pressure term; the same global efficiency factor $\eta = 0.95$ is applied as for CEA. The resulting $I_{sp}(O/F)$ curves are shown in Figure 5.6a and Figure 5.6b.

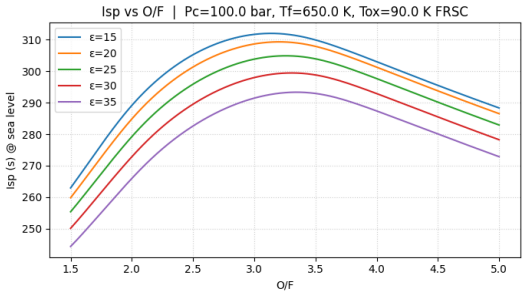

(a) Sea-level I_{sp} versus mixture ratio for the FRSC case (hot CH_4 at 650 K, cold LOX at 90 K) at $P_c = 100$ bar with an expansion-ratio sweep ε = 15-35.

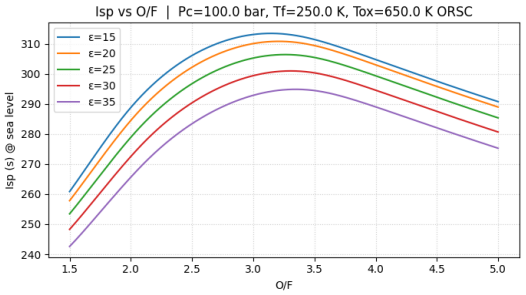

(b) Sea-level I_{sp} versus mixture ratio for the ORSC case (cold CH_4 at 250 K, hot LOX at 650 K) at $P_c = 100$ bar with an expansion-ratio sweep ε = 15-35.

Figure 5.6: Sea-level I_{sp} comparison between RocketCEA and Cantera at $P_c = 100$ bar and $\varepsilon = 35$: FRSC (left; $T_f = 650$ K, $T_{ox} = 90$ K) and ORSC (right; $T_f = 250$ K, $T_{ox} = 650$ K).

These differences are consistent with expected variations between thermochemical databases and equilibrium solvers, and are deemed acceptable for sizing the fluid supply system.

Validation

As validation of the above-mentioned results, the values for the BE-4 engine, Blue Origin's oxidizer-rich LOX-LCH4 staged-combustion engine, Vulcain 2.1 and LE-7 are used. For BE-4, these numbers are

Table 5.5: Sea-level I_{sp} comparison: RocketCEA vs. Cantera at $P_c = 100$ bar and $\varepsilon = 35$.

(a) FRSC: $T_f = 650$ K, $T_{ox} = 90$ K

MR	$I_{sp_{CEA}}$ [s]	$I_{sp_{CT}}$ [s]	Δ [s]	Δ [%]
3.1	289.54	292.37	2.83	0.98
3.2	290.25	292.99	2.74	0.94
3.3	290.67	293.30	2.63	0.90
3.4	290.77	293.29	2.52	0.87
3.5	290.54	292.94	2.40	0.83
3.6	289.97	292.26	2.29	0.79
3.7	289.09	291.29	2.20	0.76

(b) ORSC: $T_f = 250$ K, $T_{ox} = 650$ K

MR	$I_{sp_{CEA}}$ [s]	$I_{sp_{CT}}$ [s]	Δ [s]	Δ [%]
3.1	291.09	293.83	2.74	0.94
3.2	291.88	294.49	2.61	0.89
3.3	292.34	294.82	2.47	0.85
3.4	292.47	294.80	2.33	0.80
3.5	292.25	294.45	2.20	0.75
3.6	291.68	293.76	2.08	0.71
3.7	290.80	292.79	1.99	0.68

unverified, but reasonable estimates exist [8][73][72]. For Vulcain, the numbers used are the only official ESA numbers released in 2001 [13]. The results are closer to reality with the numbers released since, but these are not official. For LE-7, which is an LH_2/LOX FRSC engine, the values are taken from [36].

For the BE-4, the nozzle expansion ratio is between 21 and 25, and the temperature of the gas exiting the turbine before injection into the main chamber is between 650 and 750 Kelvin, as higher temperatures might melt the turbine. Running the turbine cooler increases the lifetime of the turbine, and thus improves reusability. Running the code for the values known for the BE-4, the results look as shown in Table 5.6. A mixture ratio of 3.5 is used, along with a chamber pressure of 140 bar. The temperature of the regeneratively-cooled methane is set to 250 K [45]. Figure 5.7 shows the results for Vulcain 2. As the parameters for this engine are known, a range of values is unnecessary. One additional assumption for the Vulcain is that 2%[2] of the specific impulse is lost through the expelled propellants used to run the turbine [9].

Table 5.6: Sea-level I_{sp} of the BE-4 at O/F = 3.5 and P_c=140 bar with CH_4 at 250 K, for varying LOX temperatures and expansion ratios.

LOX T (K)	ϵ	I_{sp} (s)
650	21	318.37
650	25	317.11
700	21	318.86
700	25	317.61
750	21	319.36
750	25	318.12

[2]Personal correspondence with Amaya Espinosa Ramos

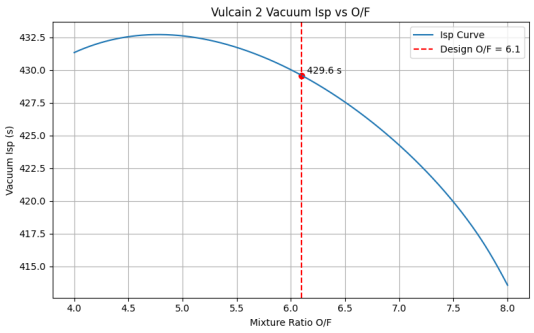

Figure 5.7: Vulcain 2 vacuum I_{sp} at O/F 6.1 and P_c=115 bar with CH_4 at 250 K and $\epsilon = 58.2$.

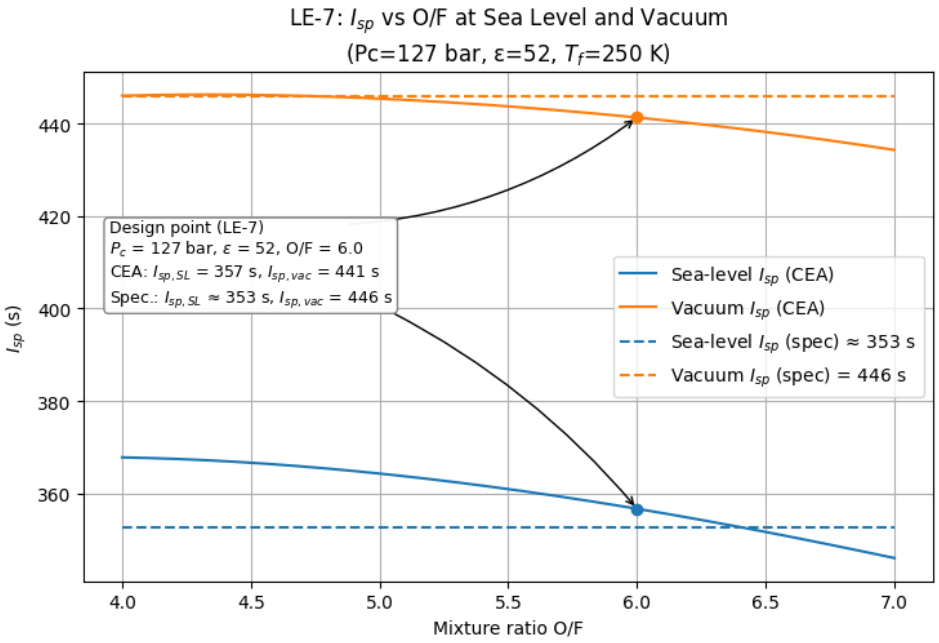

Figure 5.8: LE-7 I_{sp} vs O/F at Sea Level & Vacuum and P_c=127 bar with CH_4 at 250 K and $\epsilon = 52$.

From the plots it can be deduced that the I_{sp} of the BE-4 should be within the range of 317.11-319.36 s, and the Vulcain should be around 429.6 s. For the BE-4 and the Vulcain, both values are within one percent of the reported values for these engines, 315 s and 433 s. This is an error that is considered acceptable, as a worst-case specific impulse is used to size the propellant supply system.

5.2.1. Ullage Volume

A cryogenic run tank cannot be filled to the brim. Having a so-called ullage volume, the gas space above a liquid in a cryogenic tank, is essential for several reasons, which are listed below.

1. **Boil-off:** A cryogenic tank is, even though it is vacuum-insulated, not exempt from radiative heating and heat conduction through support structures. This makes some of the liquid boil-off. If there was no ullage volume, the pressure in the tank would rapidly rise, forcing to vent propellant. Boil-off rates for H_2, CH_4 and LOX are 0.5, 0.4, and 0.3 % of total volume per day respectively. [66]
2. **pressurisation:** The ullage volume is used to pressurise the propellant, allowing for a constant feed pressure to the pipe subsystem and thus the engine.
3. **Cavitation prevention:** Pressure-fed lines require liquid to fully occupy their inlets. If vapour pockets are drawn in, cavitation can occur, leading to pump damage or flow instabilities.
4. **Sloshing:** As the engine is fired, the propellant will shift ('slosh'). To make sure the outlet is not exposed, ullage volume is necessary.
5. **Stratification:** Cryogenic liquid that is under constant pressure stratifies, after which it hydraulically expands to a percentage of the total volume. This makes the bulk liquid expand, resulting in an increased volume. The effect for LH2 is 22.5%, 12.5% for LOX and 7% for LCH4. [3]

The void space is often set empirically. The test data informs the adjustments based on actual boil-off rates, heat soak and sloshing dynamics. A high performance engine test that requires ultra-stable inlet pressures may require a larger ullage or accumulator to compensate for transients in the feed line. Cryogenic systems start with a relatively big empty space and then adjust the values based on test behaviour and thermal load evaluation.

[3] Personal correspondence with Jörn Bellermann

Besides the empiric approach, there are reasons to consider different ullage volumes for different propellants. A percentage of about 5-30% is a typical ullage volume in cryogenic running tanks, depending on the liquid, operating pressure and tank dynamics. H_2 tends to have the highest ullage volume percentage, followed by O_2, and then CH_4. This is mostly due to the earlier mentioned stratification. H_2 tanks are typically filled to a maximum of 70-72%, while LOX and LCH_4 have a maximal liquid volume of 89% and 92-94% respectively, also dependent on the shape of the tank. For the results from the analysis performed earlier this chapter, this results in total (rounded) tank volumes as shown in Table 5.7. The last factor that should be included in this is the volume left in the tank at the end of the test. To avoid cavitation, this is typically between 5-10%. The values are rounded from 998 to 1000, 399 to 400 and 309 to 310 respectively, and then a 5% buffer is applied.

Table 5.7: Volumes of H_2 and LOX Tanks

Tank	Volume (m^3)
H_2	1050
LOX	420
CH_4	326

5.2.2. Tank Setup

Because of the large volume required to run an engine for 10 minutes, which is an industrial wish, considering the possibility of using multiple tanks is relevant. Moreover, investigating the possibility of using a single tank for both H_2 and CH_4 can be a major cost saver. First, the advantages and challenges of a system using multiple tanks are listed below.

Advantages

- **Redundancy:** Individual-tank failures, like pressure control or valve failure, can be isolated without shutting down the entire supply system. Secondary tanks can take over feed duties or permit partial-load testing while repairs are made.
- **Staggered Operations:** You can pre-cool, pressurise or fill one tank while another remains operational. This can shorten turnaround times between tests and allows planned maintenance on one tank without interrupting the flow from the others.
- **Flow Management:** Multiple tanks permit progressive valve sequencing and differential tank discharge rates. This is critical in case of a multi-engine setup, precision mixture-ratio adjustments or rapid throttling profiles.
- **Thermal Control:** Smaller vessels have higher surface-area-to-volume ratios, making them easier to insulate, pre-cool or prepare for cryogenic operations.
- **Scalability:** New tanks can be added in parallel to expand capacity as testing needs grow, without major re-engineering of pipework.

Challenges

- **System Complexity:** Each additional tank brings extra valves, piping, pressure regulators and sensors, complicating the supply system.
- **Synchronization Difficulties:** Managing equal flow and pressure between multiple tanks requires careful design.
- **Additional Failure Modes:** Every new component (valve, sensor or fitting) adds a potential leak path or failure point, increasing the overall risk of system faults.
- **Infrastructure:** Multiple vessels take more space than a single tank, increasing the cost of foundations, frames and any infrastructure related to safety.
- **Higher Operational Overhead:** The cost of purging, cooling and standby checks increases with the number of tanks.

The conclusions that can be drawn from the pros and cons are that the development and creation of a system using multiple tanks is more expensive, but the cost of operations, and the flexibility it offers regarding testing of engines is superior. In a test bench that is to be used for multiple years, it would be worth it to build a multi-tank system, even though the initial investment might be high.[4]

Closely related to the logistical considerations around the use of one or more tanks is the possibility to use a tank for more than one propellant. In principle, a single run-tank can be engineered to alternate between liquid hydrogen (LH_2) and liquid methane (LCH_4), since the stainless-steel or nickel-alloy construction used to prevent hydrogen embrittlement is also compatible with methane. However, seals and elastomers selected for hydrogen service may swell or degrade under hydrocarbon exposure, and vacuum-jacketed, actively cooled insulation sized for LH_2 is inefficient for CH_4; repeated thermal cycling between the two temperature regimes further stresses the insulation and tank walls. Hydrogen's small molecules penetrate materials and form flammable mixtures at very low concentrations, making cleaning a difficult process. Switching from LH_2 to LCH_4 demands extensive purging, leak testing and outgassing, while the reverse change, although somewhat safer, still requires absolute cleanliness. Because hydrogen systems must maintain explosion-proof zoning, running methane in a hydrogen-rated facility poses no extra hazard, but transitioning back remains an important task. Methane's higher density and lower volatility also mean very different delivery pressures and pump dynamics: large LH_2 tanks must be checked to ensure their supports can handle heavier methane loads, and pipes must be dimensioned or throttled accordingly. A 200 m^3 tank designed for hydrogen will reach it weight load limit at $1/6^{th}$ that volume when it is filled with CH_4. The control behaviour is completely different because of the large gas volume that is now above the liquid phase. With careful choice of dual-compatible materials and seals, adaptable insulation and venting, and acceptance of the downtime, the same infrastructure can serve both propellants, as long as the system is extremely cleanable and flushable.[5]

Two separate tank systems are always more expensive overall, but if quick turnaround times are required to switch between a LOX/LH_2 and LOX/CH_4 engine, which is highly unlikely, this is not feasible. The combination of having multiple tanks per propellant and this dual-use property is in the long run the most beneficial option.[6]

5.3. Pressurisation

Maintaining a constant tank pressure during running is critical to have a stable engine feed and avoiding cavitation or flow instabilities. In propulsion run tanks, but also in rocket propellant tanks, this is done by introducing a pressurant gas into the tank to occupy the volume vacated by the liquid propellant, the earlier discussed ullage volume (and more). Because the gas may exist under high-pressure conditions, it is essential to account for real-fluid behaviour rather than relying on ideal approximations. In the following subsections, the methodology for calculating the required gas mass flow rate and sizing the pressurant supply cylinders is presented.

5.3.1. Thermodynamic Properties

Consider a tank of total internal volume V_t containing a liquid propellant at pressure P (in pascals) and temperature T_ℓ (in kelvins). Above the liquid surface resides a layer of pressurant gas at the same pressure but potentially a different temperature T_g. Denote:

$$P = P_{\text{bar}} \times 10^5 \quad [\text{Pa}], \quad T_\ell = T_{K_\ell} \quad [\text{K}], \quad T_g = T_{K_g} \quad [\text{K}].$$

At these conditions, the liquid density $\rho_\ell(P, T_\ell)$ is obtained from a real-fluid property database, and the ullage-gas temperature T_g is estimated by treating the pressure relief to ullage pressure drop as an isenthalpic (Joule-Thomson) throttling across the filling valve. This is appropriate for a high-ΔP flow with negligible heat exchange. It is followed by a small fixed thermal offset to account for mixing and boil-off equilibration. The procedure is as follows:

[4] Personal correspondence with Jörn Bellermann, Kate Underhill and Jean-Noel Caruana
[5] Personal correspondence with Andreas Haberzettl
[6] Personal correspondence with Andreas Haberzettl

1. Enthalpy h_1 at buffer pressure P_{buffer} and temperature T_{buffer} is evaluated.
2. The corresponding expansion temperature T_2 at run-tank pressure P is solved for constant enthalpy h_1.
3. A cooling decrement (-10K, an approximation) is applied to yield the run-tank gas temperature T_g[7].
4. The gas density $\rho_g(P, T_g)$ and molar mass M are then extracted at these conditions.

The molar mass M of the pressurant gas (either nitrogen or helium) is likewise obtained from a fluid property database at (P, T_g).

5.3.2. Gas Mass Flow Rate Calculation

Let V_i be the initial volume occupied by the liquid propellant, so that the initial gas volume is

$$V_1 = V_t - V_i.$$

As the propellant is drawn from the tank, the void left by the departing liquid must be replaced by pressurant gas in order to hold the tank pressure constant. If the liquid mass flow rate $\dot{m}_\ell$ is known and maintained for a time interval t, then the volume of liquid displaced is

$$V_{\text{removed}} = \frac{\dot{m}_\ell\, t}{\rho_\ell}.$$

Consequently, the final liquid volume in the tank becomes

$$V_f = V_i - V_{\text{removed}},$$

and the final gas volume is

$$V_2 = V_t - V_f = V_1 + V_{\text{removed}}.$$

Because T_g is now computed via the post-JT expansion, the real-gas density must be recalculated at (P, T_g) both before and after refill. Denoting n_1 and n_2 as the number of moles of gas before and after refill is

$$n_1 = \frac{\rho_g\, V_1}{M}, \quad n_2 = \frac{\rho_g\, V_2}{M}.$$

Thus, the added moles of gas required to restore pressure are

$$\Delta n = n_2 - n_1 = \frac{\rho_g}{M}\left(V_2 - V_1\right) = \frac{\rho_g}{M}\, V_{\text{removed}},$$

and the corresponding added mass is

$$\Delta m = \Delta n\, M = \rho_g\, V_{\text{removed}}.$$

Dividing by the refill time t yields the pressurant mass flow rate, which is used as a time-averaged sizing relation under constant ullage pressure and constant liquid outflow:

$$\dot{m}_g = \frac{\Delta m}{t} = \frac{\rho_g}{t}\, V_{\text{removed}} = \dot{m}_\ell\, \frac{\rho_g}{\rho_\ell}.$$

5.3.3. Pressurant Cylinder Sizing

Selection of an appropriate pressurant storage system requires determining how many cylinders must be connected to supply Δn moles of gas throughout the run. Assume each cylinder has internal volume V_{cyl}, typically 50 L, and is maintained at ambient temperature T_N (293 K). The cylinder is considered charged to an initial pressure $P_{N,i}$, 200 bar, and is allowed to deplete down to $P_{N,f}$, 50 bar. The gas densities at these two pressures are

$$\rho_{N,i} = \rho_g\big(P_{N,i},\, T_N\big), \quad \rho_{N,f} = \rho_g\big(P_{N,f},\, T_N\big).$$

[7] Personal correspondence with Jörn Bellermann

Accordingly, the number of moles in one cylinder initially and finally are

$$n_{N,i} = \frac{\rho_{N,i}\, V_{\text{cyl}}}{M}, \quad n_{N,f} = \frac{\rho_{N,f}\, V_{\text{cyl}}}{M},$$

so that the usable moles per cylinder are

$$n_{\text{cyl}} = n_{N,i} - n_{N,f}.$$

The total number of cylinders required to supply Δn moles is then

$$N_{\text{cyl}} = \frac{\Delta n}{n_{\text{cyl}}}, \quad N_{\text{cyl}}^{\text{req}} = \lceil N_{\text{cyl}} \rceil,$$

where $\lceil \cdot \rceil$ denotes the ceiling function to round up to the nearest whole cylinder. For nitrogen, using $V_{\text{cyl}} = 50\,\text{L}$, $T_N = 293\,\text{K}$, $P_{N,i} = 200\,\text{bar}$, and $P_{N,f} = 50\,\text{bar}$, one obtains the required number of bottles directly. A similar calculation applies if helium is chosen as pressurant, replacing M and ρ values with those for helium.

5.4. Piping

The size and length of the pipes is important as there are limitations on the speed of fluid being transported and there is a pressure drop the fluid experiences along the pipe. This subsection goes into both these topics in depth.

5.4.1. Sizing

The sizing of the propellant feed pipes follows from the requirements on mass flow. Given a required mass flow rate, $\dot{m}$, this can be converted to a volumetric flow rate:

$$Q \;=\; \frac{\dot{m}}{\rho},$$

where ρ is the fluid density at the operating temperature and pressure.

To avoid excessive velocities (erosion, cavitation, vibration, explosion), a maximum allowable velocity $u_{\max}$ is imposed, which depends on the fluid[8]:

$$\begin{aligned}
&\text{H}_2\text{O}\text{: } u_{\max} = 10 \text{ m/s},\\
&\text{LOX} : u_{\max} = 25 \text{ m/s},\\
&\text{LCH}_4 : u_{\max} = 20 \text{ m/s},\\
&\text{LH}_2 : u_{\max} = 35 \text{ m/s}.
\end{aligned}$$

The next step is to apply continuity and relate the volumetric flow to the flow velocity. Considering a circular pipe of diameter D, the formula becomes:

$$Q = u\, A = u\, \frac{\pi D^2}{4} \quad \Longrightarrow \quad u = \frac{4\,Q}{\pi\, D^2} \leq u_{\max} \quad \Longrightarrow \quad D \geq \sqrt{\frac{4\,Q}{\pi\, u_{\max}}} = D_{\min}.$$

A nominal diameter $D \geq D_{\min}$ should be chosen for the pipe, adding a margin (10-20%) to account for future flow increases, roughness uncertainty, and possible safety constraints imposed by regulatory bodies. The minimum pipe size for the different fluids can be seen in Table 5.8.

Table 5.8: Pipe sizing from velocity limits for liquid propellants.

Fluid	$\dot{m}$ [kg s^{-1}]	ρ [kg m^{-3}]	$Q = \dot{m}/\rho$ [m^3 s^{-1}]	$u_{\max}$ [m s^{-1}]	$D_{\min}$ [mm]
LOX	650	1140	0.570	25	170
LCH_4	200	422	0.474	20	174
LH_2	84	70	1.200	35	209

[8]Personal correspondence with Jörn Bellermann

5.4.2. Pressure Drop

Accurate pressure-drop prediction is crucial for selecting pump head, sizing relief valves, and ensuring stability of the feed system. The Darcy-Weisbach equation is used for this [10]:

$$\Delta p_{\text{fric}} = f \, \frac{L}{D} \, \frac{\rho \, u^2}{2},$$

where

- f is the dimensionless friction factor, a function of Reynolds number Re and relative roughness ε/D,
- L is the pipe length,
- D its inner diameter,
- ρ the fluid density, and
- u the average velocity.

Because f does not have a closed-form solution in the turbulent regime, it is approximated using the Swamee-Jain formula [106]:

$$f = \begin{cases} \dfrac{64}{Re}, & Re < 2300, \\[2ex] 0.25 \Big[\log_{10}\!\Big(\frac{\varepsilon/D}{3.7} + \frac{5.74}{Re^{0.9}} \Big) \Big]^{-2}, & Re \geq 2300. \end{cases}$$

Figure 5.9 shows the resulting Moody chart computed for a range of relative roughnesses [47], clearly separating laminar, transitional, and fully turbulent regimes for $Re \in [10^3, 10^8]$.

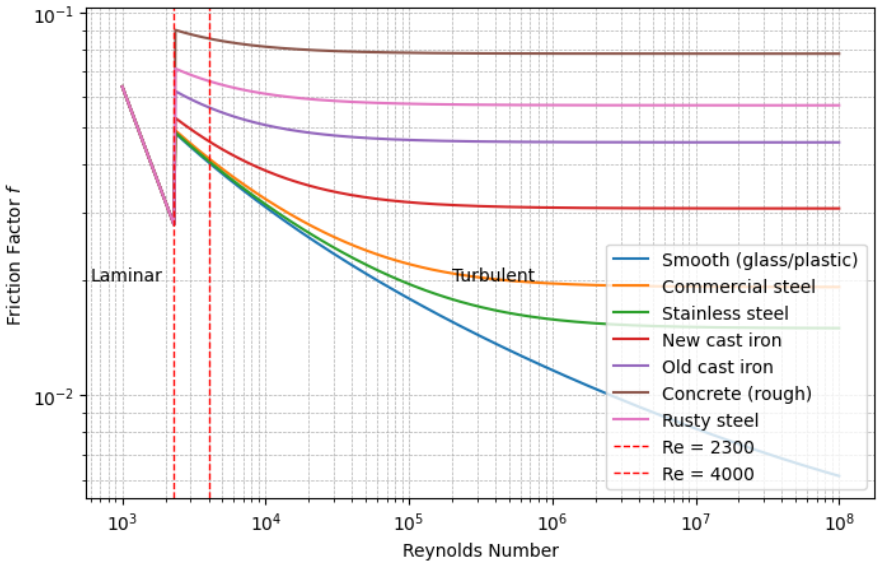

Figure 5.9: Computed friction factor f versus Reynolds number for different pipe surface roughnesses, using the Swamee-Jain approximation. Vertical dashed lines at $Re = 2300$ and $Re = 4000$ mark the laminar-turbulent transition.

To capture compressibility and temperature-pressure dependence of density, the total frictional pressure drop is evaluated by slicing the pipe into N equal segments of length $\Delta x = L/N$, and summing

$$\Delta p_{\text{fric}} = \sum_{i=1}^{N} f_i \, \frac{\Delta x}{D} \, \frac{\rho_i \, u_i^2}{2}, \quad u_i = \frac{\dot{m}}{\rho_i \, A}, \quad \rho_i = \rho\big(P_i, T\big).$$

At each segment the local pressure P_i is decremented by the previous Δp, and ρ_i is retrieved from an internal database. Gravitational effects are added via

$$\Delta p_{\text{grav}} = -\rho_0 \, g \, \Delta z,$$

where Δz is the signed elevation change and ρ_0 the inlet density. The final outlet pressure is

$$P_{\text{out}} \;=\; P_{\text{in}} - \Delta p_{\text{fric}} - \Delta p_{\text{grav}}.$$

5.5. EcosimPro Simulations

The previous sections culminate in a simulation in EcosimPro, where the behaviour of the previously discussed multi run tank setup is assessed. The ESPSS library was used for this [65]. The nominal test sequence for the LOX setup is:

a) **Pressurise** the LOX tanks to 20 bar using a nitrogen (N_2) bottle. Once the outflow of the (N_2) tank encounters the pressure relief valve, the pressure drops to a value between 39.5 and 40 bar. The filling valve then ensures that a pressure of 20 bar is maintained in the tank through a PID controller. 20 bar is necessary, because otherwise the system cannot uphold the 650 kg/s outflow.

b) **Open the test line** (Valve_Test) once 20 bar is reached.

c) **Natural decrease** of outlet pressure with Valve_A pre-opened to 0.292. This is the percentage of the opening of the valve, and was obtained through parameter tuning. This preopening drops the pressure from 20 bar to 4 bar when Valve_Test is opened.

d) **Closed-loop regulation** of outlet pressure at 4 bar for the commanded mass flow of 650 $\mathrm{kg\,s^{-1}}$ using a PI controller on Valve_A. From 2400 to 2406 s, there is a ramp-up of the mass flow. This is necessary for the engine to start up.

For methane, the logic is as follows:

a) **Pressurise** the CH_4 tanks to 10 bar using a helium (He) bottle. Once the outflow of the helium tank encounters the pressure relief valve, the pressure drops to a value between 19.5 bar and 20.5 bar. The filling valve then ensures that a pressure of 10 bar is maintained in the tank through a PID controller. 10 bar is necessary, because otherwise the system cannot uphold the 200 $\mathrm{kg\,s^{-1}}$ outflow.

b) **Open the test line** (Valve_Test) once 10 bar is reached.

c) **Natural decrease** of outlet pressure with Valve_A pre-opened to the tuned fraction 0.246. This pre-opening sets the initial pressure drop from 10 bar to the outlet pressure band used for engine admission when Valve_Test is opened.

d) **Closed-loop regulation** of outlet pressure at $p_{\text{out,CH}_4}$ for the commanded mass flow of 200 $\mathrm{kg\,s^{-1}}$ using a PI controller on Valve_A. From 2400 to 2406 s, there is a ramp-up of the mass flow to accommodate engine start-up transients.

There are some criteria that drive the decisions made in the simulation. These are listed in Table 5.9.

Table 5.9: Criteria for the pressurisation and feed system LOX tanks.

Criterion	Target	Notes
Tank pressure during pressurisation	Slow ramp-up to 20 bar	PID regulation; Valve_Press is always open unless $p_{N_2} \leq 50$ bar. The ramp-up is slow because there is no reason to quickly pressurise the tank, which carries an inherent risk.
Relief valve	Drop pressure from 200 bar to 40 bar	Relief band 39.5 bar to 40.5 bar
Outlet pressure	≈ 4 bar	Achieved with Valve_A pre-opened at 0.292
Test mass flow	$650\,\mathrm{kg\,s^{-1}}$	From 7 seconds after the test valve is opened
Additional valve logic	Satisfied	Regulation valve opens if $p_{tank} > 25.01$ bar; pressurisation valve closes if $p_{N_2} \leq 50$ bar

5.5.1. System Overview

The system consists of an N_2 pressurant bottle (100 m^3 at 200 bar, 293 K) feeding the ullage of two LOX storage tanks (400 m^3 total volume, 85 % liquid fill). The multi-tank setup that was discussed in subsection 5.2.2 is implemented in this simulation. The tank liquid and boil-off gas initial temperatures are 90.5 K and 91 K, respectively. The tank shell is SS 304L with a 20 mm wall and 16 mm outer shell, insulated by 49.9 cm diameter vacuum panels. The pressurant line is 8 cm in diameter and 19.45 meters long. The engine feed path comprises Valve_A (regulating), Valve_Test and a 30 m long, 220 mm diameter outlet line. The flows of Tank A and B are combined through a tee junction before Valve_A. Valve_Test signifies the engine entry, and thus the end of Pipe_A_outlet_valve_A is the point where the supply pressure is measured (shown by the pressure_engine meter). The setup is divided in eight pieces, left to right, top to bottom, to ensure readability of the schematic (a 4 by 2 grid). The split-up system is visible in Figure 5.10 to Figure 5.16. The full schematic can be found in Appendix B, Figure B.5.

For methane and hydrogen, the exact same setup can be used, with a few minor tweaks; the methane setup is not shown because the layout is exactly the same and the image would be too big to show both in one. The results presented in this section are for the LOX system, because the other systems are governed by the same principles, and thus the method used for LOX translates to CH_4 and H_2 (with helium pressurisation). Methane is pressurised using helium, because it can possibly react with nitrogen; the N_2 pressurant is thus swapped with helium. A flare stack is typically used instead of venting to get rid of the excess gas. Assuming a CH_4 flow of 200,kg/s, the minimum diameter of the lines is 17,cm; this limits the velocity of CH_4 below 20,m/s, which is the maximum flow speed to stay within safety constraints. For hydrogen the same holds: the mass flow is smaller (84-85,kg/s), thus the necessary pressure in the tank is lower, and the minimum line diameter for an 85,kg/s flow of H_2 is 21,cm to limit the flow velocity to 35,m/s. Hydrogen is also pressurised with helium, because nitrogen would solidify in an LH_2 tank. CH_4 needs two tanks as well, while hydrogen, if 200 m^3 is considered to be the default size of tanks, needs 6 propellant tanks. Hydrogen embrittlement is not a problem with the tank used in the simulation, and is also not an issue with commercial off-the-shelf (COTS) tanks provided by Air Liquide or other cryogenic tank providers. The pressurisation using helium differs from nitrogen in several ways: the density and molar mass of He is significantly smaller than that of nitrogen, which means helium either has to be stored at a higher pressure to have the same storage volume as nitrogen, or more storage volume is needed; furthermore, helium has a higher permeability, it leaks more, so the requirements on anything that is not a pipe will have to be tighter than for nitrogen. The pressurisation infrastructure for a H_2 tank would be more sophisticated, and thus more expensive, than

that for a LOX tank, as the requirements on seals and elastomers are stricter. Lastly, helium is very expensive, so a recovery mechanism would be a good investment.

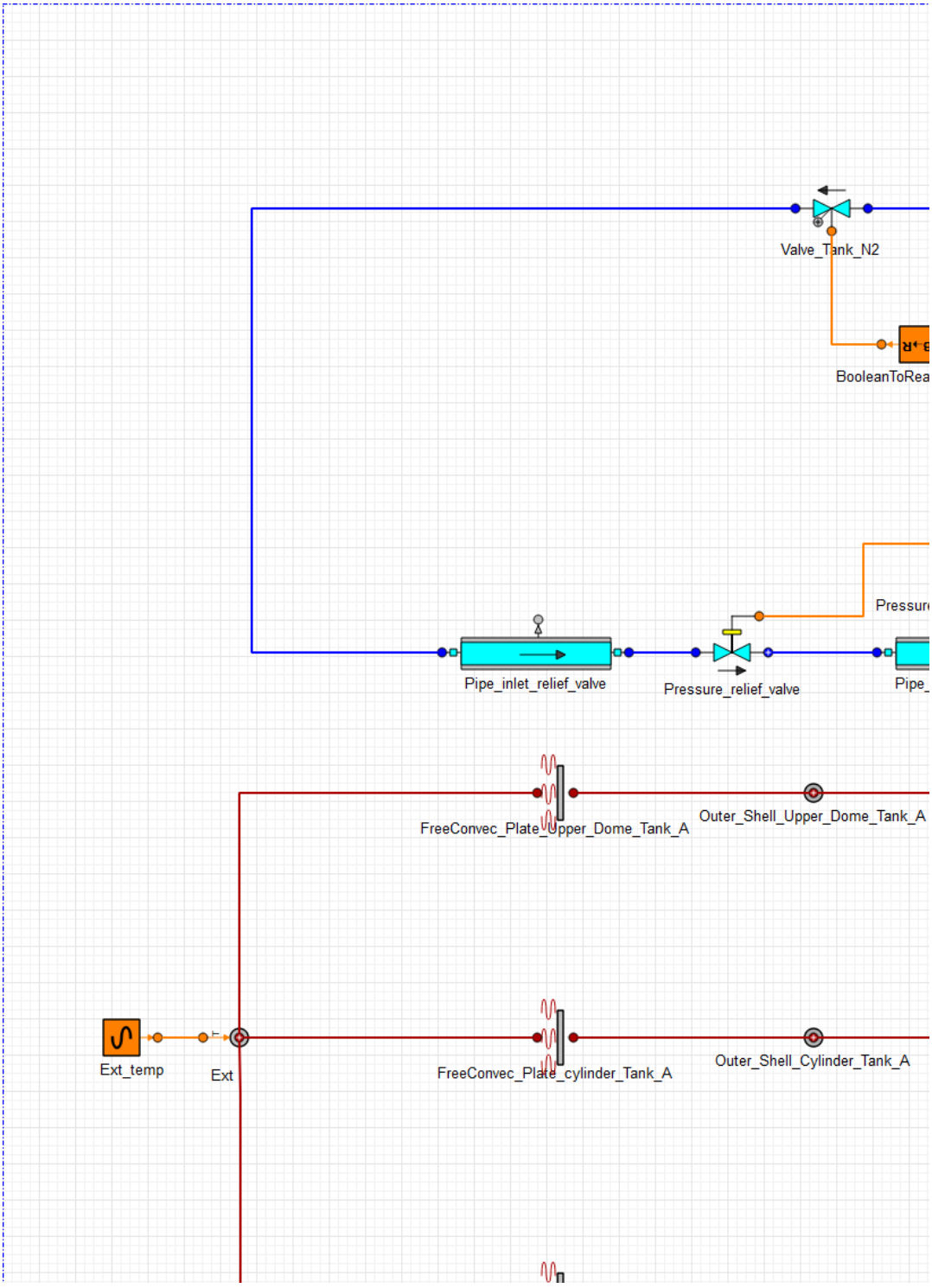

Figure 5.10: System schematic two tanks - top, tile 1 of 4.

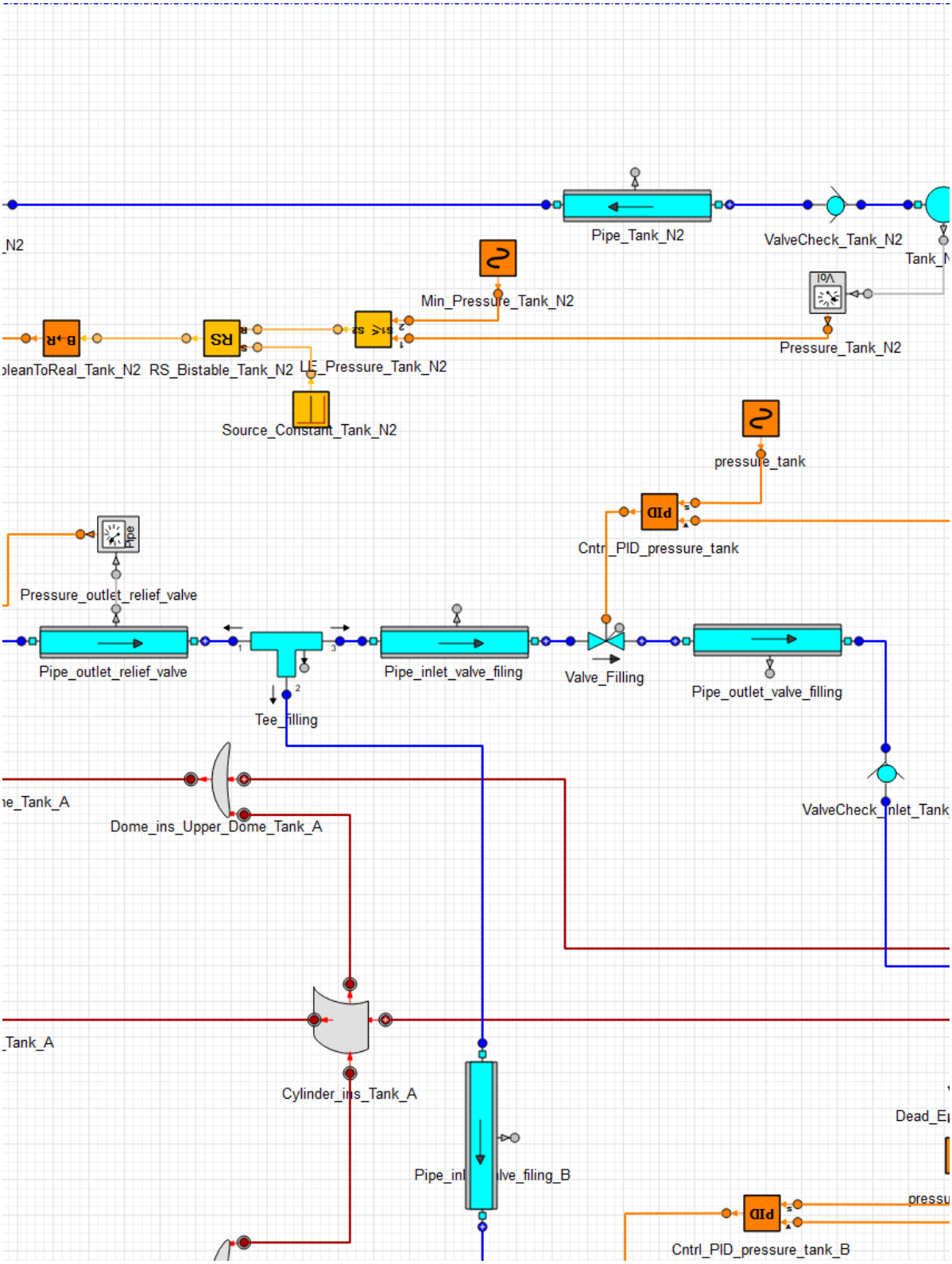

Figure 5.11: System schematic two tanks - top, tile 2 of 4.

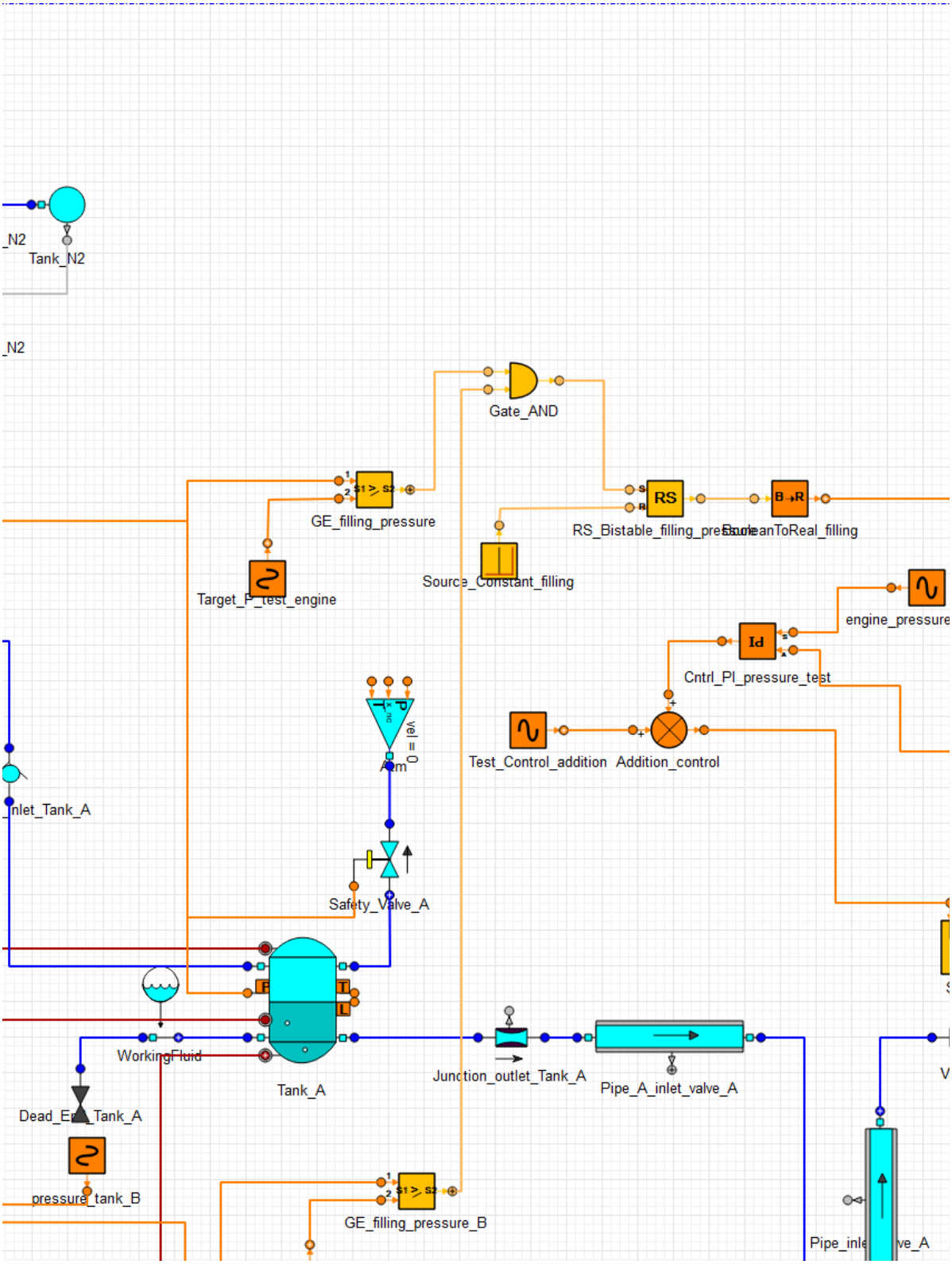

Figure 5.12: System schematic two tanks - top, tile 3 of 4.

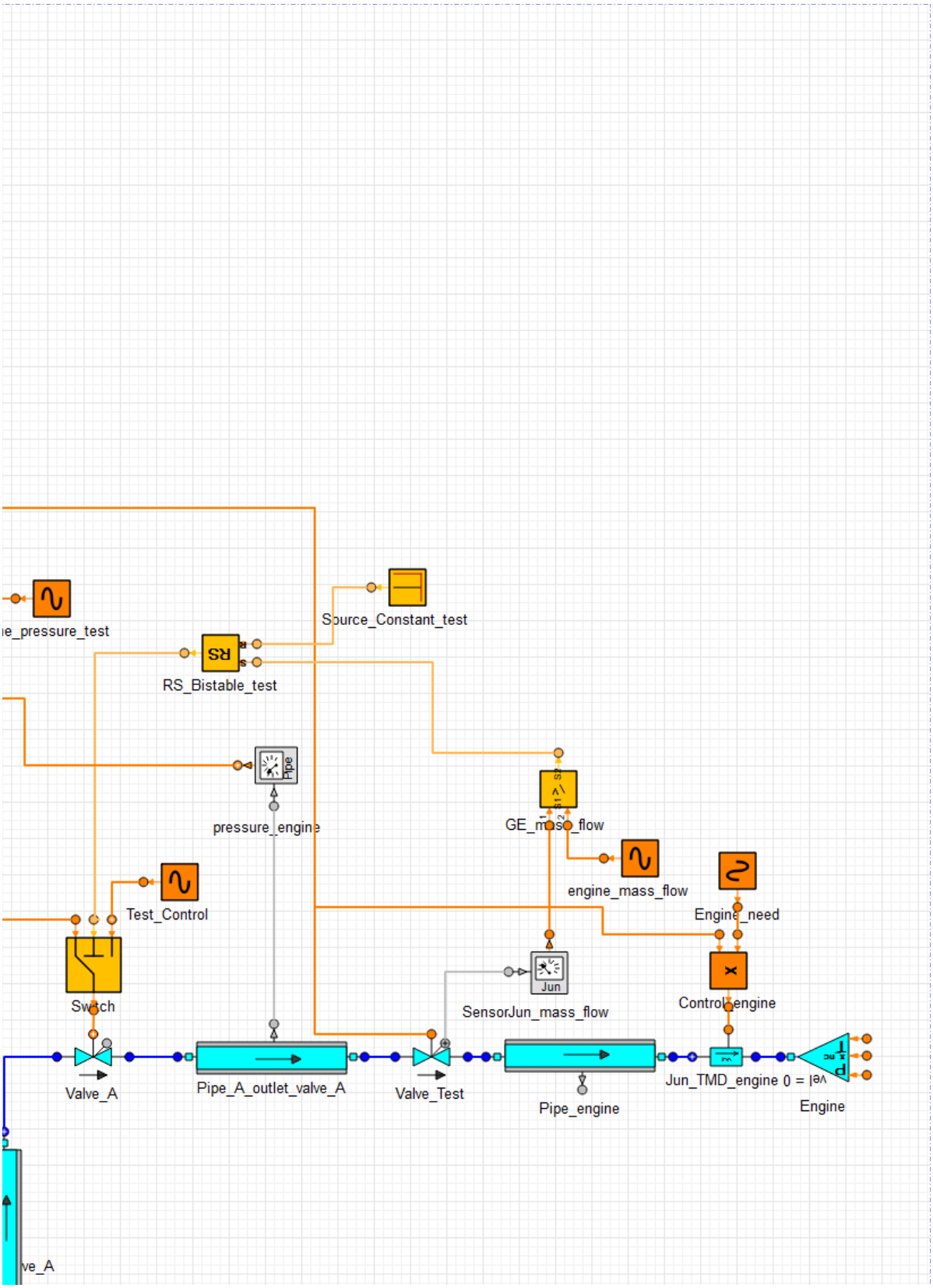

Figure 5.13: System schematic two tanks - top, tile 4 of 4.

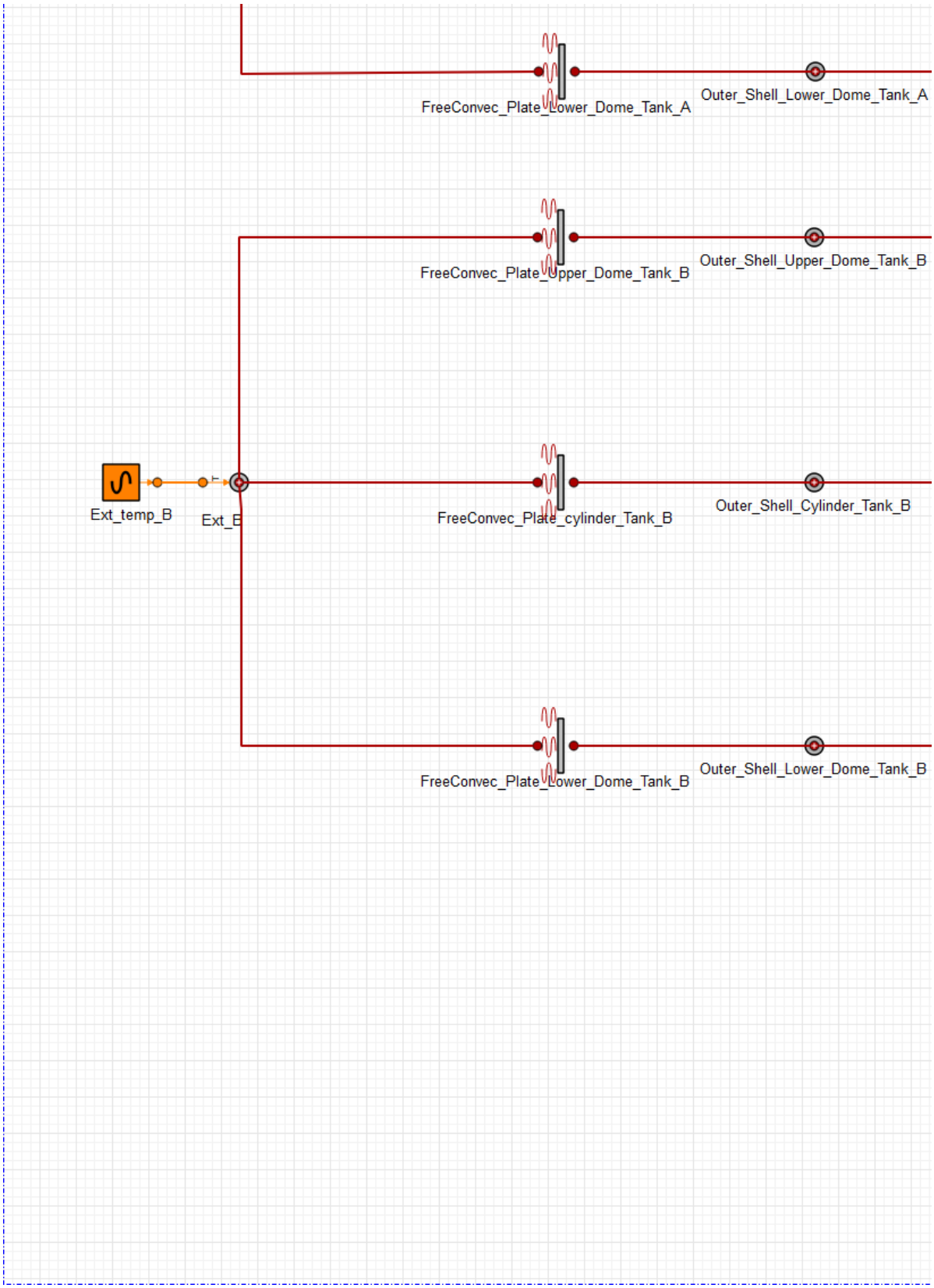

Figure 5.14: System schematic two tanks - bottom, tile 1 of 4.

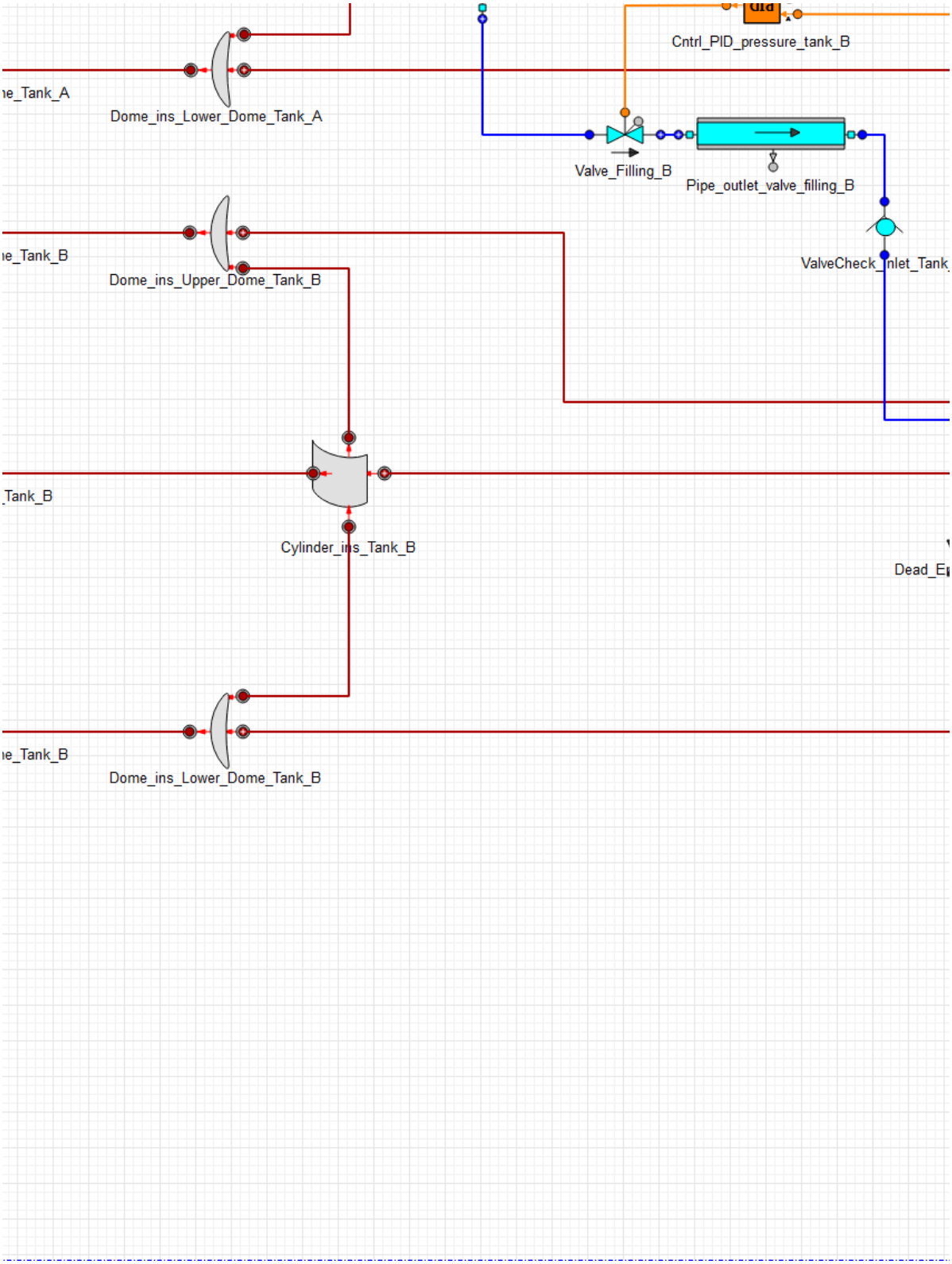

Figure 5.15: System schematic two tanks - bottom, tile 2 of 4.

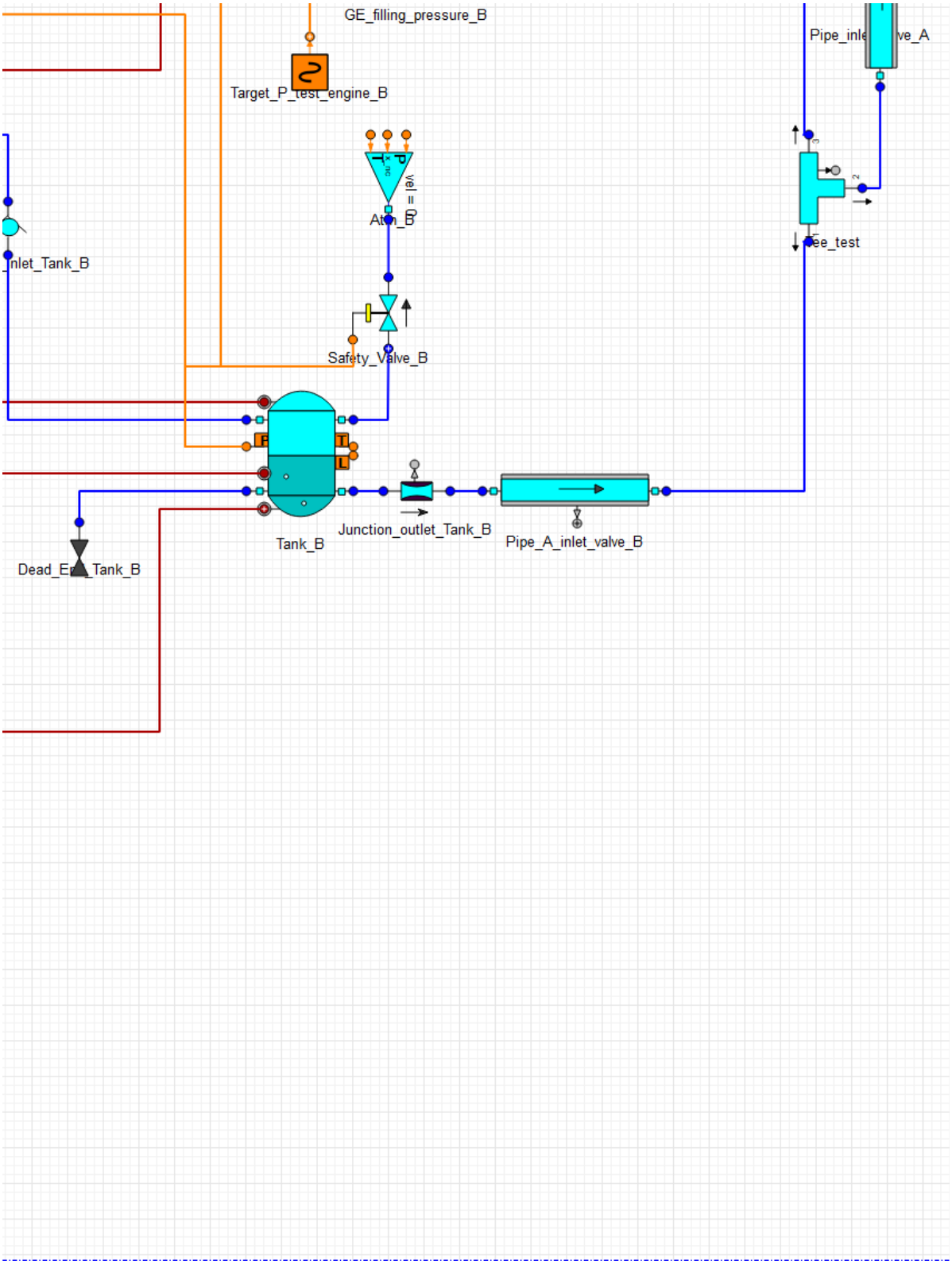

Figure 5.16: System schematic two tanks - bottom, tile 3 of 4.

The bottom right image is left out, as this is empty. Therefore, the figures only run until 'bottom, tile 3 of 4'.

5.5.2. Ecosim Pressurisation

The pressurisation sequence can be seen below. The valves are opened at t=0, making the pressure rise in Tank A and B and drop in the nitrogen tank. The pressurisation phase is taken to be 2400 seconds, or 40 minutes, because there is no reason to rush the pressurisation, and it is safer to take time doing it. This is common behaviour in test bench operation[9]. Figure 5.17 shows the pressure build-up in Tank A and B, while Figure 5.18 shows the N_2 tank pressure decreasing as the pressure rises in both run tanks.

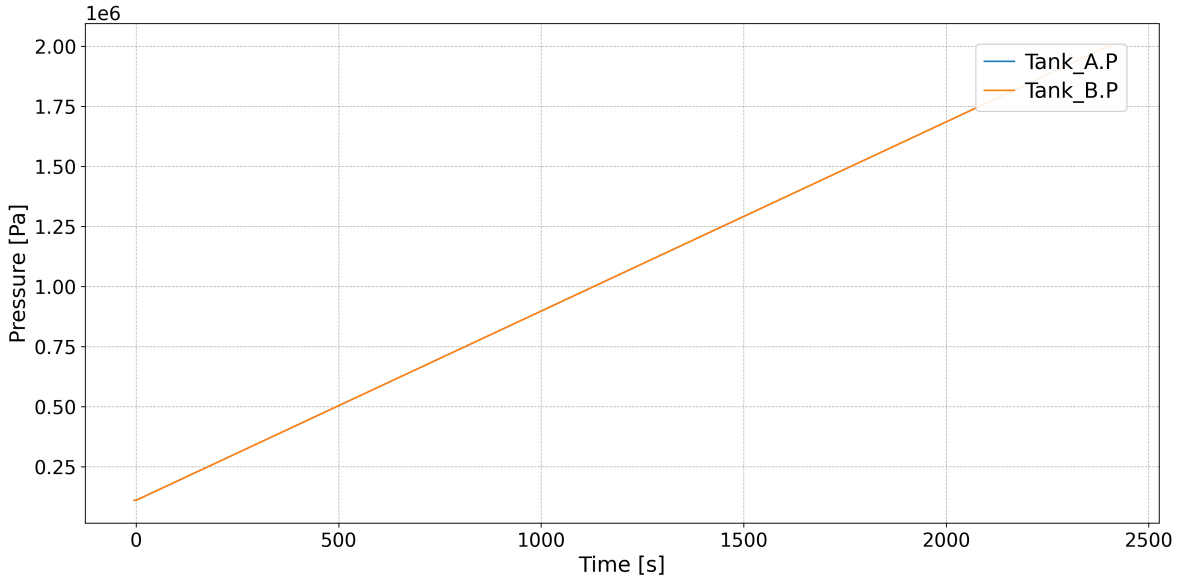

Figure 5.17: Tank pressure build-up

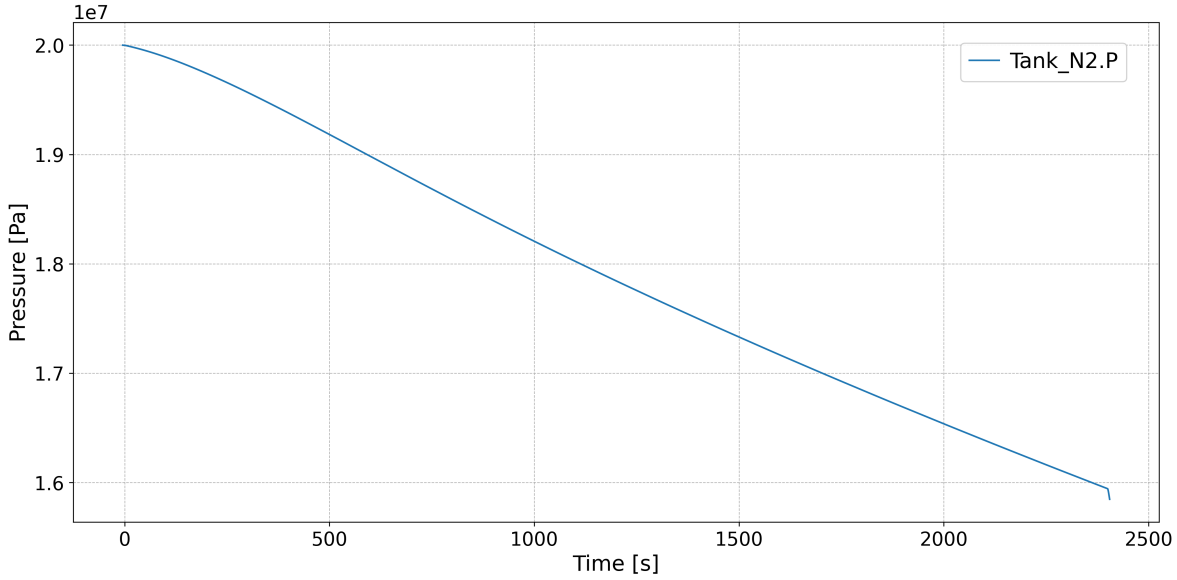

Figure 5.18: N_2 tank pressure

Figure 5.19 shows the N_2 pressurant mass flow while the controller tracks a *ramped* LOX tank-pressure reference that increases to 20 bar over 2400 s. Early in the ramp the pressure error and upstream-

[9]Personal correspondence with Jörn Bellermann (ESA) and Andreas Haberzettl (DLR)

downstream Δp are largest, so the pressurisation valve opens and the N_2 mass flow rises, aided by Joule-Thomson cooling and gas densification. As the ramp progresses, the error diminishes and the available Δp falls slightly because of decreasing pressure in the N_2 tank, so the valve trims back and the mass flow gently decreases. Consequently, tank pressure increases monotonically with a slope that is highest early in the ramp and slowly tapers, consistent with pressure being the time-integral of ullage inflow and the ullage gas temperature approaching steady state.

Figure 5.20 shows the mass of the non-condensable gas in the tank along with any other gas in the tank. When the run starts, there is only boiled-off oxygen in the tank. After 2400 seconds, there is 1210 kg of N_2 in the tank. This is important information to verify the behaviour of pressurisation.

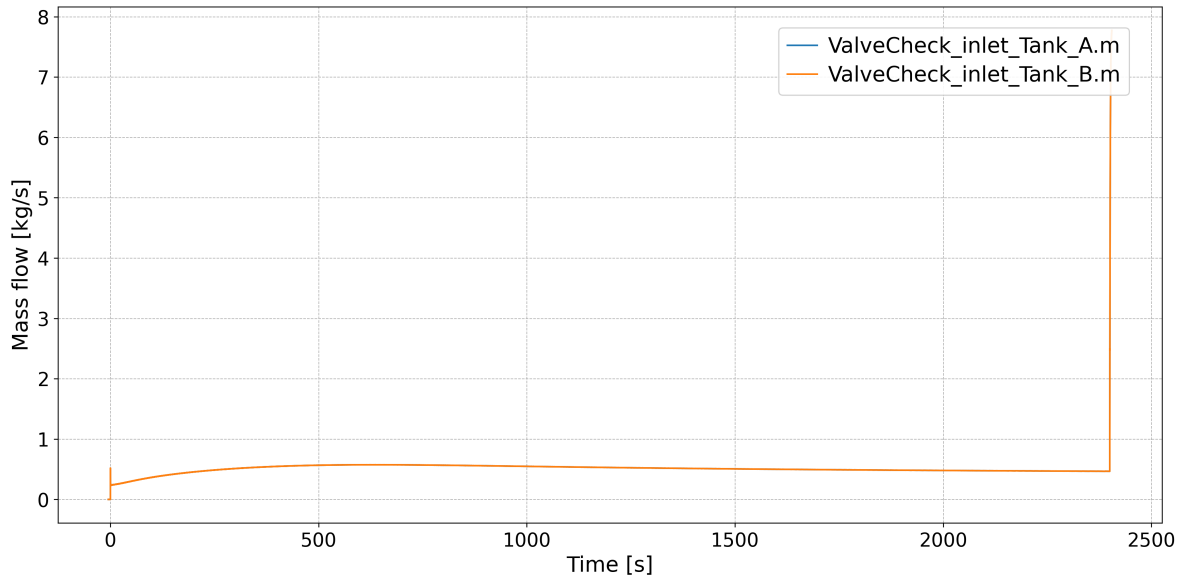

Figure 5.19: Mass flow of nitrogen into the tanks

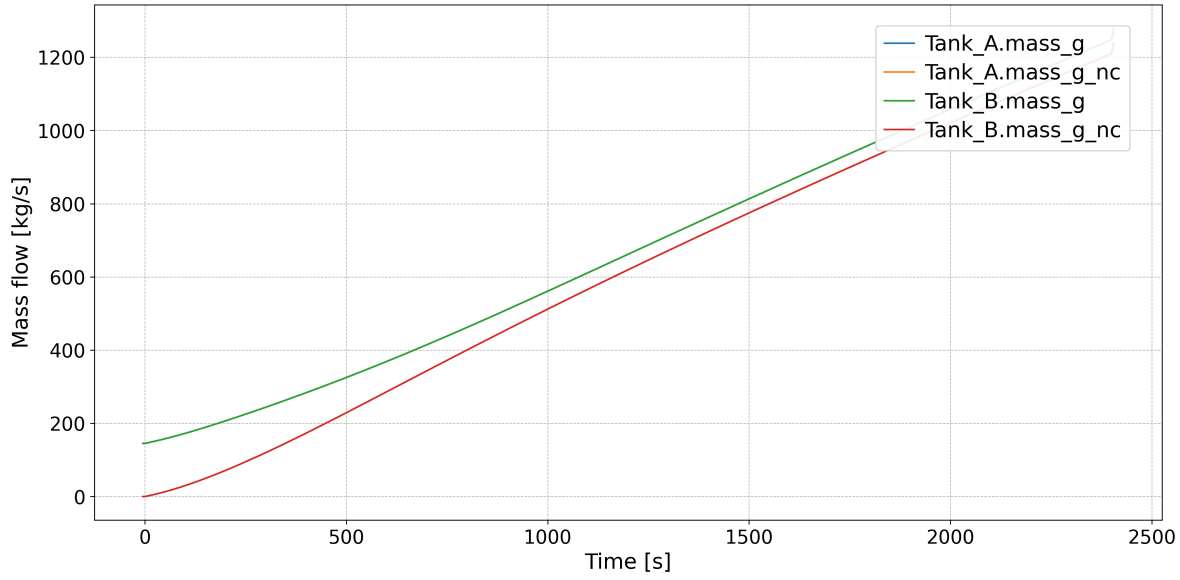

Figure 5.20: Gas mass of non-condensable gas (N_2) and boil-off in the run tanks

The aformentioned mass of non-condensable gas in combination with the gas temperature of the upper control volume of the tank can be used to assess the similarity between calculations and the EcosimPro

results. This gas temperature per control volume can be seen in Figure 5.22. Furthermore, a more complete overview of the changing pressures in the system is shown in Figure 5.21.

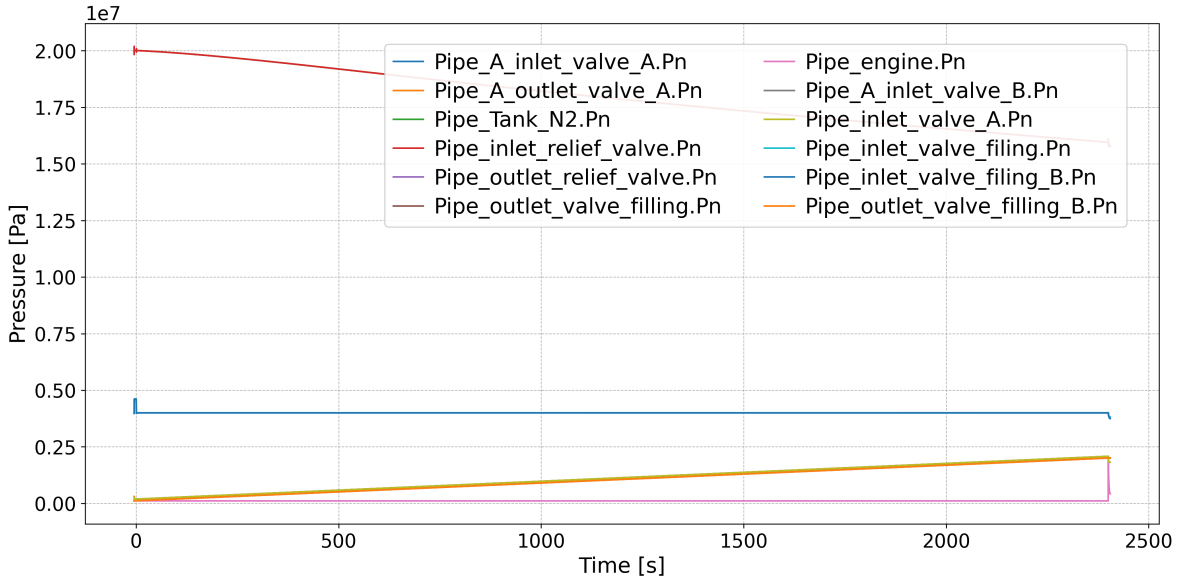

Figure 5.21: Pressure at different points in the system

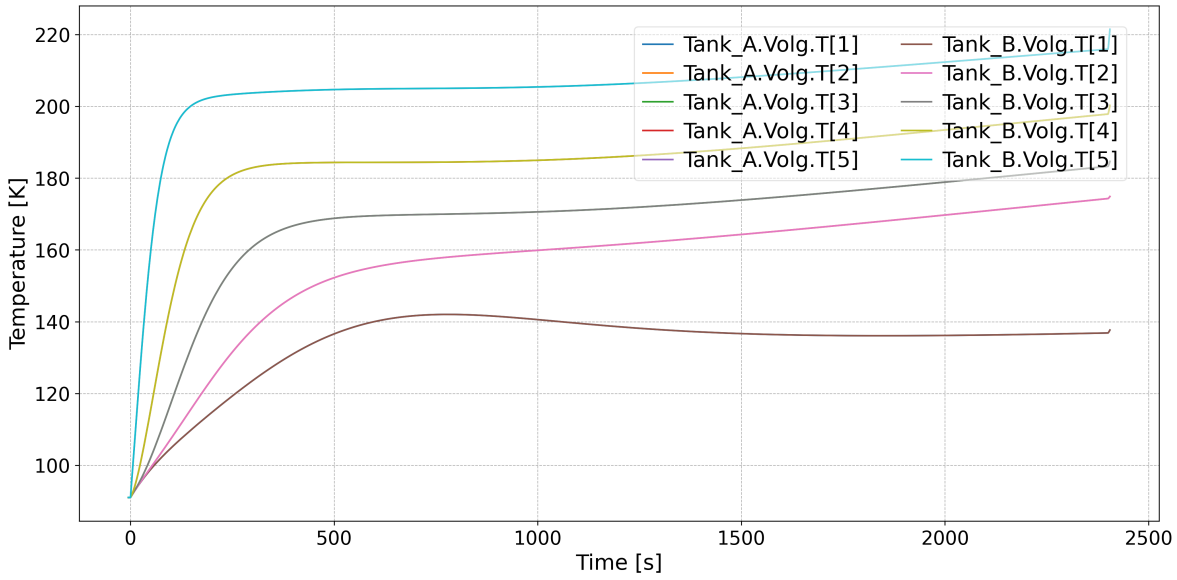

Figure 5.22: Gas temperature of control volumes in the tanks

5.5.3. Ecosim Engine Running

In this subsection, the running of the engine is simulated and explained using graphs. The logic is the following:

At 2400 seconds, the LOX tanks are pressurised to 20 bar. At this moment, the engine asks for 650 kg/s using a step function. Valve_Test opens linearly in one second, and the mass flow into the engine builds up. It takes 7 s for the mass flow to settle at 650 kg/s. The mass flow is extremely stable, only deviating 0.01% at the end of the run, while subject to the non-stationary effects native to the ESPSS library. This process can be seen in Figure 5.23.

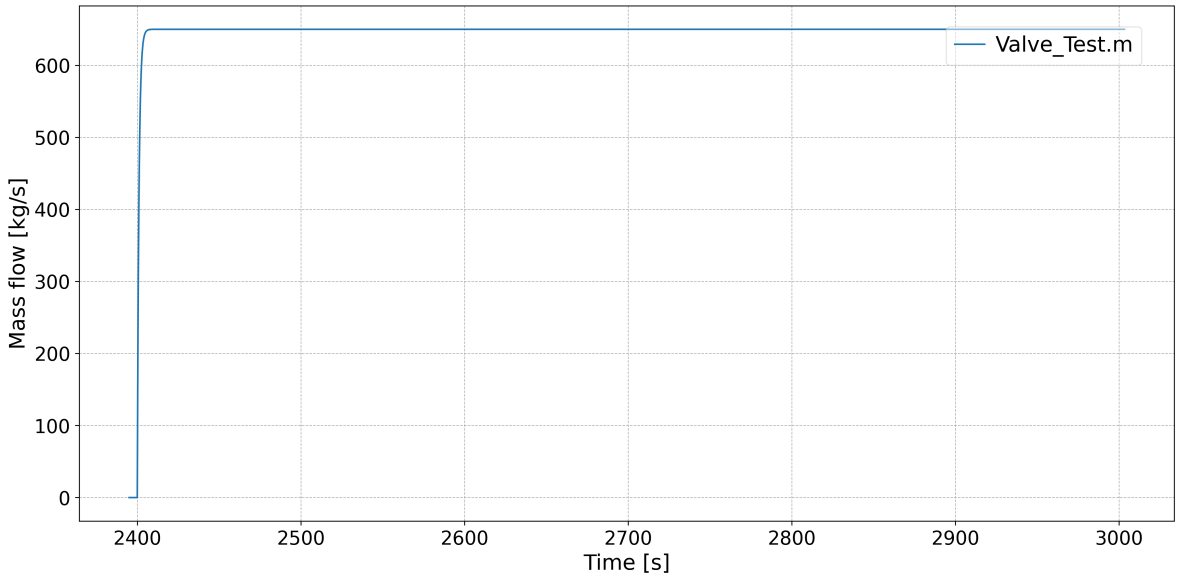

Figure 5.23: Mass flow starting from t=2400

Once the mass flow hits 650 kg/s, the controls of Valve_A start working.Valve_A is crucial to the operation of the bench. This is normally not only one valve, but multiple, focused on carefully managing the pressure of the flow [7][97]. In this study, a single valve was used to simplify the operations. The pressure at the inlet of Valve_A exceeds 20 bar at the beginning. This is because the liquid in Tank A and B is pushing down (gravity) on the liquid further in the pipe. Valve_A is pre-opened at 0.292 to ensure a drop to 4 bar, but this means that as liquid is depleted from the tanks, the valve should open more and more. This is visible in Figure 5.24, where the operations of multiple valves is shown, and Figure 5.25, where the increase in Valve_A opening is visible. In the former, the increase for both pressurisation valves is also shown, showcasing that the N_2 supply, that is decreasing in pressure, needs a higher mass flow to sustain 20 bar in both tanks.

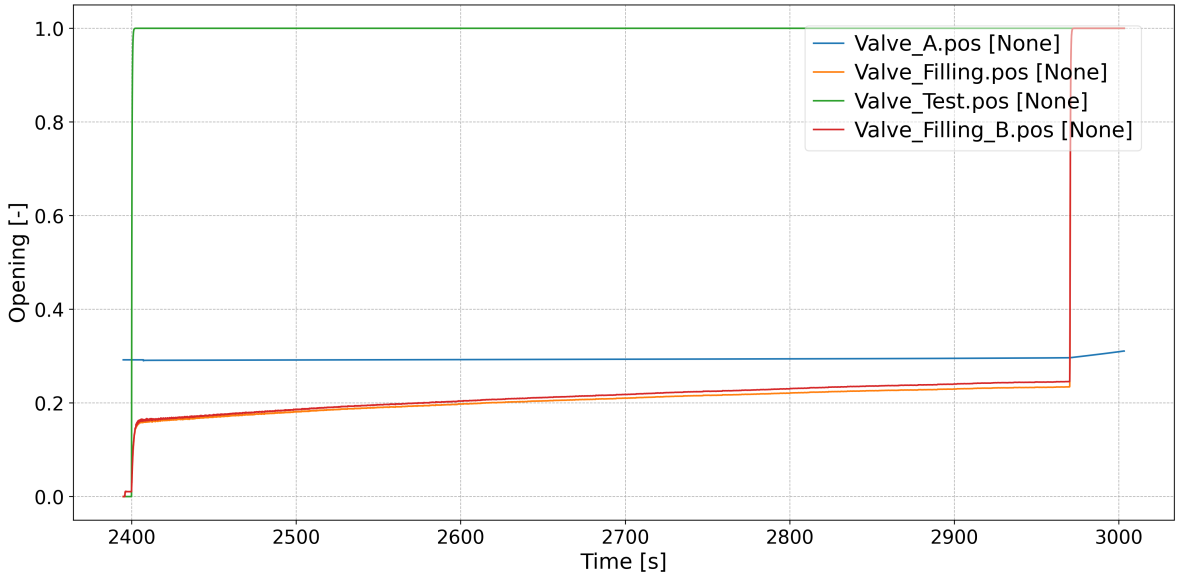

Figure 5.24: Valve position for multiple important valves

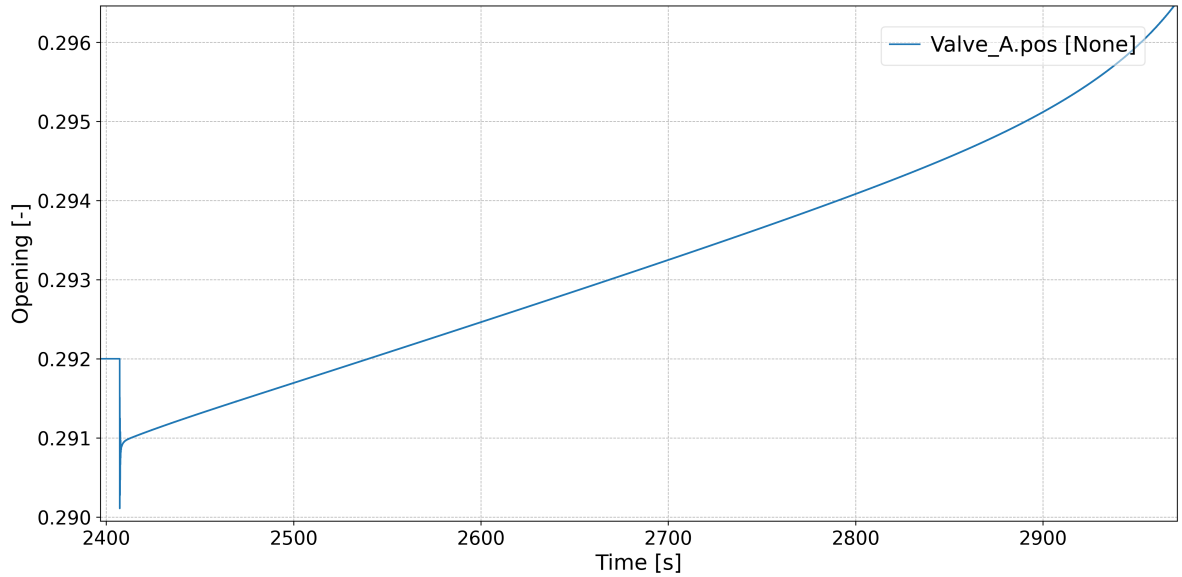

Figure 5.25: Position of Valve_A throughout the run

The pressure at which the 650 kg/s is supplied to the engine starts at 4.03 bar, and drops to 3.88 bar at the end of the run. This happens because the control is not properly tuned. Valve_A adjusts its position based on to ensure a stable pressure, but because of incorrect gain tuning and integral time, the pressure drops slowly. Figure 5.26 clearly shows this pressure drop.

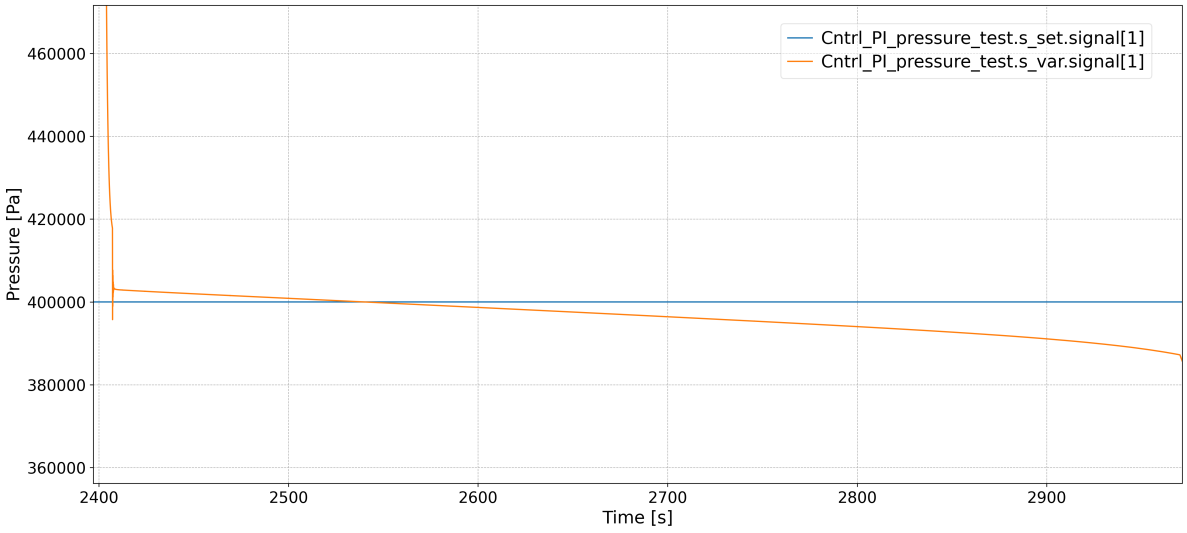

Figure 5.26: Engine supply pressure during the run

The pressure in the tanks stays constant at 20 bar during the entire run, with a maximum error ($|20e5 - P\_Tank|$) of 5 to 10 Pa, or 0.00025%. This is shown in Figure 5.27, where the error is displayed, and Figure 5.28, which shows the tank pressure for Tank_A and Tank_B for the duration of the entire run. Only one line is visible because the pressures are equal.

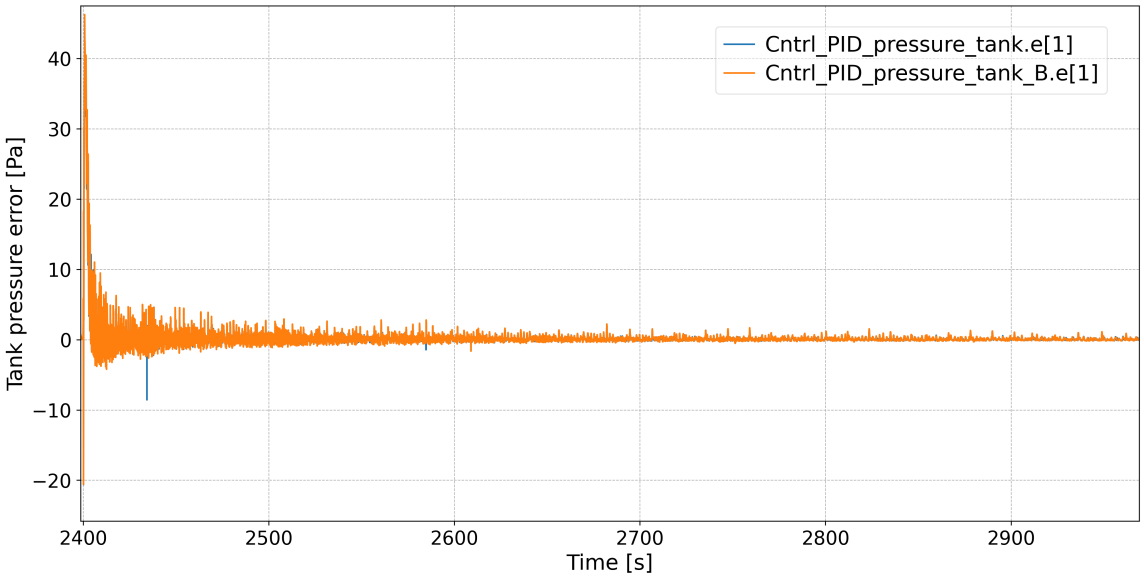

Figure 5.27: Error in tank pressure

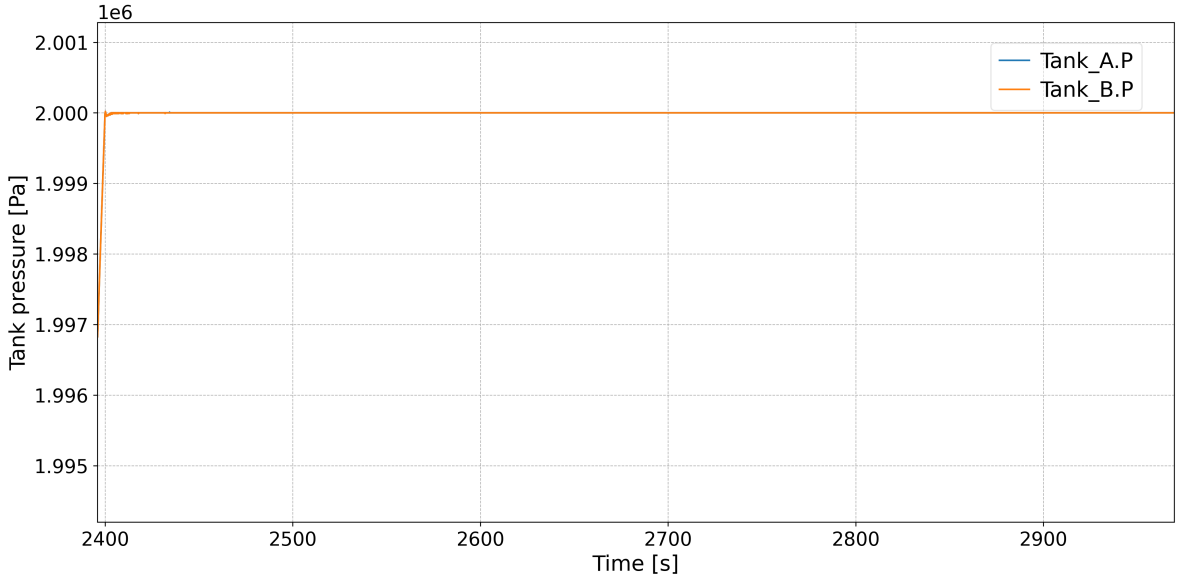

Figure 5.28: LOX tank pressure

After 2970 s, the run abruptly stops because the pressure of the nitrogen tank has dropped to 50 bar. This ends the run. It should be noted that 100 m^3 is not enough nitrogen to both pressurise the tanks and run the test. The testing does not take into account the pressurisation phase, which is separated from the run phase and shown in Appendix B.

The pipes are 220 mm in diameter to ensure the velocity of oxygen stays at 15 m/s. The velocity of LOX in the engine, as well as the velocity of fluids at other points in the system, can be seen in Figure 5.29, where it is obscured by Pipe_inlet_valve_A. The steady decrease of the N_2 tank pressure is visible in Figure 5.30.

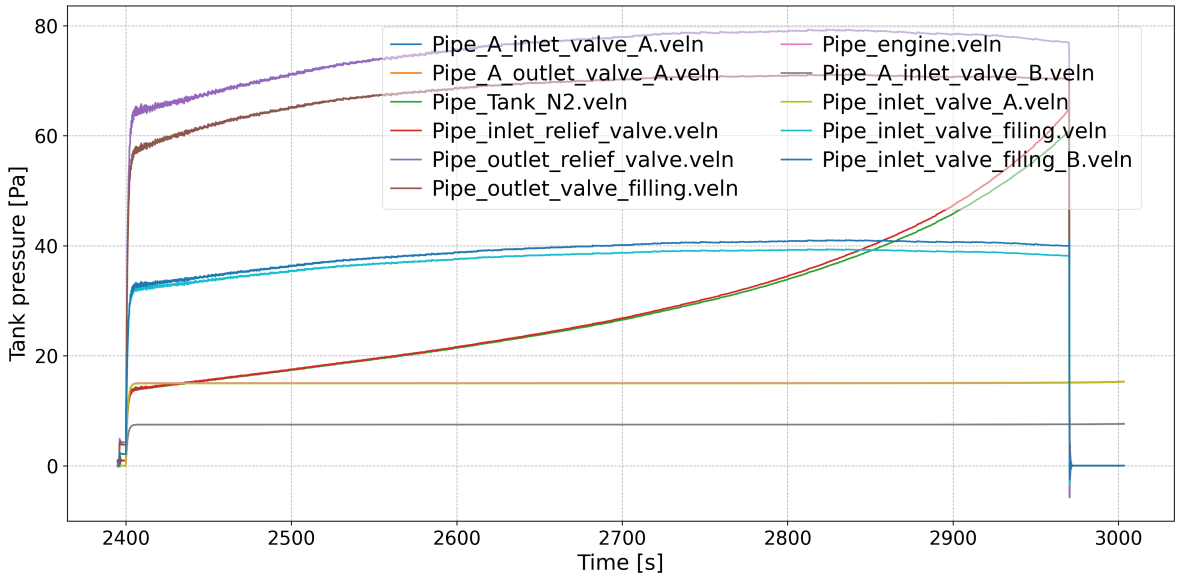

Figure 5.29: Velocity of oxygen and nitrogen in different parts of the system

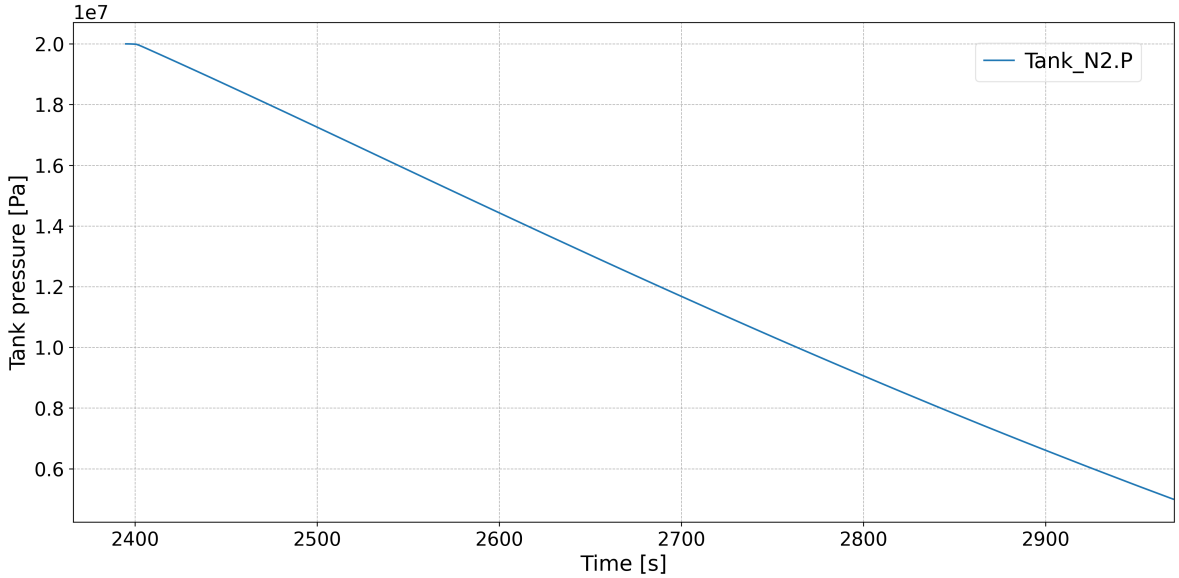

Figure 5.30: N_2 tank pressure

The decrease in tank level can be seen in Figure 5.31. Theoretically, if the nitrogen tank had been larger, the test could have run for 20 more seconds, before the fuel would be between 5 and 10% and the test would be stopped.

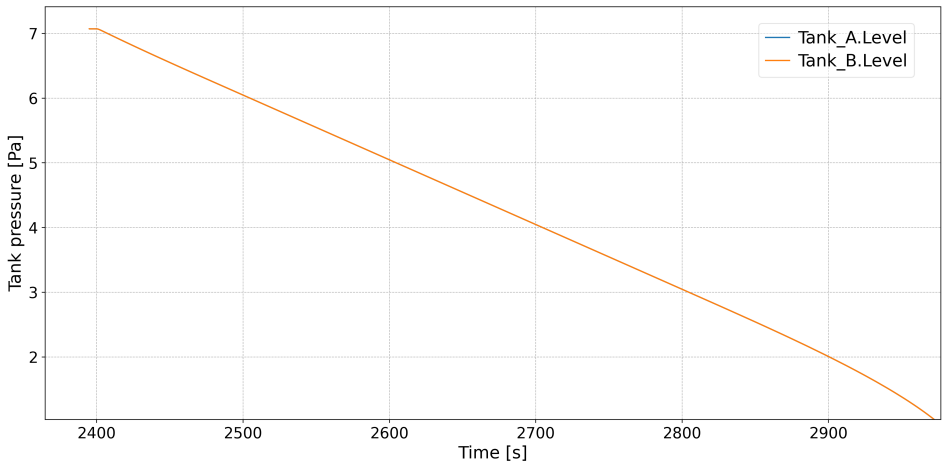

Figure 5.31: Fill level of Tank A and B

Table 5.10: Assessment of pressurisation and feed-system criteria.

Criterion	Target	Met?	Evidence
Tank pressure during pressurisation	Slow ramp-up to 20 bar	✓	Figure 5.17, 2400 s
Relief valve	Drop from 200 bar to 40 bar	✓	Figure 5.27, Figure 5.28, Figure 5.21
Regulated outlet pressure (during test)	4.00 bar ± 5%	✓	Figure 5.26, max 3%
Test mass flow	650 $\mathrm{kg\,s^{-1}}$	✓	Figure 5.23
Additional valve logic	Satisfied	✓	Figure 5.30

Verification

To verify the simulation results, the governing relations from chapter 5 are applied. For steady, incompressible flow in a straight pipe of constant diameter, the pressure drop is described by the Darcy-Weisbach formulation,

$$\Delta p \;=\; f\,\frac{L}{D}\,\frac{\rho u^2}{2} \;+\; \rho g\,\Delta h \;+\; \Big(\sum K\Big)\frac{\rho u^2}{2}, \qquad u \;=\; \frac{\dot m}{\rho A}, \quad A = \frac{\pi D^2}{4}, \quad \mathrm{Re} = \frac{\rho u D}{\mu}.$$

Verification is carried out for liquid oxygen flowing out of Tank A, at a operating pressure of $p \approx 20.3$ bar. The roughness used in the Swamee-Jain approximation is $\varepsilon = 5 \times 10^{-5}\,\mathrm{m}$, which differs from the $\varepsilon = 1.5 \times 10^{-5}\,\mathrm{m}$ value in the Moody chart shown in chapter 5. This reflects the stainless-steel grade assumed in the Ecosim configuration, which has a higher representative roughness than the material used to generate that chart.

$$\dot m = 325\ \mathrm{kg\,s^{-1}}, \quad T = 90\ \mathrm{K}, \quad p_1 = 20.30\ \mathrm{bar},$$
$$D = 0.22\ \mathrm{m}, \quad L = 15\ \mathrm{m}, \quad \varepsilon = 5 \times 10^{-5}\ \mathrm{m}, \quad \Delta h = 0, \quad \sum K = 0.$$

These values, together with LOX properties from taken from CoolProp at 90 K, $p = 20.3$ bar yield

$$A = 0.0380\ \mathrm{m^2}, \quad u = 7.46\ \mathrm{m\,s^{-1}}, \quad \mathrm{Re} = 9.42 \times 10^6, \quad f = 0.0142.$$

Hence,

$$\Delta p_{\mathrm{total}} = f\,\frac{L}{D}\,\frac{\rho u^2}{2} \;=\; 0.309\ \mathrm{bar}, \qquad p_2 = p_1 - \Delta p = 19.991\ \mathrm{bar}.$$

This is exactly the pressure drop observed in the simulation, as shown in Figure 5.32 at 2412 seconds.

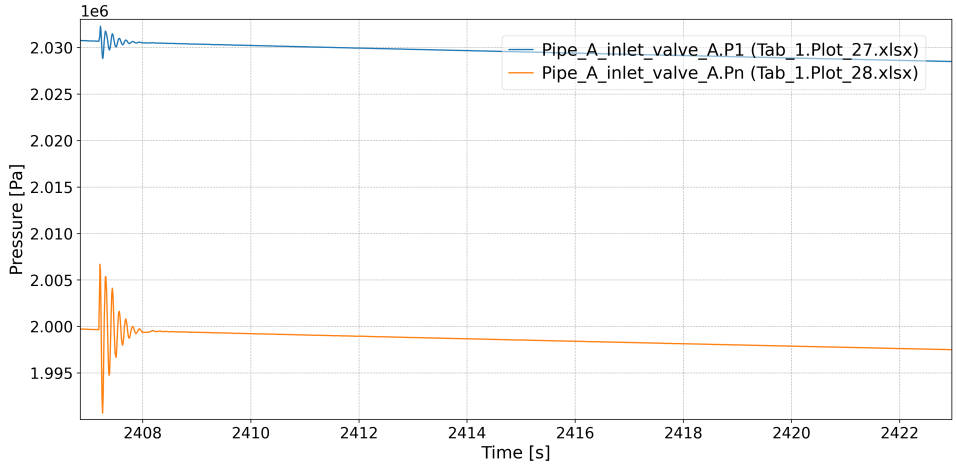

Figure 5.32: Pressure drop in Pipe_A_inlet_valve_A (15 m length, 22 cm diameter)

1210 kg was the amount of nitrogen in the tank at the end of the pressurisation sequence, as shown in Figure 5.20. There are two ways to determine this mass, first using the approximation presented in chapter 5, and then using this same approximation, but with the control volume gas temperatures to compute the post-JT temperature.

(a) Constant post-JT temperature from the buffer. Buffer conditions $T_1 = 205\,\mathrm{K}$, $P_1 = 40\,\mathrm{bar}$ throttled to $P_2 = 20\,\mathrm{bar}$ at constant enthalpy give

$$T_{2,\mathrm{JT}} = 196.55\,\mathrm{K}, \qquad T_{2,\mathrm{est}} = 186.55\,\mathrm{K}.$$

With ullage volume $V_1 = V_t - V_i = 200 - 170 = 30\,\mathrm{m}^3$, the added nitrogen mass to raise the tank from $P_{\mathrm{start}} = 1.01\,\mathrm{bar}$ to $P_2 = 20\,\mathrm{bar}$ at $T = T_{2,\mathrm{est}}$ is

$$\Delta m = \left[\rho_{\mathrm{N_2}}(20\,\mathrm{bar}, 186.55\,\mathrm{K}) - \rho_{\mathrm{N_2}}(1.01\,\mathrm{bar}, 186.55\,\mathrm{K})\right] V_1.$$

From the property library, $\rho_{\mathrm{N_2}}(20\,\mathrm{bar}, 186.55\,\mathrm{K}) = 38.22\,\mathrm{kg\,m^{-3}}$ and $\rho_{\mathrm{N_2}}(1.01\,\mathrm{bar}, 186.55\,\mathrm{K}) \approx 1.83\,\mathrm{kg\,m^{-3}}$. Hence

$$\Delta m = (38.22 - 1.83) \times 30 = \boxed{1{,}091.7\,\mathrm{kg}},$$

(b) Using Figure 5.22. Let $\overline{T}_g$ be the time-average of the ullage temperature during the pressurisation ramp,

$$\overline{T}_g = \frac{1}{t_f - t_0} \int_{t_0}^{t_f} T_g(t)\,dt \approx 170\ \mathrm{K}.$$

$$\Delta m = \left[\rho_{\mathrm{N_2}}(20\,\mathrm{bar}, 170\,\mathrm{K}) - \rho_{\mathrm{N_2}}(1.01\,\mathrm{bar}, 170\,\mathrm{K})\right] V_1.$$

With $\rho_{\mathrm{N_2}}(20\,\mathrm{bar}, 170\,\mathrm{K}) \approx 42.98\,\mathrm{kg\,m^{-3}}$ and $\rho_{\mathrm{N_2}}(1.01\,\mathrm{bar}, 170\,\mathrm{K}) \approx 2.01\,\mathrm{kg\,m^{-3}}$,

$$\Delta m = (42.89 - 2.01) \times 30 = \boxed{1{,}226.4\,\mathrm{kg}},$$

which matches the Ecosim result to within $\leq 1.5\%$. The approximation thus nudges the result in the right direction, but is insufficient to get close enough to the result. Diving further into the verification would impede progress in other aspects of this thesis, which are more important for the high-level design. The validity of this tool has been proven over time, as it is an industry favourite. This does not mean further verification is unnecessary, however it is the reason why no verification is performed.

5.5.4. Conclusions from Simulation

The EcosimPro/ESPSS runs demonstrate that the baseline LOX architecture achieves the principal functional requirements for a 2 MN test bench at sea level. First, the dual run-tank configuration can be brought to 20 bar with a controlled, low-risk ramp (2400 s) using N_2 ullage pressurisation. The

tank-pressure PID holds 20 bar with an error of 10 Pa during the hot run, indicating steady operation (Figure 5.27, Figure 5.28). Second, the feed system stably delivers the target 650 $\mathrm{kg\,s^{-1}}$ at an engine-interface pressure of approximately 4 bar. The mass flow settles within ∼7 s after Valve_Test opening and remains within ±0.01% of the command despite ESPSS non-stationary effects (Figure 5.23). Third, the line losses are consistent with first-principles hydraulics: the measured Δp across the 15 m, 0.22 m line matches the Darcy-Weisbach prediction using the Swamee-Jain friction factor at the simulated Reynolds number (Figure 5.32).

Operationally, the runs reveal two important implications. Firstly, the 100 $\mathrm{m^3}$ at 200 bar N_2 pressurant is not enough for a combined pressurisation+600 s hot run at 650 $\mathrm{kg\,s^{-1}}$: the pressurant depletes to ∼50 bar around $t \approx$2970 s, terminating the sequence (Figure 5.30). This is however after a second initialisation: the pressurisation and hot run were initialised separately, thus the volume should have run out earlier. This sets a clear requirement for a larger N_2 storage. Secondly, the outlet pressure regulation exhibits a slow drift from 4.03 bar to 3.88 bar over the run (Figure 5.26), attributable to conservative PI tuning and changing hydrostatic head as the tanks empty. This is not a fundamental limitation, but it highlights the need for a focus on control tuning.

Taken together, the simulations verify the bench can ramp and hold ullage pressure at the demanded set-point, meet the peak mass-flow requirement with relatively stable delivery at the interface, and keep pipe velocities within the adopted safety limits through the selected diameters. These are the core functional requirements for the fluid supply system.

Limitations of the simulations

The present results reflect the fidelity and scope of a deliberately streamlined EcosimPro/ESPSS model whose objective is feasibility and sizing rather than full operational certification. The model as presented in this chapter has several limitations, which are discussed below.

First, the control architecture is intentionally minimal. A single regulating element (Valve_A) is tasked with outlet pressure control where industrial benches commonly employ a staged train of valves. As a consequence, the slow drift from 4.03 bar to 3.88 bar is explained by conservative PI tuning and changing hydrostatic head as tanks empty, but other real-world contributors are not represented in this simplified loop. A staged valve sequence would yield different results than a single valve.

Second, the scenario coverage is narrow by design. Although the system overview motivates that the same architecture translates to CH_4 and H_2, the pressurisation and hot-run shown and verified are for LOX only. Methane and hydrogen differences are discussed qualitatively, but no full transient runs with those fluids are included in this section, so cross-propellant conclusions remain inferential.

Thirdly, the verification was carried out only for the pressurisation and feed simulations because these cases admit fixed, well-posed checks: for a commanded 650 $\mathrm{kg\,s^{-1}}$ and a ∼4 bar interface, line losses follow Darcy-Weisbach (with Swamee-Jain), ullage temperature follows a JT estimate, and mass/energy balances can be computed independently and compared one-to-one with the EcosimPro results. By contrast, the other runs in this chapter deliberately use time-varying conditions: valve openings evolve, and the PI loop retunes the effective flow area, so the state is path-dependent. There is no stationary 'reference point' to verify against. Any check would require time-resolved acceptance data for the exact command trajectory, which is outside the scope here. Therefore, those transients are reported as operability evidence rather than as verification cases.

Lastly, the pressurant supply sizing is demonstrated with a single storage configuration, while the 50 litre tanks depleting might cause a different pressure profile, and there is an operational split between 'pressurisation' and 'hot run'. The termination around $t \approx$2970 s due to the N_2 bottle reaching 50 bar highlights the iterations on storage volume are not complete. Because the pressurisation phase is modelled separately from the hot run in the figures, the exact depletion crossover for a continuous

end-to-end timeline is not captured in one pass. The conclusion that $100\,\mathrm{m}^3$ at $200\,\mathrm{bar}$ is insufficient is correct, but the buffer margin necessary for a full operation sequence is not yet quantified.

6

Site Selection

In this section, a high-level, qualitative trade-off approach is applied to narrow down the candidate countries for site construction. Given that many of the relevant aspects, like political, strategic, and regulatory aspects, are inherently qualitative, a full systems engineering trade-off was deemed unnecessary. Instead, the proposed approach relies on an iterative screening process based on key criteria extracted from customer requirements, especially CR-3.

Initially, quantitative measures such as cost serve as a primary filter, as these are easiest to compare. For this, average labour cost data for European countries is used. Countries that clearly exceed acceptable cost thresholds are immediately excluded from further consideration. This first-level elimination is efficient, as it ensures no unnecessary considerations are done in further stages of the trade-off.

Following this initial cull, the remaining countries are further evaluated using additional qualitative factors, which will be discussed later. The goal of the analysis is not to fix the country selection, but rather to provide an insight into which countries should be considered.

6.1. Labour Cost

For the assessment of the performance of countries based on the operational cost for a potential test bench, the UNECE statistics for gross average monthly wage in purchasing-power-parity dollars is used [115]. Furthermore, as an initial benchmark, the statement by ESA professionals that "for technology demonstration and maturation projects the balance of cost should be on the technology and not on the test infrastructure, as well as the fact that currently the principal engine test facility used by larger engine projects is based in Germany (DLR Lampoldshausen)" [1], will be used to create the following criterion: the gross average monthly wages in the country of interest shall not exceed 80% of that of Germany. 80% is chosen, because this still leaves a large pool of countries to choose from, but the cost reduction regarding wages is still a meaningful amount. Labour cost is a big factor in the operation of a test bench, and can account for a third of the yearly operational expenditure of a test facility [54]. Simply looking at countries that have a lower wage than Germany is not going to have a large impact unless the reduction of salary budget is significant.

The countries that will be assessed in this analysis, and their respective gross average monthly wages are shown in Figure 6.1. The bar plot shows countries exceeding the 80% benchmark in red, and countries below in green. Changing the benchmark between >70 and 90% yields the same result.

[1] Personal correspondence with Kate Underhill and Jean-Noel Caruana

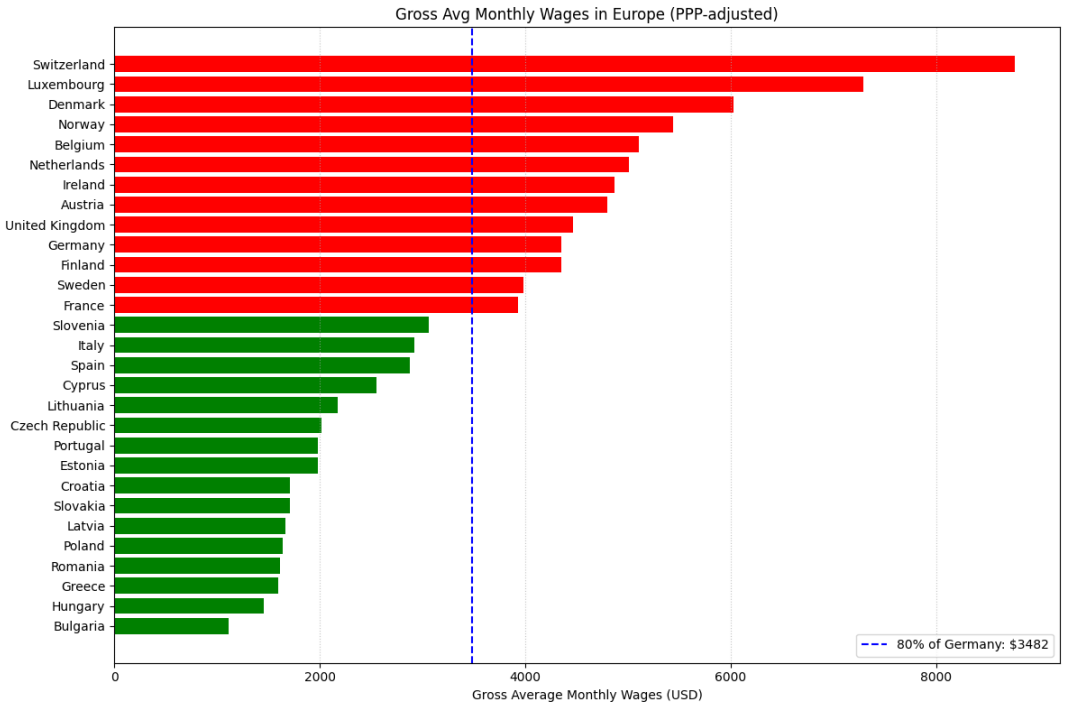

Figure 6.1: Gross Average Monthly Wages by Country

The result of this first iteration is that there are only 16 countries left to consider, from an initial 29. The countries are listed below, in Table 6.1

Table 6.1: European countries with average monthly wages below 80% of Germany's (in PPP USD)

Bulgaria	Hungary	Greece	Romania
Poland	Latvia	Slovakia	Croatia
Estonia	Portugal	Czech Republic	Lithuania
Cyprus	Spain	Italy	Slovenia

6.2. Ease of Doing Business

In 2020, the World Bank Group released a ranking of 190 economies on their ease of doing business (it was the last version of the Ease of Doing Business ranking, because of corruption around some Middle-Eastern countries). The ranking assesses the conductivity of the regulatory environment to starting a business. Among the criteria in this ranking is the category 'Dealing with construction permits', which is very relevant to this project. A smooth and streamlined process to construction will ensure that the requirement to be operating in three years is met. The respective ranking of these countries is given in Table 6.2. The lower the rank, the better the country performs in the category. [118]

Table 6.2: Dealing with Construction Permits: Rankings and Scores from Doing Business 2020

Country	Rank	Score
Poland	39	76.4
Bulgaria	43	75.9
Portugal	60	73.2
Spain	79	70.8
Greece	86	69.5
Italy	97	68.3
Hungary	108	67.0
Slovenia	119	65.3
Cyprus	125	64.2
Slovakia	146	59.4
Romania	147	58.4
Czech Republic	157	56.2

6.3. Population Density and Logistics

To minimize external disturbance from test-stand operations, site selection was guided by a quantitative measure of regional 'remoteness'. Eurostat's NUTS 2 population and land-area datasets were combined to compute density (inhabitants per km^2) for every NUTS 2 unit across the candidate countries. [31]

For each nation, its NUTS 2 regions were ranked by ascending density, and the three least-populated regions were identified. The mean of those three densities then defined a country-level remoteness index, ensuring that isolated locations drive the score.

As the dataset still contains 12 countries, the computed population density of Portugal is given as an indication in Figure 6.2.

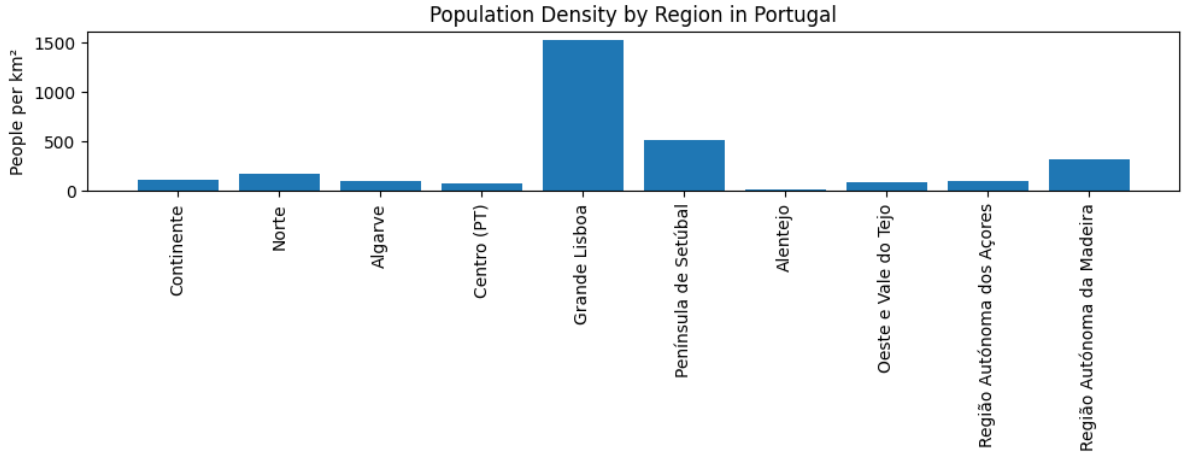

Figure 6.2: Population Density by Region in Portugal

To reflect the need for logistics, two transport/infrastructure metrics (motorway density and railway density) were incorporated. All three indicators (remoteness index, motorway density, railway density) were normalized to a 0 to 1 scale and combined into a single Suitability Score according to project-specific priorities: 45% weight on remoteness, 35% on motorway connectivity, and 20% on rail access. The results of this analysis can be seen below, first showing how each metric was analysed.

Regional remoteness was quantified using Eurostat NUTS 2 population P_r and area A_r data to compute regional density

$$d_r = \frac{P_r}{A_r}.$$

For each country c, the three NUTS 2 regions with lowest d_r were selected (denoted S_c) and an area-weighted average density was calculated:

$$\text{Remoteness}_c = \frac{\sum_{r \in S_c} d_r \, A_r}{\sum_{r \in S_c} A_r}.$$

Larger values of Remoteness_c correspond to greater isolation, which is a pro when considering the noise of a 2 MN rocket engine.

Transport connectivity metrics were drawn from the European Environment Agency [29], comprising total motorway length and total railway length per 1000 km^2, denoted MotorwayDensity_c and RailwayDensity_c. Each raw indicator $X_{i,c}$ with $X_{\text{Pop},c} = -\,\text{Remoteness}_c$, to ensure that higher isolation yields a larger score, was rescaled to the $[0, 1]$ interval via a Min-Max transform:

$$S'_{i,c} = \frac{X_{i,c} - \min_c X_{i,c}}{\max_c X_{i,c} - \min_c X_{i,c}}, \quad i \in \{\text{Pop}, \text{Motorway}, \text{Railway}\}.$$

The composite Suitability Score is given by

$$S_c = 0.45\, S'_{\text{Pop},c} + 0.35\, S'_{\text{Motorway},c} + 0.20\, S'_{\text{Railway},c}.$$

These scores were determined as follows:

- **Population density (0.45)** For a 2 MN engine stand, blast/noise hazard distances, public exposure, and social licence to operate dominate site feasibility. Low surrounding population directly reduces exclusion zones, mitigations, and legal challenge risk; hence the largest weight.
- **Motorway access (0.35)** Day-to-day logistics depend primarily on road: oversize components (turbomachinery, ducts, valves), frequent dangerous-goods traffic (LOX, LH_2/CH_4, LN_2/He), and emergency access. Proximity to high-capacity roads lowers transport cost, schedule risk, and response times, thus resulting in a substantial weight.
- **Railway access (0.20)** Rail is valuable for bulk and occasional heavy lifts, but is less time-critical and more substitutable via road than motorway access. Useful, but not decisive in most European contexts; thus a supportive, lower weight.

Robustness of the resulting country ranking was assessed via a Monte Carlo procedure. Weight vectors $\mathbf{w} \sim \text{Dirichlet}(100\,[0.45, 0.35, 0.20])$ were drawn $n_{\text{sim}} = 1000$ times and used to compute perturbed scores

$$S_c(\mathbf{w}) = \sum_i w_i \, S'_{i,c}.$$

Distributions of $\{S_c(\mathbf{w})\}$ were summarised by mean, standard deviation and quartiles, and visualised in a box-plot, shown in Figure 6.3 (for k=3), where k is the number of sparsest regions used to create the baseline for population density. The choice for three (k=3) NUTS regions is backed up by the stability that can be seen in Figure 6.4. Furthermore, having more than one region is essential for proper selection of a country, because this increases the probability that a proper site can be found in this region.

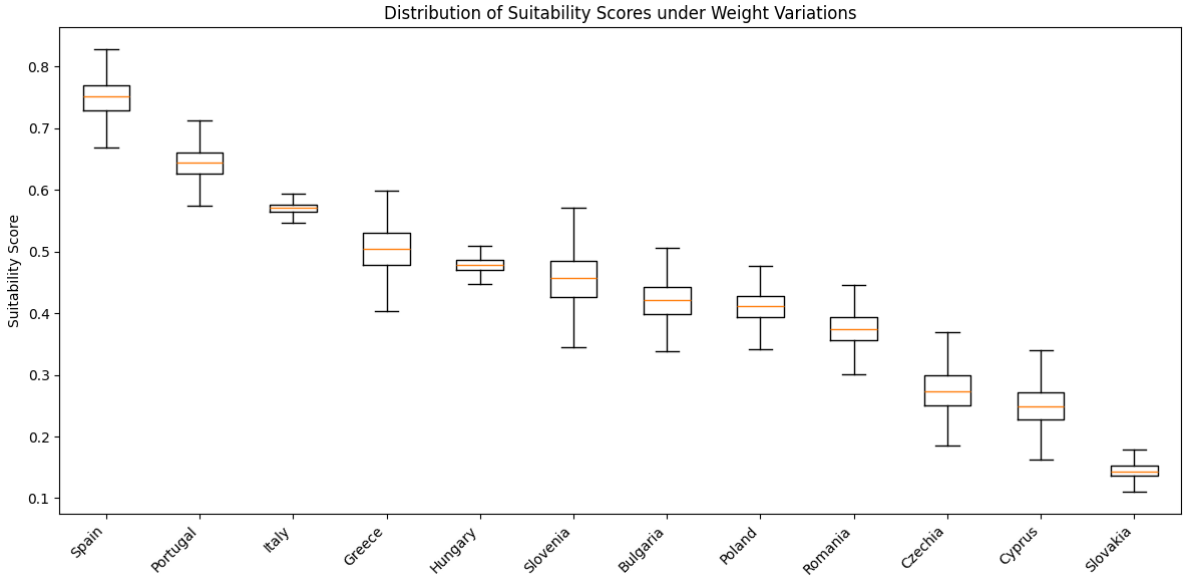

Figure 6.3: Distribution of Suitability Score by Country under Weight Variations

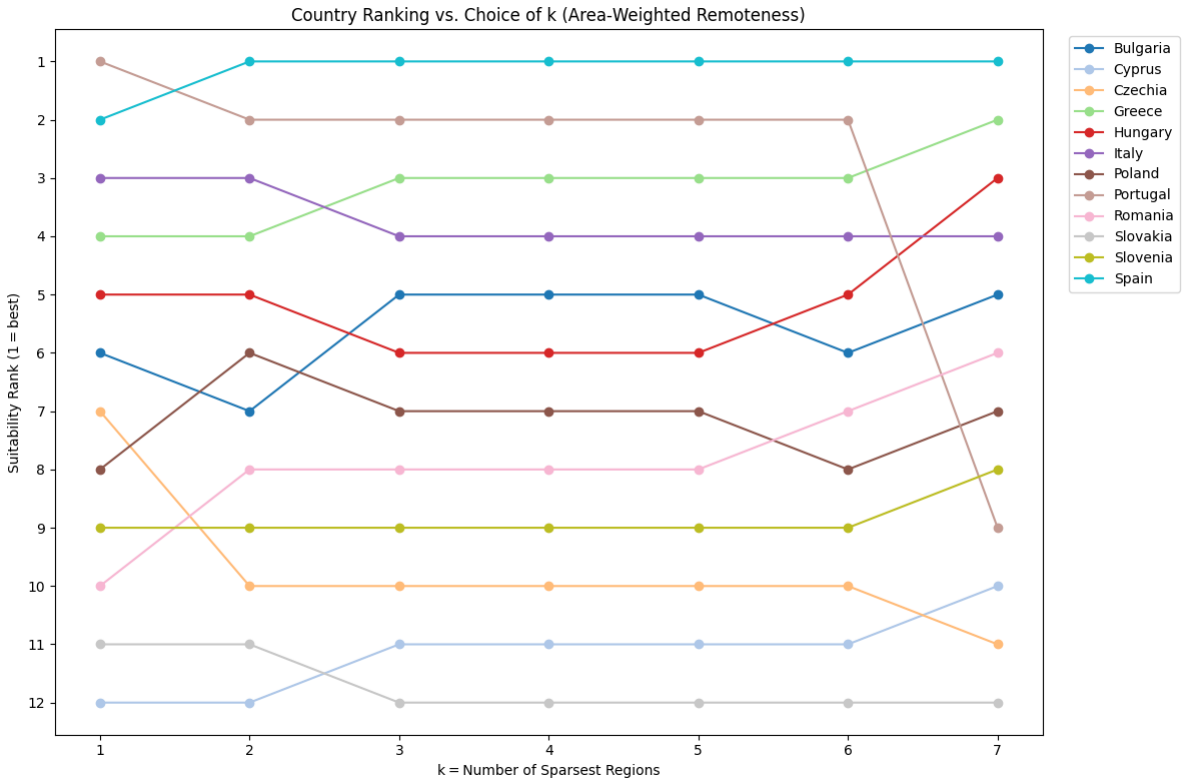

Figure 6.4: Stability of the Country Selection based on k-Selection

6.4. Availability of Skilled Workforce

A test bench cannot operate without operators. For these operators, it is essential that they have a background in their respective fields. Standard practice is to have someone with a university degree as responsible person for the test bench. The level of education is preferable tertiary for the people working on the test bench. Tertiary education means education after high school. This can be university, but also vocational schooling or any other type of education after high school. This is why the tertiary

education attainment rate per country is relevant for shortlisting countries. These rates are shown in Table 6.3.

Table 6.3: Tertiary Education Attainment Rates (Age 25–64) [88]

Country	Rate (%)
Spain	41.0
Slovenia	40.0
Greece	35.0
Poland	34.0
Cyprus	33.2
Portugal	31.0
Bulgaria	30.0
Hungary	29.0
Slovakia	29.0
Czech Republic	27.0
Italy	20.0
Romania	20.0

This data is used under the assumption that in a country with a higher tertiary rate of education, it is easier to get a skilled workforce. The size of the population is not taken into account, because the criterion is how likely is it that any candidate will already be qualified, which depends on the share of tertiary-educated adults rather than the total head-count. If a specific number of hires per year needs to be ensured, the population of working-age adults can be incorporated to get absolute figures.

6.5. Final Results

By combining the results from all previous subsections, a shortlist of potential countries can be made. To integrate the four quantitative indicators, which are labour cost, ease of doing business, site suitability, and workforce education into a single metric for each country, the following steps are performed:

1. **Normalization of individual scores.** The first step is to derive four normalized indices on a common scale [0-1]. The logic behind this derivation is shown below.

$$\tau = 0.8\, W_{\mathrm{DE}}, \quad W_{\mathrm{DE}} = 4353 \tag{6.1}$$

$$\mathrm{CostScore}_i = \frac{\tau - W_i}{\tau} \tag{6.2}$$

$$\mathrm{BizScore}_i = \frac{P_i}{100} \tag{6.3}$$

$$E_{\mathrm{Canada}} = 63\%(\text{Canada has the highest tertiary education rate in the world}) \tag{6.4}$$

$$\mathrm{EduScore}_i = \left(\frac{E_i}{E_{\mathrm{Canada}}}\right) \tag{6.5}$$

   - W_i: average monthly wage of country i (in PPP USD).
   - P_i: raw permit-score (0-100) for country i.
   - E_i: tertiary-education attainment rate (%) for country i.
   - E_{Canada}: reference tertiary-education rate for Canada.

2. **Composite score under scenario s.** For each weighting scenario s with weight vector

$$(w_c^s,\, w_b^s,\, w_s^s,\, w_e^s),$$

   the composite score for country i is

$$S_i^{(s)} = w_c^s\, \mathrm{CostScore}_i + w_b^s\, \mathrm{BusScore}_i + w_s^s\, \mathrm{SuitabilityScore}_i + w_e^s\, \mathrm{EduScore}_i. \tag{6.6}$$

3. **Weight-scenario generation.**
   The weights in weight vector are determined as follows:

   - Cost (30): The cost of labour is one of the driving requirements of building a new test bench altogether. The weight of this requirement is determined as such.
   - Business (30): Building a test bench is a difficult endeavour that requires complex permits and multi-agency approvals. Countries with clear, predictable, and timely administrative processes cut schedule risk and uncertainty, hence the high weight.
   - Suitability (20): Adequate safety/exclusion zones, favourable topography, logistics infrastructure, and low natural-hazard exposure determines feasibility and performance for a 2 MN staged-combustion stand. It is important, but some deficits can be engineered at cost, justifying a medium-high weight.
   - Education (20): Availability of experienced propulsion/test engineers, cryogenic technicians, controls/safety specialists, and QA reduces ramp-up time and incident risk. This criterion is significant but augmentable via training and mobility, resulting in a 20% weight.

   Starting from a baseline weight vector

   $$\mathbf{w}^{(0)} = (w_c, w_b, w_s, w_e) = (0.30, 0.30, 0.20, 0.20),$$

   the following scenarios are considered:

   - *Original:* keep $\mathbf{w}^{(0)}$.
   - *Equal:* $\big(0.25, 0.25, 0.25, 0.25\big)$.
   - k*-Heavy* (for $k \in \{\text{cost}, \text{biz}, \text{suit}, \text{edu}\}$): double the kth weight and scale the others to sum to 1:

   $$w'_k = 2\, w_k, \tag{6.7}$$

   $$w'_i = w_i \, \frac{1 - 2\, w_k}{1 - w_k} \quad (i \neq k). \tag{6.8}$$

   This preserves the ratios among the non-bumped weights.

4. **Composite score and ranking.**
   For each country i and scenario s with weights $(w_c^s, w_b^s, w_s^s, w_e^s)$, compute

   $$S_i^{(s)} = w_c^s \, \text{CostScore}_i + w_b^s \, \text{BizScore}_i + w_s^s \, \text{SuitabilityScore}_i + w_e^s \, \text{EduScore}_i.$$

   Countries are then sorted by $S_i^{(s)}$ (highest first) and assigned integer ranks (1 = best).

Weight Scenarios

The different weight scenarios that have been established following the principles of the previously described step 3 result in the weight vectors given in Table 6.4.

Table 6.4: Weight Vectors

Scenario	Cost	Business	Suitability	Education
Original	0.30	0.30	0.20	0.20
Equal	0.25	0.25	0.25	0.25
Cost-focus	0.60	0.1714	0.1143	0.1143
Biz-focus	0.1714	0.60	0.1143	0.1143
Suit-focus	0.225	0.225	0.40	0.15
Edu-focus	0.225	0.225	0.15	0.40

Using these weights, it is possible to generate the composite score for each country, for each scenario. This is shown in Figure 6.5.

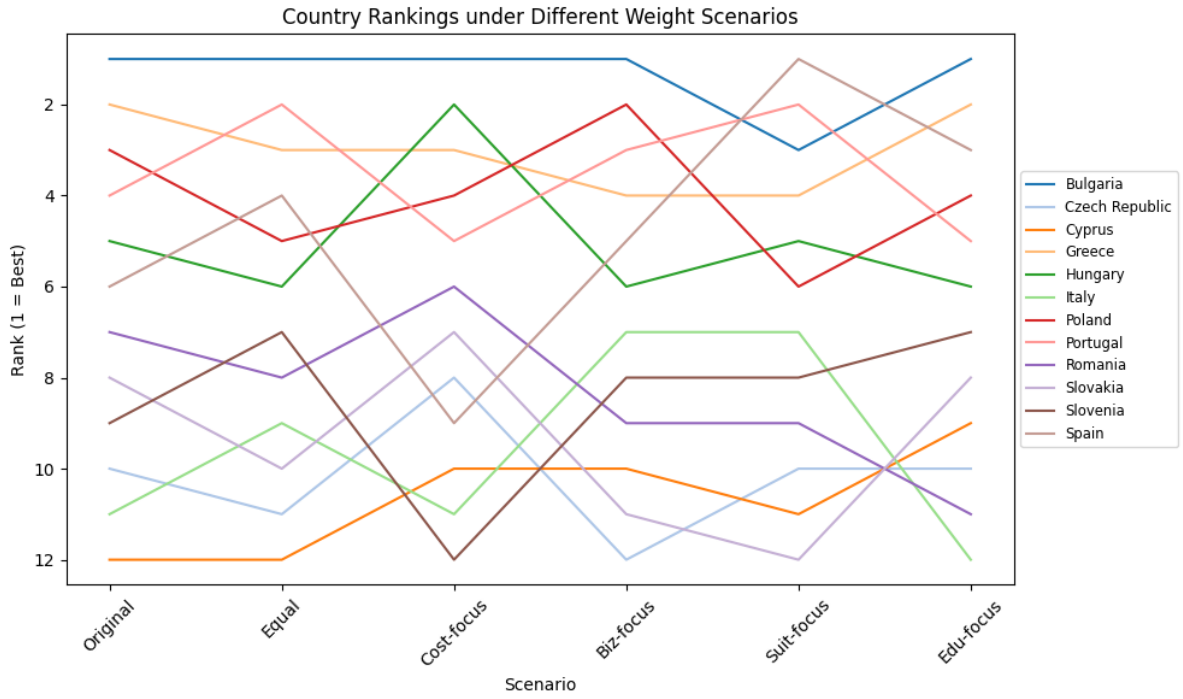

Figure 6.5: Ranking of Countries by their Composite Score, per Scenario

By aggregating the composite ranks from all six scenarios and computing the average rank for each country, we obtain the following ordered list (lowest average rank = best):

Country	Average Rank
Bulgaria	1.33
Greece	3.00
Portugal	3.50
Poland	4.00
Spain	4.67
Hungary	5.00

6.5.1. Shortcomings of the Selection

There are a few shortcomings to this method of country shortlisting. These problems are listed below, in no particular order.

- Short supply lines are important to minimise cost of propellant, but this is not quantifiable. The availability of liquid methane, liquid hydrogen and liquid oxygen can be a deal-breaker for the selection of a country: even though Bulgaria has low wages, a few low density regions and good overall infrastructure, if there are no LOX or LCH4 plants, the test bench cannot be built there.
- The analysis of population density would have been better with the NUTS 3 regions, because this divides the country in even more regions. When looking at SpaceX's McGregor test facility, it is indeed quite in the middle of nowhere, but Waco, a city with 150,000 inhabitants, is still within 30 km. Ideal data would have been a Gini coefficient of the degree of urbanization per NUTS 3 region, along with its population density, to assess the availability of city clusters in relative proximity to the test site. Having cities close means that the infrastructure is better, and coming back to the previous shortcoming, better infrastructure and (relative) proximity to a city increase the chances for a working propellant infrastructure, and it can be easier to retain employees. These employees can live in the city, and don't have to live in the middle of nowhere to go to work. Lastly, the terrain of the respective regions is not taken into account. Building a bench in a sparsely populated mountainous area is a lot more costly than on flatland.

- For the analysis on infrastructure, only nationwide numbers are available on motorway and railway density. There is therefore no information on the density of these two criteria in the 'sparsest regions', rendering conclusions uncertain. Regional data, when available, can refine and potentially strengthen these conclusions.
- The 'Ease of Doing Business' metric, and then especially the ease of getting a construction permit, is a general metric that is in this case used to describe a quite intricate process. The fact that tanks that can explode, containing liquids (gases at room temperature) that are bad for the environment, are on the premises might make it more difficult to get permits in some countries than in others.
- Export control rules are largely the same in Europe, but some countries have extra strict policies when it comes to their equipment being transported out of the country. France and Italy are examples of countries that have stricter export control. This would argue in their favour, because a lot of aerospace companies making engines in Europe are based in one of these two countries.
- (Geo-)Politics are not taken into account. This would require a scrutinization of the entire political history and current political course of the country. Other large developments, especially economic development, are also not taken into account. This would be an economics thesis by itself. The Polish economy is steadily growing, as are the Polish wages. It is not unlikely that in 10 to 15 years, the wages in Poland are on par with the wages in Western Europe. This would make Poland a significantly less attractive option than a country with a stagnant economy, where wages are low and will remain on the low end of European wages.
- Military test sites can provide a remote test location to local, regional, or national test companies. Old military sites often already have some of the necessary infrastructure, like anchored, reinforced concrete walls, and proper roads that lead to the site. This makes them very feasible locations, but they also tend to be nationalistic in their approach. Testing an Italian engine on an old French military base might cause diplomatic issues that would rather be avoided, or rule out the testing from happening at all. A country with a lot of abandoned military bases would be a good option. The same holds for mines, as these already have the necessary documentation surrounding explosives that is necessary to build a test bench, and noise constraints are typically less stringent.
- Heritage in propulsion testing is not considered, even though this is a very important metric. Building a bench is significantly easier if you have the experience readily available in your country, rather than starting from scratch. Heritage is difficult to quantify, but when considering the countries in the final selection, this could be an argument to choose Poland, where ILOT is experienced in testing (smaller scale) engines, and Spain, where PLD, a recent winner of the European Launcher Challenge (ELC), tests their engines.

7

Cost Modelling

Building a test bench is, based on historical data, not a cheap endeavour. The scarce data that is available sketches an image of concrete and steel superstructures that are 60 years old and that were built in a time when budget did not matter: the Cold War and the associated Space Race. The transparency of cost towards the public was non-existent, thus there is no information on the cost of benches that were built in this period. They would also not be proper representations of the current reality: as budget was not an issue, building a cost-effective bench was not really on the agenda. Furthermore, the capacity that the benches were built for at the time is exorbitant. As an example, the Stennis B test complex was designed for a thrust of 11 million lbf, approximately equivalent to 48.9 MN, or 24 times the capacity of the bench considered in this thesis. In this chapter, the cost of the bench will be assessed by using a dual approach. First, a top-down approach is performed, after which a bottom-up approximation is done based on the PBS and ESA asset information.

7.1. Top-Down Cost Approximation

To know the cost of a propulsion test bench, it is necessary to know the costs of the subsystems, add them up and add construction cost. But the cost of these subsystems is not known, and the design is not in-depth enough to approximate it. It is however possible to use information from benches built in other parts of the world, or Europe, of which there is cost data available. With this cost data, a parametric model can be built [81]. The input data for this model was acquired through extensive research, and is gathered in Table 7.1.

Region	Test Stand	Currency	Amount	Cost Type	Thrust Range	Orientation	Year	Source
USA	NASA A-3 (SSC)	MUSD	349.0	Full	Up to 4.4 MN	Vertical	2014	[74], [70]
USA	NASA B-2 (SSC)	MUSD	230.0	Partial (Renovation)	Up to 13.3 MN	Vertical	2023	[75], [70]
USA	NASA A-2 (SSC)	MUSD	267.0	Partial (Modernization)	2.9 MN to 14.7 MN (Upgrade)	Vertical	2023	[109]
USA	Stand 4670 (MSFC)	MUSD	62.5	Partial (Refurbishment)	3.3 to 4.4 MN	Vertical	2019	[77], [78], [28], [60]
USA	USAF 2-A (Edwards)	MUSD	18.5	Partial (Refurbishment)	Up to 2.05 MN	Vertical	2004	[1]
Europe	DLR P5.2	MEUR	70.0	Full	0.18 MN	Vertical	2023	[39]
India	Semi-cryogenic Integrated Engine and stage Test facility (SIET)	MINR	7400.0	Full	Up to 2.6 MN	Vertical	2016	[12], [94], [99], [3], [14], [53]
China	Vertical High-Altitude Simulation Test Stand	N/A	-	-	6.9 MN	Vertical	-	[120]
Russia	NPO Energomash	N/A	-	-	Up to 1.92 MN	Vertical	-	[110]

Table 7.1: Overview of Rocket Engine Test Stands by Region

Notes: Amounts are in the stated currencies and millions thereof (MUSD, MEUR, MINR).

For the Russian and Chinese bench, hardly any information is available. These were added for completeness of the table, when it comes to countries developing high-thrust engines. All costs mentioned in the table can be found in the sources mentioned in the table, except for the cost of the Indian test bench, the MSFC 4670 stand and the A-2 stand.

The cost for the Indian bench was deduced using [12], [94], [99], [3], [14], and [53]. It is stated that India initiated three space projects at a cost of ₹1800 crore[1]. The three projects are the PSLV Integration Facility, a Trisonic Wind Tunnel and the Semi-cryogenics Integrated Engine and stage Test facility (SIET). Firstly, the PSLV Integration Facilities, is a project costing ₹475 crore. The cost of the Trisonic Wind Tunnel was estimated using the Current Replacement Value (CRV) of a trisonic wind tunnel that is used at Marshall Space Flight Center. Using a value of $ 15 million for this trisonic wind tunnel (MSFC TWT)[12], the cost of the Indian Trisonic Wind Tunnel can be established. This was done the following way:

$$\left.\begin{array}{l}\underbrace{(15 \times 0.5)}_{\substack{\text{(1) Base}\\ \text{cost [USD]}}} + \underbrace{(15 \times 0.5 \times 15)}_{\substack{\text{(2) Variable}\\ \text{cost [USD]}}}\end{array}\right\} \times \underbrace{0.86}_{\substack{\text{(3) Exchange}\\ \text{rate [USD-EUR]}}} \times \underbrace{\frac{0.55}{1.30}}_{\substack{\text{(4) Regional}\\ \text{adjustment}}} = €43.66 \text{ million (2016)}$$

The factors mentioned in the equation above are the following:

(1) Base cost: Original cost (15 M) x fixed cost factor (0.5). Approximately 50% of the costs are fixed for big construction projects. This means that 50% of the 15 million can be considered as the first factor of cost.

(2) Variable cost: The other part of the cost is variable. As the two wind tunnels are not of similar size, the Indian one being significantly larger than the American one, the diameter of the tunnels is compared, and a factor is associated to this. $\frac{5.4m}{0.35m} \approx 15$, which will be multiplied by 15, and 0.5 as it represents 'the other 50% of the cost' [2].

[1] A crore is 1,00,00,000 rupees, or 10,000,000 when formatted as the decimal quantity.
[2] Established in discussion with ESA cost engineers

(3) Exchange rate USD-EUR: This signifies the exchange rate between USD and Euro. All costs are assessed in Euro, to create a common axis.

(4) Regional adjustment USA=1.30, Europe=1.00, India=0.55. Construction in India is cheaper than in Europe. For this, an established factor is used.

Especially step 2 is not very accurate, but for the parametric cost model, an approximation is all that is necessary.

For the MSFC 4670 bench, the cost mentioned in the relevant sources is $50 million. However, when these projects are announced in the US, they typically underestimate the cost, as exemplified by work on the B-2 at Stennis, which was supposed to cost $143 million (2014), and ended up costing $230 million (2023). The inflation in this time was 28.71% [52], so the multiplication factor is $\frac{230}{143 \times 1.2871}$, resulting in a factor of 1.25. This results in a cost of $ 62.5 million. For the A-2 stand at Stennis, the given total investment that Relativity Space is doing in Stennis is given to be $267 million [109]. There is a discrepancy in sources, where some sources mention the investment is only in the development of A-2 [119], and others mention it to be investment in its Stennis operations, being more vague [109][35]. In this analysis, it is assumed that the investment is only done on modernizing the A-2 bench.

There are various steps in establishing the equivalent cost for 2025 in euros. Firstly, every project was initiated or finished in a certain year. The fact that the cost is in some cases only mentioned before the project, and in some cases is the total project cost, makes the estimate slightly more inaccurate. However, as it is all that is available, this is an acceptable limitation. The year and mentioned budget together give an idea what effect inflation has on this number: a bench constructed in 2025 is 28% more expensive than it would have been in 2014. Secondly, the exchange rate needs to be taken into account, to ensure all currencies mentioned are the same. Thirdly, a regional cost adjustment is necessary. A bench constructed in the US is more expensive than in Europe, and building in India is significantly cheaper than either.

The initial adjustment factors (inflation to 2025, currency conversion, and regional cost indices) are objective and verifiable from published datasets[3]. By contrast, the factor distinguishing maintenance, refurbishment/modernization, and new-build construction is judgment-based rather than directly measurable; it is modelled with discrete levels (0.25, 0.50, 0.75, 1.00) derived from the documented scope of works, which is analysed in Appendix C, and should be interpreted as indicative rather than exact. Lastly, a performance factor is assigned. For a bench that can test at sea-level conditions in one position, a factor of 1 is applied. If a bench has the capability to test in multiple positions, a factor of 1.33 is applied. In case the bench can test multiple engines at the same time in different configurations, a factor of 1.66 is used. When vacuum testing is possible, a factor is 2 is used. The rationale for this can also be found in Appendix C. By multiplying the costs mentioned in Table 7.1 with the first two factors, and dividing by the last three, an equivalent cost in 2025 euros is found.

$$F_{\text{total},r} = \frac{F_{\text{infl},r}\, F_{\text{FX},r}}{F_{\text{region},r}\, F_{\text{refurb},r}\, F_{\text{perf},r}}$$

By combining this with the thrust, a graph can be made that provides an estimate of the cost evolution of a test bench with increasing thrust. The factors are shown in Table 7.2, and the resulting graph is shown in Figure 7.1.

[3]The Regional Cost Adjustment was provided by ESA cost engineers Javier Serrano Gomez and Andrea Polomini

Table 7.2: Adjustment factors and 2025-equivalent costs for rocket test stands [52][50][51]

Test Stand	Raw EC to 2025 EC	Exchange Rate to EUR	Regional Cost Adjustment (Europe=100%)	Refurbishment vs Construction	Performance Factor (e.g., vacuum)	Total Adjustment Factor	Equivalent Cost (2025 MEUR)
NASA A-3 (SSC)	1.36	0.86	1.30	1.00	2.00	0.44985	157.00
NASA B-2 (SSC)	1.06	0.86	1.30	0.75	1.00	0.93497	215.04
NASA A-2 (SSC)	1.06	0.86	1.30	0.75	1.00	0.93497	249.64
Stand 4670 (MSFC)	1.19	0.86	1.30	0.50	1.33	1.18381	73.97
USAF 2-A (Edwards)	1.71	0.86	1.30	0.50	1.00	2.26246	41.86
DLR P5.2	1.06	1.00	1.00	1.00	2.00	0.53000	37.10
SIET	1.54	0.01	0.55	1.00	1.66	0.01855	137.30

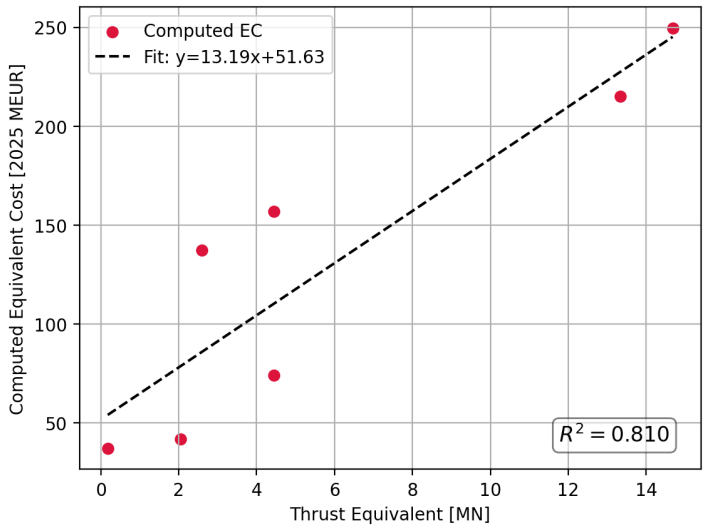

Figure 7.1: Computed equivalent cost (in 2025 MEUR) as a function of thrust equivalent (MN), including a linear regression fit ($R^2 = 0.810$).

From this graph, an estimate can be made that a 2 MN, *vertical* test bench would cost approximately 80 million euros in Europe. This is only the capital expenditure (CAPEX) within Europe, there are again differences in price levels, as also exemplified in the chapter on site selection. The figure presented here is a European average. This does not yet take into account that big construction projects cost tends to be underestimated. An extra 28% will be added to this 80 million in section 7.4 to calculate operating expenses and return on investment, a value that is backed by [2][34]. To create an estimate of the cost saving, considering the horizontal nature of the bench, and hence the less complicated structure, another approach is necessary. Therefore, a bottom-up approach, where the known cost of subsystems is used to create an estimate for the whole, horizontal system, is performed in the following section.

7.2. Bottom-up Cost Assessment

ESA has a large amount of assets when it comes to propulsion testing. The costs of these assets is known and managed by the Infrastructure and Value Chain team (STS-I). This means that it is possible to build a model of a test bench from the ground up from a PBS, and gauge the total cost of a bench based on that. The hypothesis for a cost estimate like this is that the outcome is lower than the cost estimate done in the top-down approach, since the design is considering a horizontal test bench, which is inherently cheaper than a vertical bench. Furthermore, for the top-down approach, the final reported cost of the benches is used. This cost does not only include the acquisition cost of the bench elements, but also the integration cost and labour cost, while the cost in the asset database is the acquisition cost with occasionally the infrastructure costs merged into it. This section will provide a Rough Order of Magnitude (ROM) estimate of what a horizontal test bench would cost, using the ESA assets database to establish the difference in cost between a horizontal and vertical bench.

A trimmed-down version of the PBS describing a test bench is used in Table 7.3. This table compares the presence of elements of a test bench between the Lampoldshausen facilities (and thus the ESA database) and a to-be-built high thrust test bench. This can then be used to determine which elements of a bench should be taken into account for costing, and which shouldn't. The full PBS can be found in chapter 2.

Table 7.3: Comparison of Lampoldshausen vs. High-thrust bench capabilities ('yes' = available, 'no' = not available).

Component	LAM	HTBench
1. Test Cell		
Engine installation structure	yes Green	yes Green
Vacuum chamber (if high-altitude simulation required)	yes Green	no Red
Microphones	yes Green	yes Green
Camera system	yes Green	yes Green
Crane and support tools	yes Green	yes Green
2. Exhaust Gas Guiding System		
2.1. Diffuser		
Traditional diffuser or Centre body diffuser	yes Green	no Red
Water cooling system	yes Green	no Red
2.2. Guide Tube		
Water cooling system	yes Green	no Red
2.3. Flame Deflector		
Redirect exhaust flow	yes Green	no Red
(Optional) water-cooling system	yes Green	no Red
2.4. Exhaust Duct (if applicable)	yes Green	no Red
3. Engine Propellant Supply System		
3.1. Propellant Storage Tanks		
Cryogenic tanks (LH_2, LOX, LCH_4)	yes Green	yes Green
1000 m^3 LH_2, 400 m^3 LOX, 310 m^3 methane	yes Green	yes Green
Non-cryogenic tanks (ambient-temperature fluids)	yes Green	yes Green
3.2. Buffer Tanks (optional)	yes Green	no Red
3.3. Pipe Subsystem		
Vacuum-insulated pipes (cryogenic fluids)	yes Green	yes Green
Standard pipes (non-cryogenic fluids)	yes Green	yes Green
Valves and control elements	yes Green	yes Green
Filters for cryogenic fluid supply	yes Green	yes Green
Chill-down systems (cryogenic)	yes Green	yes Green
4. Gaseous Supply System		
4.1. Gas Storage & Pressurization Tanks		
Nitrogen (GN_2)	yes Green	yes Green
Hydrogen (GH_2)	yes Green	no Red
Helium (GHe)	yes Green	yes Green
Oxygen (GOX)	yes Green	no Red
Methane and Propane	yes Green	yes Green
4.2. pressurisation Subsystem		

Table 7.3 (continued)

Component	LAM	HTBench
Tank pressurisation lines	yes Green	yes Green
Line pressurisation and purge lines	yes Green	yes Green
4.3. Ignition Gas Supply		
Gaseous H_2 & O_2 to igniters	yes Green	no Red
Ignition system valves and regulators	yes Green	yes Red
4.4. Venting System		
Neutral gas (He, N_2) venting lines	yes Green	yes Green
5. Water Supply System (noise abatement)		
Water storage tank	yes Green	yes Green
Refrigeration system	yes Green	no Red
Pumping system	yes Green	no Red
Distribution pipe network	yes Green	yes Green
Water-cooled subsystems (EU noise rules):		
Diffuser cooling system	yes Green	no Red
Guide tube cooling	yes Green	no Red
Flame deflector cooling	yes Green	no Red
Condenser/steam-generator cooling lines	yes Green	no Red
Fire-extinguish system	yes Green	yes Green
6. Measurement, Command & Control (MCC) System		
Centralized real-time monitoring & control	yes Green	yes Green
Data acquisition (low/high-frequency)	yes Green	yes Green
Data processing & storage infra.	yes Green	yes Green
Safety and emergency shutdown	yes Green	yes Green
Control room infrastructure (remote monitoring)	yes Green	yes Green
7. Flare Stack		
Gas combustion chamber	yes Green	yes Green
Ignition device	yes Green	yes Green
Exhaust gas dispersion nozzle	yes Green	yes Green

Using the ESA assets database, it is possible to determine the cost of most element as percentage of the whole bench. The analysis has been performed based on the data from the ESA asset database related to test benches but limited to the analysis of acquisition costs. All subsequent investments have been excluded as to separate maintenance or upgrade costs. After mapping the assets in the database as closely as possible from the PBS, the following cost shares, shown in Table 7.4 have been identified.

Table 7.4: PBS element cost shares. Yes = excluded from horizontal bench. [4]

Block 1			Block 2			Block 3		
PBS	**%**	**Excl.**	**PBS**	**%**	**Excl.**	**PBS**	**%**	**Excl.**
1.1	0.3		2	4.5	Yes	3	12.0	
1.2	1.6	Yes	**Total (2)**	**4.5**		**Total (3)**	**12.0**	
1.3	0.4							
1.5	0.3							
1.6	0.2							
Misc	1.2							
Total (1)	**4.5**							
Block 4			**Block 5**			**Block 6**		
PBS	**%**	**Excl.**	**PBS**	**%**	**Excl.**	**PBS**	**%**	**Excl.**
4.1.1	8.3		5	5.2	Yes	6.1	9.0	
4.1.2	1.2	Yes				6.2	2.8	
4.1.3	5.4					6.5	1.7	
4.1.4	0.5	Yes				Misc	7.2	
4.1.5	0.1							
4.4	0.9							
Total (4)	**15.5**		**Total (5)**	**5.2**		**Total (6)**	**20.7**	
Block 7			**Infrastructure**					
PBS	**%**	**Excl.**	**PBS**	**%**	**Excl.**			
7	0.9		I	36.5				
Total (7)	**0.9**		**Total (Infra)**	**36.5**		**Total**	**100%**	

The rationale for the exclusions is the following:

- The water supply system is partially excluded, and exhaust gas guiding system fully excluded, because noise rules are not taken into account.
- The ignition gas supply is excluded because staged combustion engines have built-in igniters.
- Buffer tanks are excluded because this is extra cost that is unnecessary with proper valve sequencing. Buffer tanks are sometimes present to account for a pressure drop, and can be used to provide more stable flow.
- The bench does not need GOX nor GH_2, which would have been used for ignition.

Some exclusion costs have not been specifically identified in the database and are thus still included in the cost. As the infrastructure costs register in the ESA database lacks details (and includes civil engineering activities not to be considered in this case), the analysis has been performed with and without those costs in order to identify a range. As a result, the calculation shows that the share of costs not to be considered for a horizontal bench range between 13% and 21% of the bench total cost. The 13% corresponds to the table above, and the 21% is the result when you remove infrastructure from the table and scale the other values. As a fire suppression system is a necessity, this range should be lowered to 10 - 17%, because some water infrastructure is necessary, but the database lacks granularity to distinguish this from the whole water infrastructure. As noise reduction can be a future requirement, already having the (partial) water infrastructure for this is beneficial.

Using the parametric model established in the previous subsection, it is possible to determine a range for the cost of a horizontal bench. Using the 102.4 million deduced in the previous section (80 million + 28%), a 10-17% reduction for a horizontal layout yields a cost range of **€92.16 M (-10%)** to **€84.99 M (-17%)**. It is very important to note that this cost does not take into account licensing for the site. The other sites considered in the parametric model already have (almost) all the necessary licenses, because they are on established testing grounds. These licenses are also the reason that defining a timeline for building a bench is not possible with the information presented in this thesis. For this, a deep dive

[4] Personal correspondence with Edouard Gourier

into the regulatory environment of each site selection country is necessary. Besides this additional cost, there is a discrepancy between the bottom-up and top-down model that has to be addressed. It is unknown which costs are exactly taken into account in the reported values of the test benches, while for the bottom-up model, this is quite clear. This uncertainty is why the upper bound of the range, €92.16 M (-10%), will be used in further analyses.

7.3. OPEX

NASA's Rocket Propulsion Test Program had a yearly budget of $46-49 million per year, before the major budget cuts at NASA in 2025, which terminates the NASA Rocket Propulsion Test Program [76]. For ESA, this number is confidential, but it is a non-negligible amount of money. Operational expenditures (OPEX) for a rocket propulsion test program typically include personnel costs for staff, utilities, like compressed gases and cryogens; maintenance, including periodic refurbishment of test stands, replacement of valves; and compliance activities such as emissions monitoring, and hazardous-materials handling.

Annual operating expenses are often benchmarked as a percentage of the initial CAPEX. Table 7.5 summarizes typical OPEX ranges by facility type and age for the aviation industry, which serves as an indication. Note that these percentages cover only day-to-day facility maintenance.

Table 7.5: Annual OPEX as a percentage of initial CAPEX, by facility type and age[5]

Facility Type	0-10 years	10-20 years	20-30 years
Category I: Regular buildings (offices, apartments, etc.)	1.00%	1.25%	1.50%
Category II: Industrial buildings (warehouses, maintenance facilities, workshops)	2.00%	3.50%	4.00%
Category III: Civil works (pavements, bridges, car parks)	0.50%	1.00%	2.00%

Notes:
(1) OPEX here covers only the facilities themselves, not specialized systems or machinery inside.
(2) Repex (heavy maintenance) such as HVAC replacement, major overhauls, or resurfacing is additional and highly facility-specific.
(3) Technological equipment (PCs, printers, data systems) is typically amortized and fully replaced within 10 years, rather than maintained.

The values in this table do not properly cover the annual OPEX that would be spent in the space transportation industry. The complexity of a rocket engine test facility is significantly higher than that of a warehouse or plane hangar. For a test bench, the value hovers around 4%, but it hardly grows, and can even decrease with cost-effective measures. OPEX in the space context is usually called ordinary maintenance (OM). The 4% doesn't usually go up, even after decades, because of extraordinary maintenance (EM). Every x years on a given segment, EM happens to keep the facility running, which gives a skewed view of the annual OPEX as percentage of the initial CAPEX. Changes that are applied to the functionality of a bench, like the methane capabilities of P5 Lampoldshausen for Prometheus, are not included in the OM or EM, because they are not included in the nominal operations that the bench is designed for.

For a commercial bench, the cost of OM and EM has to be included in the user fees, as the operation would be loss-making if it was not. The business plan that would work for such a bench is discussed in the next section. The logic presented in this section is used to support the business model, and a breakdown of the OPEX factors used in the model and the logic behind their respective values can be found in Appendix D.

7.4. Business Plan

To operate a commercial test bench, a solid business plan is necessary. With significant running costs, a high initial CAPEX and a goal to earn back the initial investment and generate margin, this section formalises a quantitative operating and valuation model. Specifically, it establishes the price per

[5]Provided by Javier Serrano Gomez

test day and utilisation required for breakeven and assesses profitability under inflation and discounting.

To establish a model that quantifies what a feasible operation looks like, an economic analysis is performed. The assumptions used in this analysis are shown in Table 7.6.

Table 7.6: Base assumptions and dynamics

Parameter	Symbol	Base	Unit	Dynamics / Notes
Horizon	T	35	years	Aim is a positive NPV after 25 years. For completeness, 35 years are analysed.
Currency	-	1	kEUR	All amounts expressed in thousands of euros.
Inflation	π	2.5	%/yr	Price/cost index $I_t = (1+\pi)^{t-1}$.
Discount rate	r	4.0	%/yr	NPV factor $d_t = 1/(1+r)^t$.
Price per test day	P_1	85	kEUR/day	Bi-yearly escalated with inflation. Flexible depending on ROI.
Utilisation (days used)	D_t	$60 \rightarrow 110$	days/yr	Ramp: 60, 80, 90, 100; then 110 maximum. During a typical test campaign, utilisation is maximally 3 days per week.
Annual revenue	R_t	-	kEUR	$R_t = P_t \cdot D_t$.
Inelastic OPEX (year 1)	Inel_1	1 844	kEUR/yr	Escalated yearly with inflation. In base year it is equal to 2% of CAPEX.
Elastic OPEX (year 1)	Elas_1	1006	kEUR/yr	Escalated yearly with inflation, and is based on the amount of test days: the more test days, the higher the elastic OPEX.
Repex (year 1)	Repex_1	922	kEUR/yr	Escalated yearly with inflation. Initial value is 1% of CAPEX.
Initial CAPEX (at $t = 0$)	CAPEX_0	92 200	kEUR	Based on the parametric model.
Amortization	Amo	2 634	kEUR/yr	92,200/35; yearly earn-back of initial investment. Purely an indicative column.
Net cash flow	NCF_t	-	kEUR	$\text{NCF}_t = R_t - \text{Inel}_t - \text{Elas}_t - \text{Repex}_t$.
Net present value	NPV	-	kEUR	$-\text{CAPEX}_0 + \sum_{t=1}^{T} d_t \, \text{NCF}_t$. This value determines whether an investment is interesting to make. It has to be positive.

As can be read in the table, an initial CAPEX of €92.2 million is used, as well as an initial test cost of €85 thousand per day. For the CAPEX in this analysis, a range of €70-115 million, a ≈€22 million range around €92.2 million, is considered. The initial cost value is achieved by parameter tuning in Excel. The figures that follow will provide more depth into the full range of values. First, one term that is mentioned in the analysis has to be discussed in more depth:

NPV measures today's value of all future cash flows after the initial outlay. Future euros are discounted using the **hurdle rate** r via $d_t = (1+r)^{-t}$. Example: at $r = 4\%$, one euro received in year 10 is worth $1/1.04^{10} \approx 0.68$ EUR today. In this analysis, a discount rate of 4% is used. This is based on data available from Norway, Great Britain and France, where the typical discount rate for projects of up to 30 years are 4%, 4.5% and 4% respectively [83, 84, 87]. These discount rates decrease after 30 years. Discount rates are different in the US, but considering this is a European test facility, this is irrelevant for the analysis. [38, 40, 42, 43]

With nominal cash flows NCF_t and horizon T,

$$\mathrm{NPV} = -\,\mathrm{CAPEX}_0 + \sum_{t=1}^{T} \frac{\mathrm{NCF}_t}{(1+r)^t}, \tag{7.1}$$

where amortisation is non-cash and therefore excluded from NCF_t; the investment appears as $-\mathrm{CAPEX}_0$ at $t = 0$.

A commercially viable project requires $\mathrm{NPV} \geq 0$ by a finite horizon K for investor acceptability. Define the present-value splits up to K,

$$\mathrm{PV}_R(K) = \sum_{t=1}^{K} \frac{R_t}{(1+r)^t}, \qquad \mathrm{PV}_C(K) = \sum_{t=1}^{K} \frac{\mathrm{Inel}_t + \mathrm{Elas}_t + \mathrm{Repex}_t}{(1+r)^t}.$$

If the entire price path is scaled by a uniform uplift u ($P_t \mapsto (1+u)P_t$), then

$$\mathrm{NPV}_K(C, u) = -C + (1+u)\,\mathrm{PV}_R(K) - \mathrm{PV}_C(K),$$

and the zero-NPV frontier is

$$u(C) = \frac{C + \mathrm{PV}_C(K)}{\mathrm{PV}_R(K)} - 1.$$

Comparing $K = 20$ with $K = 30$ quantifies the trade-off: a shorter recovery horizon demands a higher starting price. This can be seen in Figure 7.2.

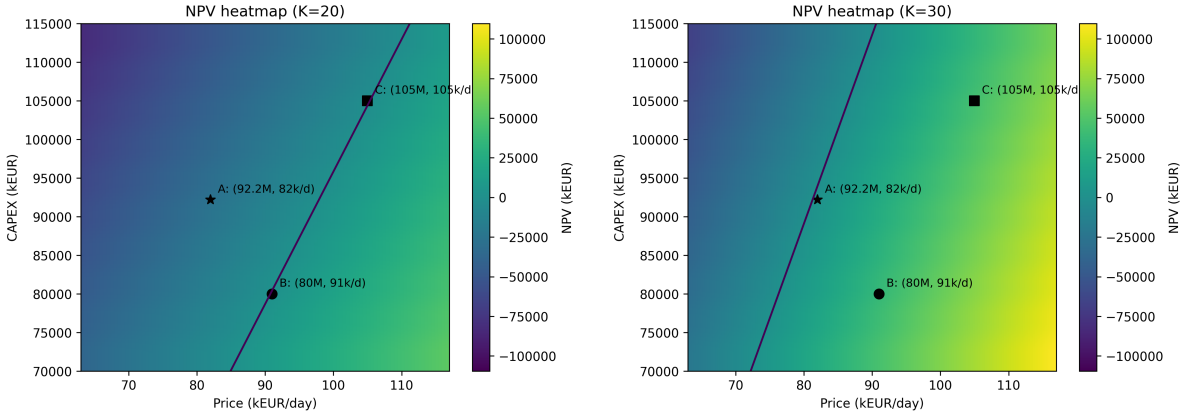

(a) NPV heatmap, target horizon $K = 20$. (b) NPV heatmap, target horizon $K = 30$.

Figure 7.2: NPV vs. CAPEX and P_1 (evaluated at $r = 4\%$); zero-NPV frontier shown.

For a realised CAPEX C, any point right of the frontier in Figure 7.2 (higher price or lower CAPEX) yields $\mathrm{NPV}_K \geq 0$; points below/left do not. The upward shift from $K = 30$ to $K = 20$ reflects the higher price level required for earlier recovery. Figure 7.2 also shows three indicative operating points. **A** (€92.2 M, €82 k/day) represents an institutional access model of the bench. At this combination of CAPEX and test cost, the project remains to the left of the K=20 zero-NPV frontier (negative discounted value by year 20, achievable with €98 k/day), but achieves break-even at a longer horizon (K=30). **B** (Bulgaria: €80 M, €91 k/day) reflects a cost-advantaged build. It lies to the right of the frontier and thus achieves NPV ≥ 0 within 20 years. **C** (Germany: €105 M, €105 k/day) represents a higher-cost build priced to remain on the profitable side of the K=20 frontier. The location effect is transparent: to clear the 20-year hurdle, the German build requires a day-rate that is about *€14 k/day* higher than the Bulgarian build (105 vs. €91 k/day). In other words, the cost advantage of the Bulgarian site converts directly into a pricing advantage of roughly 15 % for achieving the same discounted breakeven horizon, which is strategically important in a competitive test-services market. Following the logic presented in [4], the difference might be even bigger. While Sofia scores a 95 in the construction

cost index, German cities score consistently higher (135 for Frankfurt, 155 for Berlin, and 196 for Munich). This suggests a difference in construction cost of a factor 1.5-2x.

The discounted cash balance over time is

$$\mathrm{CumNPV}(t) = -\,\mathrm{CAPEX}_0 + \sum_{\tau=1}^{t} \frac{\mathrm{NCF}_\tau}{(1+r)^\tau},$$

starting at $-\mathrm{CAPEX}_0$ in year 0. Figure 7.3 reports when the project pays back in discounted terms and how value accumulates thereafter. In this model, operating cash flows do not depend on CAPEX. Therefore, alternative CAPEX values shift the curve vertically. As can be deduced from the figure below, 85k/day is not enough to hit positive NPV in 25 years.

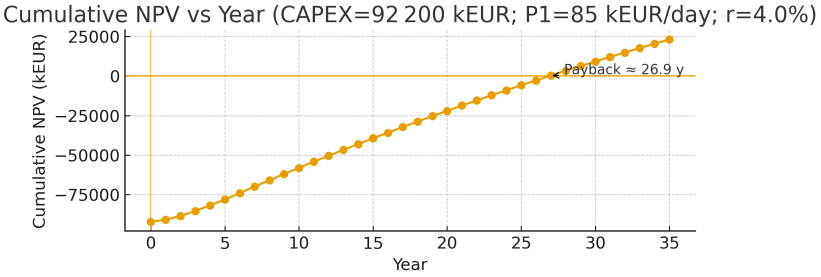

Figure 7.3: The cumulative NPV plotted over time, payback at 26.9 years.

Different test bench operators prioritise the outputs of Figure 7.2 differently. For a commercial operator, the primary objective is value creation at a finite investor horizon with a relatively high hurdle rate. The heatmap is used as a pricing indication: for the achieved CAPEX C, tariffs are set such that the operating point lies safely right of the $K = 20$ frontier, or any other short horizon that is deemed necessary by investors. In practice, the price lever is the base-year day rate P_1; a target is

$$P_1(K) = \frac{C + \mathrm{PV}_C(K)}{\sum_{t=1}^{K} d_t\, \alpha_t D_t}, \qquad \alpha_t = \frac{P_t}{P_1},$$

evaluated at the commercial K, in this case set at 20 years.

On the other hand, an institutional operator's most important goals are access, capability retention and schedule assurance. Tolerance for a longer horizon and lower financial return is higher. Pricing aims at long-run cost recovery rather than maximising the margin, so the relevant period and price is in this case is the $K = 30$ frontier and $P_1(30)$. Multi-year agreements can reduce volatility in cash flows.

Further details of the spreadsheet structure and formulas used to generate the figures are provided in Appendix D.

8

Failure Mode, Effects, and Criticality Analysis

This chapter compiles a FMECA for the rocket engine test bench. For each credible failure scenario (cryogenic flow, start/combustion transients, pressurisation/purge, structures, instrumentation and controls), a Severity (S), Probability of occurrence (P), and Detection (D) rating is assigned; their product gives the Criticality Number (CN = S×P×D). Initial and post-mitigation values are reported to show risk reduction. Entries that remain at high criticality (CN $\geq$ 12) after mitigations are highlighted, requiring additional design controls or procedural barriers. Each entry has a unique identifier, and is called a Critical Item (CI).

For each failure mode, consequences are stated at bench and test-article level, then ranked on a 1-4 scale, 1 being the best and 4 the worst score, for

- Severity: the impact on the bench or test object
- Probability: the likelihood of such a failure occurring
- Detection: the ability of the bench to detect anomalies before there are consequences

The Criticality Number is

$$\mathrm{CN} = \mathrm{S} \times \mathrm{P} \times \mathrm{D}.$$

Initial values reflect the baseline design, final values include the mitigation listed in the table. The intent is to surface the small set of residual high-CN hazards. It is important to keep into account that the Severity is intrinsic to the consequence and is not reduced by mitigations: risk reduction can be achieved through P and D.

Table 8.1: Pressurisation/purge, instrumentation/controls, and utilities FMECA items

CI	Scenario	S/P/D (init)	S/P/D (final)	CN init	CN final	Primary mitigation
CI-01	Delayed internal ignition, causing a hard start	4/3/3	4/2/2	36	**16**	Enforce tight start-sequence windows with automatic cut-off on delay.
CI-02	No ignition detected within the permitted window	3/3/3	3/2/2	27	**12**	Block further propellant admission and abort the sequence if no light-off is detected.
CI-03	Rough combustion or high-frequency instability in main chamber	4/3/3	4/2/2	36	**16**	Apply redlines on p_c oscillations that command immediate cut-off.

Continued on next page

CI	Scenario	S/P/D (init)	S/P/D (final)	CN init	CN final	Primary mitigation
CI-04	Ignition of residual propellant vapours around the stand	4/2/3	4/1/2	24	8	Purge the engine before and after start attempts.
CI-05	LOX main valve fails to close	4/2/3	4/1/2	24	8	Use fail-closed spring-return actuation, as these have a safe default state.
CI-06	LOX line rupture	4/2/2	4/1/2	16	8	Install mechanical restraints and size reliefs to prevent overpressure.
CI-07	CH_4 or LH_2 leak	4/2/3	4/1/2	24	8	Fit flammable-gas detectors that trigger automatic abort.
CI-08	Ice blockage at LOX valve or orifice	3/3/2	3/2/2	18	**12**	Perform controlled chill-down and temperature conditioning of the valve, and system as a whole.
CI-09	Water-hammer in cryogenic line	3/3/2	3/2/2	18	**12**	Limit valve closure rate or increase the diameter of the pipes to limit the flow velocity.
CI-10	Cavitation in CH_4/LH_2 feed	3/3/2	3/2/2	18	**12**	Control inlet temperature, flow velocity, and pressure.
CI-11	Cross-connection mis-routing of propellants	4/2/3	4/1/2	24	8	Use keyed quick-disconnects and interlocks so wrong hookups cannot be made.
CI-12	Embrittlement crack in cryogenic piping	4/2/2	4/1/2	16	8	Conduct periodic checks on cryogenic lines. Keep track of the producer provided life-limit of the pipes.
CI-13	Pressurisation regulator fails high	3/3/2	3/2/2	18	**12**	Add a downstream slam-shut valve that trips if regulator spikes the pressure.
CI-14	Over-pressurisation of run tank	4/2/2	4/1/1	16	4	Install pressure relief valves, and possibly even a burst disc sized for the worst case.
CI-15	He/N_2 supply depletion mid-test	3/2/2	3/2/2	12	**12**	Cut-off test, and evaluate tank sizing.
CI-16	Purge not established / lost purge flow	3/3/2	3/2/2	18	**12**	Prove purge flow with a switch and hold the countdown if not met.
CI-17	Sensor drift causing false safe reading	3/2/3	3/2/2	18	**12**	Implement 2oo3 voting.
CI-18	Safety comms loss during firing	4/2/2	4/2/1	16	8	Provide a hard-wired safety PLC with an independent emergency stop.
CI-19	Interlock logic error, or misconfiguration of software	4/2/3	4/1/2	24	8	Run a dry-run of all interlocks before hot-fire.

Table 8.2: Structures/mechanical, operations/human factors, and architecture-specific FMECA items

CI	Scenario	S/P/D (init)	S/P/D (final)	CN init	CN final	Primary mitigation
CI-20	Restraint/hold-down failure (engine movement)	4/2/3	4/1/2	24	8	Proof-load all anchors and fit secondary restraints.
CI-21	Lifting/crane incident during integration	4/2/2	4/1/2	16	8	Execute a certified lift plan with exclusion zones.

Continued on next page

CI	Scenario	S/P/D (init)	S/P/D (final)	CN init	CN final	Primary mitigation
CI-22	Wrong unit or wrong set-point in redlines	3/3/3	3/2/2	27	**12**	Apply a two-person check of all limits before arming.
CI-23	Countdown procedural error (wrong step order)	3/3/2	3/2/2	18	**12**	Use read-do checklists with enforced hold points.
CI-24	Foreign-object debris left in line	3/2/1	3/2/1	6	6	Conduct checks on bench close environment before test.
CI-25	Hydrocarbon contamination in oxygen-rich environments	4/2/3	4/1/2	24	8	Enforce oxygen-clean materials and cleanliness certification.
CI-26	Wrong run-tank selected in sequence (routing error)	4/2/3	4/1/2	24	8	Verify the active tank map before arming.
CI-27	Unequal pressurisation across tanks	3/3/2	3/2/2	18	**12**	Use per-tank pressure control with independent set-points.
CI-28	Common-cause failure of pressurisation manifold	4/2/2	4/1/2	16	8	Split the manifold into two independent regulator trains.
CI-29	Orifice installed in the wrong branch of pipes	3/3/2	3/2/2	18	**12**	Part-number check at installation with sign-off.
CI-30	Vent header capacity exceeded during abort dump	4/2/2	4/1/2	16	8	Size the vent header for worst-case simultaneous dump and prove using cold-flow.
CI-31	System purge leaves dead-leg pockets unpurged	3/3/2	3/2/2	18	**12**	Add multiple points where the purge enters the system.
CI-32	Transient spike when multiple tanks open to a common line	3/3/2	3/2/2	18	**12**	Stagger valve openings with ramped commands or merge flow while filling tanks.
CI-33	Back-pressure on an inactive tank after a downstream closure	3/3/2	3/2/2	18	**12**	Fit a relief valve to vent.
CI-34	He/N_2 supply routed to the wrong pressurisation branch	3/2/3	3/1/2	18	6	Use couplings and validate pressurisation is only on the selected tank.
CI-35	Temperature stratification biases density in mass-flow calculation	2/3/2	2/2/2	12	8	Place a temperature sensor adjacent to the metering element and compensate in real time.
CI-36	Helium blow-by cools an actuator causing a seal to shrink	3/2/2	3/2/2	12	**12**	Heat-trace vulnerable actuators and limit the He purge temperature ramp rate.
CI-37	Wrong valve-stroke calibration creates partial flow area	3/3/2	3/2/2	18	**12**	Calibrate stroke versus C_v (valve flow coefficient) and store a signature before enabling automatic control.
CI-38	Logic enables two tanks to shut simultaneously, causing water-hammer	3/3/2	3/2/2	18	**12**	Create a sequence in which valves are closed with a minimum separation time.
CI-39	Purge valve stuck closed near engine inlet	4/2/3	4/1/2	24	8	Verify local purge flow with a switch that inhibits the main-valve from opening.
CI-40	Software error toggles the wrong physical valve	4/2/3	4/1/2	24	8	Run a test before each campaign.
CI-41	Loss of site electricity during test	4/2/2	4/1/1	16	4	Provide UPS autonomy and automatic transfer to a generator sized to complete the full safe-down sequence.
CI-42	Loss of test data storage (disk or network failure)	3/2/2	3/2/1	12	6	Use dual recorders; verify logging before arming.

Continued on next page

CI	Scenario	S/P/D (init)	S/P/D (final)	CN init	CN final	Primary mitigation
CI-43	Environmental conditions outside limits (too hot / too cold / high wind)	2/3/2	2/2/2	12	8	Define environmental go/no-go limits and postpone or precondition hardware if limits are exceeded.
CI-44	Key test roles not staffed (for example, test conductor or safety responsible)	3/2/2	3/1/2	12	6	Enforce a sign-in staffing checklist; test is no-go if any critical role is unfilled.
CI-45	Fire crew not on standby	4/2/2	4/1/2	16	8	Confirmation of fire coverage before arming; otherwise hold.

The performed FMECA highlights several important trends regarding the residual risks within the test bench design. After mitigation, most failure scenarios are reduced to acceptable levels, with only a limited amount of scenarios remaining above the criticality threshold of CN $\geq$ 12. The highest residual criticalities are associated with ignition and early-combustion events, pressurisation, procedural errors and purging. These items, except for the procedural errors, share a common characteristic: they involve fast physical processes where procedural mitigations alone are insufficient, and where safety must therefore be achieved through a robust architecture and automatic detection.

The ignition sequence remains the dominant contributor to risk. Delayed ignition and rough combustion, CI-01 and CI-03, retain the highest CN value even after mitigation, while CI-02 also has a criticality value of 12. This stresses that the start sequence represents the most safety-critical phase of a test. The detection of ignition and instability must therefore occur within milliseconds. This suggests some future work on monitoring chamber pressure oscillations and the control system in general.

A second cluster of residual CN=12 items originates from the pressurisation system. Failures such as regulator malfunction, unequal tank pressurisation, and transient spikes when multiple tanks interact reveal that the dynamics of the pressurisation circuit can introduce coupling between otherwise independent subsystems. However, in this case, these subsystems are dependent, as the same pressurisation infrastructure is connected to both tanks. Using individual pressurisation infrastructures for both might be the way to solve these issues, or at least mitigate them to below CN=12. A trade-off would have to be performed to weigh the benefits of the same pressurisation infrastructure versus individual.

A third theme concerns the purge and vent systems. Several failure modes (CI-16, CI-31, CI-39) show that purge performance is sensitive to the configuration of lines and the ability to verify flow at different points. A purge system that is only monitored upstream cannot guarantee that hazardous pockets near the engine are cleared. This analysis therefore supports a design philosophy in which purge is treated with the utmost care, with proper measurement taken along the line to ensure the MCC has a good overview of the quality of the purge. Such instrumentation should form part of the go/no-go criteria in the start sequence.

Human-factor related errors, such as incorrect limit settings or installation mistakes (CI-22, CI-23, CI-29, CI-37), remain a residual risk. The procedures laid out in chapter 2 are critical in successfully testing an engine. Automated verification tools, proper communication on redlines, and consistency checks between physical hardware and control logic are recommended.

Finally, several residual CN=12 items are linked to detection capability. Sensor drift (CI-17) and similar issues show that limited anomaly detection capability can create unsafe conditions. Increasing redundancy on critical measurements can provide significant safety improvement without any advanced redesign on the bench side.

9

Conclusion

This thesis addressed a concrete gap in Europes propulsion ecosystem: the lack of an affordable, high-capacity sea-level facility for routine hot-fire testing of 2 MN staged-combustion (SC) engines. The central research question was:

> *What high-level architecture and configuration of a sea-level propulsion test bench best enables routine hot-fire testing of 2 MN staged-combustion engines in Europe, while remaining economically viable under realistic utilisation?*

To answer this, the work integrated requirement derivation, architecture definition, and analytical sizing of cryogenic storage, pressurisation, and feed lines with dynamic verification of engine-interface stability using EcosimPro/ESPSS, a multi-criteria European site selection analysis, and a two-tier cost model coupled to an operational day rate. The findings are summarised below in line with the initial research questions.

(1) How do the specific characteristics of high-thrust staged-combustion engines influence the design? The defining parameter is the propellant mass flow ($\dot{m}_{\mathrm{LOX}} = 650\,\mathrm{kg/s}$, $\dot{m}_{\mathrm{CH_4}} = 200\,\mathrm{kg/s}$, and $\dot{m}_{\mathrm{H_2}} = 85\,\mathrm{kg/s}$). These drive large tank volumes, reinforced piping, and stable pressurisation control. Simulation results confirmed that the proposed dual LOX tank setup, regulated-outlet concept can sustain 4 bar at the engine interface with 20 bar ullage pressure, maintaining flow stability within $\pm 3\%$ during transients. The design therefore meets the dynamic interface requirements imposed by SC engines.

(2) What location for a bench is both feasible and cost-effective? The site-selection trade-off based on labour cost, ease of construction, logistics, and education levels identified Eastern and Southern Europe as favourable regions. Bulgaria, Greece, and Portugal consistently ranked highest. Bulgaria emerged as the most attractive overall when combining cost, infrastructure, and workforce indicators. These findings confirm that a low-cost site in Europe is feasible without compromising access or staffing.

(3) What are the critical technical and programmatic requirements for a 2 MN staged-combustion test bench? Key technical requirements include stable propellant delivery over 600-second firings, compatibility with both CH_4O_2 and H_2O_2 propellant combinations, and a dual pressurisation loop for cost reduction. Programmatically, schedule feasibility is out of scope: without jurisdiction-specific permitting and licensing timelines, this thesis cannot substantiate a construction duration or verify a 36-month target.

(4) What are the RAMS and safety implications of testing high-chamber-pressure engines? The FMECA identified ignition and pressurisation transients, purge loss, and configuration errors as the dominant residual risks (CN $\geq$ 12). These require architectural rather than procedural mitigation: re-

dundant sensing, automatic abort logic, and independent pressurisation regulation significantly reduce criticality. The resulting design philosophy prioritises fast detection during high-energy phases.

(5) What are the key cost drivers of test bench development and operation? Civil infrastructure (flame duct, foundations, and deluge), cryogenic storage, and staff costs dominate the capital and operational expenditures. Labour cost was found to be the most influential programmatic parameters, accounting for roughly one-third of annual operating expenses. Propellant logistics, and the associated maintenance, is the major recurring cost drivers.

(6) What are benchmark costs from similar facilities globally, and how would this bench compare? Comparisons with DLR, NASA, and ISRO facilities show that the proposed concept lies in a realistic cost envelope of 8592.2 million capital investment and a competitive operational day rate of approximately 82 000/day, excluding propellants, for a 30-year horizon. For this thrust range, that is incredibly cheap. These figures position the facility within reach of both public and commercial customers while meeting modern SC engine requirements.

(7) What could a viable business model for operating the bench look like? The business model depends mostly on the investor horizon. Two cases were assessed in this thesis: a private model with a horizon of 20 years, and a 30-year institutional model. The private model represents a commercial operator seeking full capital recovery within two decades and therefore requires a higher day rate or lower CAPEX to achieve a positive discounted value. The institutional model represents an agency-backed or hybrid publicprivate operator, where accessibility and strategic capability retention outweigh short-term return, allowing a longer recovery horizon and thus lower user pricing. Under the base assumptions (CAPEX_0 =€92.2 M, $r = 4\%$, $\pi = 2.5\%$, and utilisation ramp $D_t = 60 \rightarrow 110$ test days/year), the model yields a positive net present value at a day-rate of approximately €82 k/day for a 30-year horizon, with a discounted payback time of 29.4 years.

In conclusion, the thesis answers the main research question affirmatively. A European sea-level test bench for $\geq$2 MN staged-combustion engines is technically feasible and economically viable. The modular, dual-propellant concept satisfies the required mass-flow, pressurisation, and stability targets, while remaining competitive in cost. The remaining steps, like detailed structural design, refined controls and safety validation, permitting, and contractor-grade cost verification, represent an implementation phase rather than a reconsideration of feasibility. The work thus provides a validated conceptual baseline for establishing a next-generation European propulsion test facility.

10

Recommendation for Future Work

This section presents the recommendation for any future work to be performed using the outcomes of this thesis, or in this field in general. Three main points are identified.

Firstly, with a changing geopolitical landscape, it is necessary to reassess the tools that are used to model combustion in rocket engines. Using NASA CEA in anything that is to be published might incur consequences once it is not open source any more and subject to export control rules. To avoid consequences of export control altogether, use Cantera instead. Cantera is open-source under the BSD-3-Clause licence. Its publicly available for anyone to use and redistribute [41]. Furthermore, it is free. RPA is another possible alternative, and does have a free 'lite' version which provides a comprehensive interface, but large parametric sweep visualisations, and as a result rapid iteration, is significantly more difficult using RPA [92]. Cantera is compatible with Python, unlike RPA Lite Edition v.1.x. NASA CEA is distributed through NASAs Software Catalog. Its broadly available, but NASA explicitly reminds users that export laws still apply [68].

Secondly, instrumentation necessary to dynamically adjust redlines should be investigated. Staged combustion engines are complex engines, and thus require more redlines than traditional gas-generator engines. Since there are more points of 'failure', this might prolong already long test campaigns. By testing and then dynamically changing the relevant redlines, based on known behaviour of heritage engines, test campaigns might run into less costly delays. Europe is moving into a new design space with the staged combustion engine, and with reusability, but responsible spending in the back of mind, effective staged-combustion test campaigns are crucial to maintain independent access to space.

Thirdly, the verification for the EcosimPro simulations has to be expanded, as does the simulation setup. As diving too deep into the EcosimPro simulations was not the goal of this thesis, the system is not fully verified. The next step is to include valve sequencing and possibly staggered operations of the individual tanks, which is most interesting to look at for H_2, as the capacity necessary for H_2 might allow for simultaneously filling one tank and depleting others, prolonging test duration.

Lastly, it would also be of great interest to expand parametric cost models of test benches with specific data from European test benches. The Arcadis report [4] can be used to establish European factors for national cost differences. Document what is included in each cost, and align these scopes before fitting, so the model does not learn artefacts of accounting. Make the model more robust and less sensitive to construction factors by using methods that down-weigh outliers and validate the fit with cross-validation. If more than eight data points become available once the confidential information is added, exclude benches for which the final cost has not been published or cannot be verified, as these entries are significantly less accurate than known cost entries. Furthermore, it is important to note that the exchange rate used in the model (April 2025) might not be correct any more when reading

this thesis. Consider deleting all overseas benches for the baseline fit, because European data is more reliable for predicting a European build. Keep an international reference set in parallel, or in the same model, to explain large discrepancies and to capture effects specific to the high-thrust domain that are better represented outside Europe. Another note on the cost model would be to include the different propellants that benches can handle. This is valuable information, as a semi-cryogenic infrastructure is cheaper than a fully cryogenic one, and a bench that has capabilities of testing with multiple fuels will be more expensive than that same bench without this capability.

References

[1] Air Force Print News (AFPN). "Rocket test stand gets facelift". In: *U.S. Air Force News* (Jan. 2004). EDWARDS AIR FORCE BASE, Calif. URL: https://www.af.mil/News/Article-Display/Article/137793/rocket-test-stand-gets-facelift/.

[2] Abdulelah Aljohani, Dominic Ahiaga-Dagbui, and David Moore. "Construction projects cost overrun: What does the literature tell us?" In: *International Journal of Innovation, Management and Technology* 8.2 (2017), p. 137.

[3] ANI. *ISRO conducts integrated test on Semicryogenic Engine*. The News Mill. May 2023. URL: https://thenewsmill.com/2023/05/isro-conducts-integrated-test-on-semicryogenic-engine/.

[4] Arcadis. *Arcadis Construction Costs Report 2025: Navigating Uncertainty*. Industry report. Arcadis, 2025. URL: https://www.arcadis.com/en/insights/perspectives/global/international-construction-costs-2025.

[5] Ian H. Bell et al. "Pure and Pseudo-pure Fluid Thermophysical Property Evaluation and the Open-Source Thermophysical Property Library CoolProp". In: *Industrial & Engineering Chemistry Research* 53.6 (2014), pp. 2498–2508. DOI: 10.1021/ie4033999. eprint: http://pubs.acs.org/doi/pdf/10.1021/ie4033999. URL: http://pubs.acs.org/doi/abs/10.1021/ie4033999.

[6] Edwin Betady et al. "Development of a Mobile Rocket Engine Test Stand (MRETS)". In: *Proceedings of the 54th AIAA/SAE/ASEE Joint Propulsion Conference*. Cincinnati, OH, USA: American Institute of Aeronautics and Astronautics (AIAA), July 2018. DOI: 10.2514/6.2018-4600. URL: https://arc.aiaa.org/doi/10.2514/6.2018-4600.

[7] A. Beune. "Analysis of high-pressure safety valves". English. Phd Thesis 1 (Research TU/e / Graduation TU/e). Mechanical Engineering, 2009. ISBN: 978-90-386-2006-0. DOI: 10.6100/IR652510.

[8] Blue Origin. *BE-4 Engine*. 2025. URL: https://www.blueorigin.com/engines/be-4.

[9] Philippe Brossel et al. "Development Status of the Vulcain 2 Engine". In: July 2002. ISBN: 978-1-62410-115-1. DOI: 10.2514/6.2002-3840.

[10] Glenn O. Brown. "The History of the Darcy-Weisbach Equation for Pipe Flow Resistance". In: *Environmental and Water Resources History*, pp. 34–43. DOI: 10.1061/40650(2003)4. eprint: https://ascelibrary.org/doi/pdf/10.1061/40650%282003%294. URL: https://ascelibrary.org/doi/abs/10.1061/40650%282003%294.

[11] Tim Dodd Cain. *Raptor - SpaceXs Full-Flow Staged Combustion Methane Engine*. Everyday Astronaut. Aug. 2019. URL: https://everydayastronaut.com/raptor-engine/ (visited on 10/27/2025).

[12] CBRE | Whitestone. *Operations & Maintenance Cost Study for NASA Facilities: Final Report for Wind Tunnels*. Final Report Contract NNC09BA14B, Task Order NNC12TA91T. Washington, DC: National Aeronautics and Space Administration, Aug. 2015. URL: https://www.nasa.gov/wp-content/uploads/2023/06/nasa-wind-tunnels-final-report-20150813-tagged.pdf.

[13] D. Coulon. "Vulcain-2 Cryogenic Engine Passes First Test with New Nozzle Extension". In: *ESA Bulletin* 102 (May 2000), pp. 123–124. URL: https://www.esa.int/esapub/bulletin/bullet102/Coulon102.pdf.

[14] DC Correspondent. "ISRO readying for a number of launches". In: *Deccan Chronicle* (Jan. 2018). 1:53 AM IST. URL: https://www.deccanchronicle.com/science/science/270118/isro-readying-for-a-number-of-launches.html.

[15] LaToya Dean. *NASA Water System Project Upgrades Critical SLS Support System*. National Aeronautics and Space Administration (NASA). Jan. 12, 2015. URL: https://www.nasa.gov/news-release/nasa-water-system-project-upgrades-critical-sls-support-system/.

[16] J Deeken, Michael Oschwald, and Stefan Schlechtriem. "Lumen Demonstrator-Project Overview". In: *Proceedings of the 32nd International Symposium on Space Technology and Science, Beppu, Japan*. Vol. 26. 2019.

[17] Lingzhi Deng, Yuqiang Cheng, and Yehui Shi. "Fault Detection and Diagnosis for Liquid Rocket Engines Based on Long Short-Term Memory and Generative Adversarial Networks". In: *Aerospace* 9.8 (2022). ISSN: 2226-4310. DOI: 10.3390/aerospace9080399. URL: https://www.mdpi.com/2226-4310/9/8/399.

[18] Björn Dierks. *Development of a bi-propellantrocket engine test facility*. 2022.

[19] Brian Donius and Joshua Rovey. "Analysis and prediction of dual-mode chemical and electric ionic liquid propulsion performance". In: *48th AIAA Aerospace Sciences Meeting Including the New Horizons Forum and Aerospace Exposition*. 2010, p. 1328.

[20] Kai Dresia et al. "Test Automation and Fault Detection for Rocket Engine Test Facilities with Machine Learning". In: *International Journal of Energetic Materials and Chemical Propulsion* 22 (Jan. 2023). DOI: 10.1615/IntJEnergeticMaterialsChemProp.2023047195.

[21] Duk. *Combustion Tap-off Rocket Cycle (SVG)*. Licensed under CC BY-SA 3.0 and GFDL; page last updated 2020-10-07. Wikimedia Commons. Oct. 12, 2008. URL: https://commons.wikimedia.org/wiki/File:Combustion_tap-off_rocket_cycle.svg.

[22] Duk. *Electric Feed Rocket Cycle (SVG)*. Licensed under CC BY-SA 3.0 and GFDL; page last updated 2020-10-07. Wikimedia Commons. Oct. 13, 2008. URL: https://commons.wikimedia.org/wiki/File:Electric_feed_rocket_cycle.svg.

[23] Duk. *Expander Rocket Cycle (SVG)*. Licensed under CC BY-SA 3.0 and GFDL; page last updated 2020-10-07. Wikimedia Commons. Oct. 11, 2008. URL: https://commons.wikimedia.org/wiki/File:Expander_rocket_cycle.svg.

[24] Duk. *Full-flow Staged Rocket Cycle*. Licensed under CC BY-SA 3.0 and GFDL; subsequent edits 2015 and 2017; page last updated 2018-07-08. Wikimedia Commons. Oct. 14, 2008. URL: https://commons.wikimedia.org/wiki/File:Full_flow_staged_rocket_cycle.png (visited on 10/02/2025).

[25] Duk. *Gas Generator Rocket Cycle (SVG)*. Licensed under CC BY-SA 3.0 and GFDL; page last updated 2020-10-07. Wikimedia Commons. Oct. 10, 2008. URL: https://commons.wikimedia.org/wiki/File:Gas_generator_rocket_cycle.svg.

[26] Duk. *Pressure-Fed Rocket Cycle (SVG)*. Licensed under CC BY-SA 3.0 and GFDL; page last updated 2020-10-07. Wikimedia Commons. Oct. 8, 2008. URL: https://commons.wikimedia.org/wiki/File:Pressure_fed_rocket_cycle.svg.

[27] Duk. *Staged Combustion Rocket Cycle (SVG)*. Licensed under CC BY-SA 3.0 and GFDL; subsequent edits 2015 and 2017; page last updated 2020-10-07. Wikimedia Commons. Oct. 9, 2008. URL: https://commons.wikimedia.org/wiki/File:Staged_combustion_rocket_cycle.svg (visited on 10/02/2025).

[28] Mike Easterling. "Blue Origins overhaul of historic NASA test stand presented challenge". In: *Huntsville Business Journal* (May 2022). URL: https://huntsvillebusinessjournal.com/news/2022/05/09/blue-origins-facelift-of-historic-nasa-test-stand-presents-challenges/.

[29] European Environment Agency. *Infrastructure density and accessibility by country*. Published 01 Dec 2016; modified 01 Dec 2016. European Environment Agency. Dec. 1, 2016. URL: https://www.eea.europa.eu/en/analysis/maps-and-charts/infrastructure-density-and-accessibility-per-country-1.

[30] European Space Agency (ESA). *P3.2 test bench*. https://www.esa.int/ESA_Multimedia/Images/2016/11/P3.2_test_bench. Photograph; Credit: Courtesy of ASL; ESA Standard Licence. Accessed 1 Oct 2025. Nov. 2016.

[31] Eurostat. *Eurostat Database*. Access to detailed datasets across nine statistical themes. European Commission. URL: https://ec.europa.eu/eurostat/data/database.

[32] Asma Fejjari et al. "A Review of Anomaly Detection in Spacecraft Telemetry Data". In: *Applied Sciences* 15.10 (2025), p. 5653.

[33] Fernando Figueroa et al. "Integrated System Health Management: Pilot Operational Implementation in a Rocket Engine Test Stand". In: Apr. 2010. ISBN: 978-1-60086-963-1. DOI: 10.2514/6.2010-3454.

[34] Bent Flyvbjerg, Nils Bruzelius, and Werner Rothengatter. *Megaprojects and Risk: An Anatomy of Ambition*. Cambridge University Press, 2003.

[35] Jeff Foust. *Relativity Space expands presence at NASA's Stennis Space Center*. News article. SpaceNews. Sept. 7, 2023. URL: https://spacenews.com/relativity-space-expands-presence-at-nasas-stennis-space-center/.

[36] Yukio Fukushima et al. "DEVELOPMENT STATUS OF LE-7A AND LE-5B ENGINES FOR H-IIA FAMILY". In: *Acta Astronautica* 50.5 (2002), pp. 275–284. ISSN: 0094-5765. DOI: https://doi.org/10.1016/S0094-5765(01)00165-5. URL: https://www.sciencedirect.com/science/article/pii/S0094576501001655.

[37] Isabel Gallo Alonso. *The European Space Agencys Strategy for New Space Propulsion Test Benches*. Tech. rep. Internal document, not publicly available. Paris, France: European Space Agency, 2023.

[38] Commissariat Général du Plan. "Révision du taux dactualisation des investissements publics". In: *Présidé par D. Lebegue, La Documentation Française* (2005).

[39] German Aerospace Center (DLR). *New test stand for Ariane 6 upper stage at DLR Lampoldshausen*. News release. DLR and ESA inaugurate test stand P5.2. Feb. 2019. URL: https://www.dlr.de/en/latest/news/2019/01/20190226_new-test-stand-for-ariane-6-upper-stage-at-dlr-lampoldshausen.

[40] Christian Gollier and James K Hammitt. "The long-run discount rate controversy". In: *Annu. Rev. Resour. Econ.* 6.1 (2014), pp. 273–295.

[41] David G. Goodwin et al. *Cantera: An Object-oriented Software Toolkit for Chemical Kinetics, Thermodynamics, and Transport Processes*. https://www.cantera.org. Version 3.1.0. 2024. DOI: 10.5281/zenodo.14455267.

[42] Paul R Grandl et al. "Application of Risk within Net Present Value Calculations for Government Projects". In: (2007).

[43] Marc W Greenberg and William Laing. "Advanced Economic Analysis". In: *International Cost Estimating and Analysis Association (ICEAA): 2013 Professional Development and Training Workshop*. HQ-STI 04-2013No. 2. 2013.

[44] Dirk Greuel et al. "Test facilities for SCORE-D". In: *CEAS Space Journal* 4.1-4 (2013), pp. 55–69. DOI: 10.1007/s12567-013-0033-x.

[45] D Haeseler et al. "Recent developments for future launch vehicle LOX/HC rocket engines". In: *6th International Symposium on Propulsion for Space Transportation of the 21st Century*. 2002.

[46] John A Halchak, James L Cannon, and Corey Brown. *Materials for liquid propulsion systems*. Tech. rep. American Institute of Aeronautics and Astronautics, 2018.

[47] Stephen Hall. "1 - Fluid Flow". In: *Branan's Rules of Thumb for Chemical Engineers (Fifth Edition)*. Ed. by Stephen Hall. Fifth Edition. Oxford: Butterworth-Heinemann, 2012, pp. 1–26. ISBN: 978-0-12-387785-7. DOI: https://doi.org/10.1016/B978-0-12-387785-7.00001-3. URL: https://www.sciencedirect.com/science/article/pii/B9780123877857000013.

[48] DH Huang and DK Huzel. "Design of Liquid Propellant Rocket Engines Second Edition. Special Publication". In: *Work of the US Gov* (1971).

[49] Ronald W Humble, Henry N Gary, and Wiley J Larson. *Space propulsion analysis and design*. McGraw-Hill, 1995.

[50] Ian Webster. *Euro Inflation Calculator: EUR from 1997–2025*. https://www.in2013dollars.com/Euro-inflation. Updated 12 August 2025. 2025.

[51] Ian Webster. *India Inflation Calculator: World Bank data, 1958–2024 (INR)*. https://www.officialdata.org/india/inflation. 2025.

[52] Ian Webster. *U.S. Inflation Calculator: 1635–2025, Department of Labor data*. https://www.in2013dollars.com/. Updated 12 August 2025. 2025.

[53] Indian Space Research Organisation. *First blow down test of Trisonic Wind Tunnel at VSSC*. Online news release. Dec. 2022. URL: https://www.isro.gov.in/First_Blow_Trisonic.html.

[54] Institute of Space Propulsion Lampoldshausen. *Status Report 2011*. Tech. rep. DLR, 2012. URL: https://uppsagd.wordpress.com/wp-content/uploads/2012/12/institute-of-space-propulsion_statusreport_teil_1_lowres_gesamt.pdf.

[55] NASA (original); Jkwchui and Chouser (SVG adaptation). *SSME schematic (updated).svg*. Public domain (NASA). Coloured/annotated SVG interpretation based on NASA schematic; see file history and licensing on Commons. Wikimedia Commons. Jan. 20, 2015. URL: https://commons.wikimedia.org/wiki/File:Ssme_schematic_(updated).svg.

[56] John Livingston. *Raptor 2 Powerhead Analysis*. Tech. rep. Astrox Corp, July 2019.

[57] Brian K. Jones et al. "NASA Plum Brook Station In-Space Propulsion Facility Test Stand Characterization Hot Fire Test". In: *AIAA Propulsion and Energy Forum*. 2018. DOI: 10.2514/6.2018-4685.

[58] II Joyner Claude R. et al. "Propulsion System Choices and Their Implications". In: *46th AIAA/ASME/SAE/ASEE Joint Propulsion Conference & Exhibit*. Nashville, TN, July 2010. DOI: 10.2514/6.2010-6506.

[59] Hyun-Duck Kwak, Sejin Kwon, and Chang-Hwan Choi. "Performance Assessment of Electrically Driven Pump-Fed LOX/Kerosene Cycle Rocket Engine: Comparison with Gas Generator Cycle". In: *Aerospace Science and Technology* 77 (2018), pp. 67–82. DOI: 10.1016/j.ast.2018.02.033.

[60] Lee Roop. "Blue Origins big job: Restoring an Apollo test stand in Huntsville". In: *AL.com* (July 2020). URL: https://www.al.com/news/2020/07/blue-origins-big-job-restoring-an-apollo-test-stand-in-huntsville.html.

[61] Joris de Lint and Giulia Shanti Andritzky. *Report: US and Indian Propulsion Test Facilities*. Tech. rep. Internal document, not publicly available. Paris, France: European Space Agency, 2025.

[62] Yu Liu et al. "Concept and Key Technology Analysis of Electric Pump-Fed Liquid Propellant Rocket Engine". In: *IOP Conference Series: Earth and Environmental Science* 781.4 (2021), p. 042016. DOI: 10.1088/1755-1315/781/4/042016.

[63] Pankaj Malhotra et al. "LSTM-based Encoder-Decoder for Multi-sensor Anomaly Detection". In: *CoRR* abs/1607.00148 (2016). arXiv: 1607.00148. URL: http://arxiv.org/abs/1607.00148.

[64] Manuel Martinez-Sánchez. *16.512 Rocket Propulsion - Lecture 26: Turbopumps*. MIT OpenCourseWare. Course 16.512, Rocket Propulsion (Fall 2005). 2005. URL: https://ocw.mit.edu/courses/16-512-rocket-propulsion-fall-2005/b1f6e25184cb98de9c147c9b4aabbd63_lecture_26.pdf.

[65] J Moral et al. "ESPSS simulation platform". In: *Space Propulsion* (2010).

[66] R. Morales-Ospino, A. Celzard, and V. Fierro. "Strategies to recover and minimize boil-off losses during liquid hydrogen storage". In: *Renewable and Sustainable Energy Reviews* 182 (2023), p. 113360. ISSN: 1364-0321. DOI: https://doi.org/10.1016/j.rser.2023.113360. URL: https://www.sciencedirect.com/science/article/pii/S1364032123002174.

[67] NASA / Stennis. *B-2 Test Stand at NASA Stennis Space Center*. https://www.nasa.gov/wp-content/uploads/2019/03/b-2-test-stand-ssc-20200124-s00620.jpg. National Aeronautics and Space Administration, 2020.

[68] NASA Glenn Research Center. *Chemical Equilibrium Applications (CEA)*. NASA Software Catalog, Reference LEW-17687-1. n.d. URL: https://software.nasa.gov/software/LEW-17687-1.

[69] NASA Office of Inspector General. *NASA's Decision Process for Conducting Space Launch System Core Stage Testing*. Tech. rep. IG-14-009. NASA OIG, Jan. 2014. URL: https://oig.nasa.gov/docs/IG-14-009.pdf.

[70] NASA Office of Inspector General. *NASAs Rocket Propulsion Test Program*. Audit Report IG-24-018 (A-23-13-00-SARD). Washington, DC: National Aeronautics and Space Administration Office of Inspector General, Sept. 2024. URL: https://www.oversight.gov/sites/default/files/documents/reports/2024-09/IG-24-018.pdf.

[71] NASA Stennis Communications. *A Defining Era: NASA Stennis and Space Shuttle Main Engine Testing*. May 2025. URL: https://www.nasa.gov/centers-and-facilities/stennis/a-defining-era-ssme/.

[72] NASASpaceFlight.com Forum Contributors. *BE-4 Reverse Engineered*. NASASpaceFlight.com Forum Thread. URL: https://forum.nasaspaceflight.com/index.php?topic=45518.0.

[73] NASASpaceFlight.com Forum Contributors. *Blue Origins BE4 Engine*. NASASpaceFlight.com Forum Thread. URL: https://forum.nasaspaceflight.com/index.php?topic=39674.0.

[74] National Aeronautics and Space Administration. *A-3 Test Stand*. Web page (NASA Stennis Space Center). Page last updated: July 27, 2023; Page Editor: LaToya Dean; Responsible NASA Official: Abigail Bowman. July 2023. URL: https://www.nasa.gov/stennis/engineering-and-test-directorate/a-3-test-facility/.

[75] National Aeronautics and Space Administration. *B-2 Test Stand*. Fact sheet, NASA Stennis Space Center. Version 1. Sept. 2020. URL: https://www.nasa.gov/wp-content/uploads/2020/09/b-2_test_stand_v1.pdf.

[76] National Aeronautics and Space Administration. *Fiscal Year 2026 Budget Technical Supplement*. Technical Supplement 002. National Aeronautics and Space Administration, May 2025. URL: https://www.nasa.gov/wp-content/uploads/2025/05/fy-2026-budget-technical-supplement-002.pdf.

[77] National Aeronautics and Space Administration. *MSFC Test Facility 4670*. Web page (Propulsion Test Capabilities, Space Operations Directorate). Page last updated: July 24, 2023; Page Editor: LaToya Dean; Responsible NASA Official: Abigail Bowman. July 2023. URL: https://www.nasa.gov/directorates/space-operations/rpt/propulsion-test-capabilities/msfc-test-facility-4670/.

[78] National Aeronautics and Space Administration. *NASA, Blue Origin Agreement Signals Rocketing Growth of Commercial Space*. News release, Release 19-021. Apr. 2019. URL: https://www.nasa.gov/news-release/nasa-blue-origin-agreement-signals-rocketing-growth-of-commercial-space/.

[79] National Aeronautics and Space Administration. *Space Operations Mission Directorate - Reports*. 2025. URL: https://www.nasa.gov/directorates/space-operations/rpt/.

[80] National Aeronautics and Space Administration. *TEST FACILITIES CAPABILITY HANDBOOK*. Tech. rep. 20070006480. NASA, 2007, pp. 173–177. URL: https://ntrs.nasa.gov/api/citations/20070006480/downloads/20070006480.pdf.

[81] National Aeronautics and Space Administration (NASA), Office of the Chief Financial Officer (OCFO). *NASA Cost Estimating Handbook (CEH), Version 4.0 - Main Body*. Handbook CEH Version 4.0. Washington, DC: NASA Office of the Chief Financial Officer, Program, Planning & Control (PP&C), Feb. 2015. URL: https://www3.nasa.gov/sites/default/files/files/01_CEH_Main_Body_02_27_15.pdf.

[82] Michael J. Neufeld. *The Rocket and the Reich: Peenemünde and the Coming of the Ballistic Missile Era*. New York: Free Press (Simon & Schuster), 1995.

[83] Jincheng Ni. *Discount Rate in Project Analysis*. English. Tech. rep. Département Développement Durable et Numérique. Paris: France Stratégie, Mar. 2017.

[84] Jincheng Ni and Joël Maurice. *Guide de l'évaluation socioéconomique des investissements publics: Complément opérationnel I — Révision du taux d'actualisation*. French. Complément opérationnel I. Validé par le comité d'experts le 21 octobre 2021 (prés. Roger Guesnerie). Paris: France Stratégie, Nov. 2021.

[85] Kyle E. Niemeyer. *Implementing CEA Calculations Using Cantera*. 2021. URL: https://kyleniemeyer.github.io/rocket-propulsion/thermochemistry/cea_cantera.html.

[86] NSF - NASASpaceflight.com. *SpaceX's McGregor test site*. Post on X (formerly Twitter). Photographs by Gary Blair. Dec. 31, 2024. URL: https://x.com/NASASpaceflight/status/1874098582338650617.

[87] Office of Management and Budget. *Circular A-94: Guidelines and Discount Rates for Benefit-Cost Analysis of Federal Programs*. Tech. rep. Circular No. A-94. Revised November 9, 2023. Washington, DC: Executive Office of the President, Office of Management and Budget, Nov. 2023. URL: https://www.whitehouse.gov/wp-content/uploads/2023/11/CircularA-94.pdf.

[88] Organisation for Economic Co-operation and Development. *OECD Data Explorer*. OECD data portal. URL: https://data-explorer.oecd.org/.

[89] Guansong Pang et al. "Deep learning for anomaly detection: A review". In: *ACM computing surveys (CSUR)* 54.2 (2021), pp. 1–38.

[90] John T. Pazos, Craig A. Chandler, and Nickey G. Raines. "The E-3 Test Facility at Stennis Space Center: Research and Development Testing for Cryogenic and Storable Propellant Combustion Systems". In: *45th AIAA/ASME/SAE/ASEE Joint Propulsion Conference*. AIAA 2009-5307; NASA/TM-2009-215706. 2009.

[91] Sr. Phillip Hebert and Alex C. Elliot. *NASA Data Acquisition System Software for Rocket Propulsion Testing*. https://www.ni.com/en/solutions/aerospace-defense/case-studies/nasa-data-acquisition-system-software-for-rocket-propulsion-testing.html?srsltid=AfmBOoolnJMBVLnI9d5PXQb6vGmoD8BDskztarLOcExFC_AMr3Hc8ME8. 2022.

[92] Alexander Ponomarenko. *RPA: Design tool for liquid rocket engine analysis*. 2009.

[93] Michael Popp et al. *Liquid rocket thrust chambers: aspects of modeling, analysis, and design*. American Institute of Aeronautics and Astronautics, 2004.

[94] Press Information Bureau, Government of India. *PM to visit Kerala, Tamil Nadu and Maharashtra on 27–28 February*. Press release. Release ID: 2009042. Feb. 2024. URL: https://www.pib.gov.in/PressReleseDetailm.aspx?PRID=2009042.

[95] A. Preuss et al. "10 Years of Subscale Testing at P8 Test Facility Lampoldshausen". In: *Proceedings of the European Conference for AeroSpace Sciences (EUCASS) -235*. Astrium GmbH, Space Transportation. 2009.

[96] Paul Prochnicki et al. "Hydra: Development of a Liquid Rocket Engine Test Stand and Feed System". In: *Proceedings of the 54th AIAA/SAE/ASEE Joint Propulsion Conference*. Cincinnati, OH, USA: American Institute of Aeronautics and Astronautics (AIAA), July 2018. DOI: 10.2514/6.2018-4601. URL: https://arc.aiaa.org/doi/10.2514/6.2018-4601.

[97] Jin-yuan Qian et al. "A comprehensive review of cavitation in valves: mechanical heart valves and control valves". In: *Bio-Design and Manufacturing* 2.2 (2019), pp. 119–136.

[98] R Anil Kumar. *ISRO Sets New Benchmark with Successful Semi-Cryogenic Engine SE2000 Test for LVM3*. Online article. URL: https://www.indiastrategic.in/isro-sets-new-benchmark-with-successful-semi-cryogenic-engine-se2000-test-for-lvm3/.

[99] Dhritiman Ray. "Stand built by SAIL subsidiary for ISRO rocket test a success". In: *The Times of India* (May 21, 2023). Updated: May 21, 2023, 14:01 IST. URL: https://timesofindia.indiatimes.com/city/ranchi/stand-built-by-sail-subsidiary-for-isro-rocket-test-a-success/articleshow/100389692.cms.

[100] Lukas Ruff et al. "A unifying review of deep and shallow anomaly detection". In: *Proceedings of the IEEE* 109.5 (2021), pp. 756–795.

[101] K. Schäfer et al. "Challenges of Test Facilities for Space Propulsion". In: *Proceedings of the 1st CEAS European Air and Space Conference*. Paper No. CEAS-2007-251. German Aerospace Center (DLR). Lampoldshausen, 74239 Hardthausen, Germany, 2007.

[102] Klaus Schäfer et al. "DEVELOPMENT OF P4.1 ALTITUDE SIMULATION FOR VINCI ő ENGINE". In: 2005. URL: https://api.semanticscholar.org/CorpusID:110079227.

[103] Klaus Schäfer et al. “P4. 1 Test Facility for Altitude Simulation of VINCI Engine, Bench Development”. In: *2005 Moscow EUCASS* (2005).

[104] L Schoenman. *Fuel/oxidizer-rich high-pressure preburners*. Tech. rep. 1981.

[105] Mark Schwabacher, Nikunj Oza, and Bryan Matthews. “Unsupervised Anomaly Detection for Liquid-Fueled Rocket Propulsion Health Monitoring”. In: *Journal of Aerospace Computing, Information, and Communication* 6 (Aug. 2009). DOI: 10.2514/1.42783.

[106] E. Shashi Menon. “Chapter Five - Fluid Flow in Pipes”. In: *Transmission Pipeline Calculations and Simulations Manual*. Ed. by E. Shashi Menon. Boston: Gulf Professional Publishing, 2015, pp. 149–234. ISBN: 978-1-85617-830-3. DOI: https://doi.org/10.1016/B978-1-85617-830-3.00005-5. URL: https://www.sciencedirect.com/science/article/pii/B9781856178303000055.

[107] Martin Sippel and Jascha Wilken. “Preliminary Component Definition of Reusable Staged-Combustion Rocket Engine”. In: *Space Propulsion 2018*. Paper 2018-309, Session 9 – ST – Reusability. 3AF, with ESA support. Seville, Spain, May 2018. URL: https://elib.dlr.de/120327/.

[108] Relativity Space. *Locations – A-2 Complex*. Web page. URL: https://www.relativityspace.com/locations#a2complex.

[109] Relativity Space. *Relativity Space Signs Lease On Historic NASA Test Stand*. Press release, Bay St. Louis, Mississippi. Sept. 2023. URL: https://www.relativityspace.com/press-release/2023/9/5/relativity-space-signs-lease-on-historic-nasa-test-stand.

[110] SpaceWatch Africa. *NPO Energomash tests the RD171MV and RD191 engines*. Online news article. Jan. 2021. URL: https://spacewatchafrica.com/npo-energomash-tests-the-rd-171mv-and-rd-191-engines/.

[111] George P Sutton and Oscar Biblarz. *Rocket propulsion elements*. John Wiley & Sons, 2011.

[112] Charlie Taylor. *RocketCEA: RocketCEA Wraps The NASA FORTRAN CEA Code And Provides Some Useful Tools*. https://rocketcea.readthedocs.io/en/latest/. Version 1.2.1 documentation. 2015.

[113] James C. Thomas et al. “Design of a Lab-Scale Hybrid Rocket Test Stand”. In: *Proceedings of the 52nd AIAA/SAE/ASEE Joint Propulsion Conference*. Salt Lake City, UT, USA: American Institute of Aeronautics and Astronautics (AIAA), July 2016. DOI: 10.2514/6.2016-4965. URL: https://arc.aiaa.org/doi/10.2514/6.2016-4965.

[114] Tobias Traudt et al. “LUMEN: Test Platform for Rocket Engine Technologies. Project Overview and Upcoming Steps in the Development”. In: *34th International Symposium on Space Technology and Science ISTS*. 2023.

[115] United Nations Economic Commission for Europe (UNECE). *Gross Average Monthly Wages by Indicator, Country and Year*. UNECE Statistical Database, 2025. URL: https://w3.unece.org/PXWeb2015/pxweb/en/STAT/STAT__20-ME__3-MELF/60_en_MECCWagesY_r.px/?rxid=0806c85a-23f8-4249-a4d0-10980df459d1 (visited on 04/20/2025).

[116] John Uri. *55 Years Ago: First Saturn V Stage Tested in Mississippi Facility*. NASA History Office, Johnson Space Center. Apr. 2021. URL: https://www.nasa.gov/history/55-years-ago-first-saturn-v-stage-tested-in-mississippi-facility/.

[117] Günther Waxenegger-Wilfing et al. “Early detection of thermoacoustic instabilities in a cryogenic rocket thrust chamber using combustion noise features and machine learning”. In: *Chaos: An Interdisciplinary Journal of Nonlinear Science* 31.6 (2021).

[118] World Bank. *Doing Business 2020: Comparing Business Regulation in 190 Economies*. Washington, DC: World Bank, 2020. ISBN: 978-1-4648-1440-2. DOI: 10.1596/978-1-4648-1440-2. URL: https://hdl.handle.net/10986/32436.

[119] Ian Wright. *Move Over SpaceX: Relativity Space Now the Largest Commercial Presence at NASA Stennis*. News article. engineering.com. Sept. 12, 2023. URL: https://www.engineering.com/move-over-spacex-relativity-space-now-the-largest-commercial-presence-at-nasa-stennis/.

[120] Deng Xiaoci. “China completes construction of Asias largest high-altitude rocket test facility”. In: *Global Times* (May 2024). URL: https://www.globaltimes.cn/page/202405/1312452.shtml.

[121] Barry Zandbergen. “Thermal rocket propulsion”. In: *Delft University of Technology* (2023).

[122] Xiaoguang Zhang et al. “Intelligent Fault Diagnosis of Liquid Rocket Engine via Interpretable LSTM with Multisensory Data”. In: *Sensors* 23.12 (2023). ISSN: 1424-8220. DOI: 10.3390/s23125636. URL: https://www.mdpi.com/1424-8220/23/12/5636.

A

Gantt Chart

On the next page, the Gantt chart for this project can be found. This is a more in-depth dive into the work performed from February to November than the preliminary timeline presented in the Research Proposal. Pink marked days are holidays, sick days, or miscellaneous days on which no full-time work on the thesis was performed. The diamonds show milestones in the project.

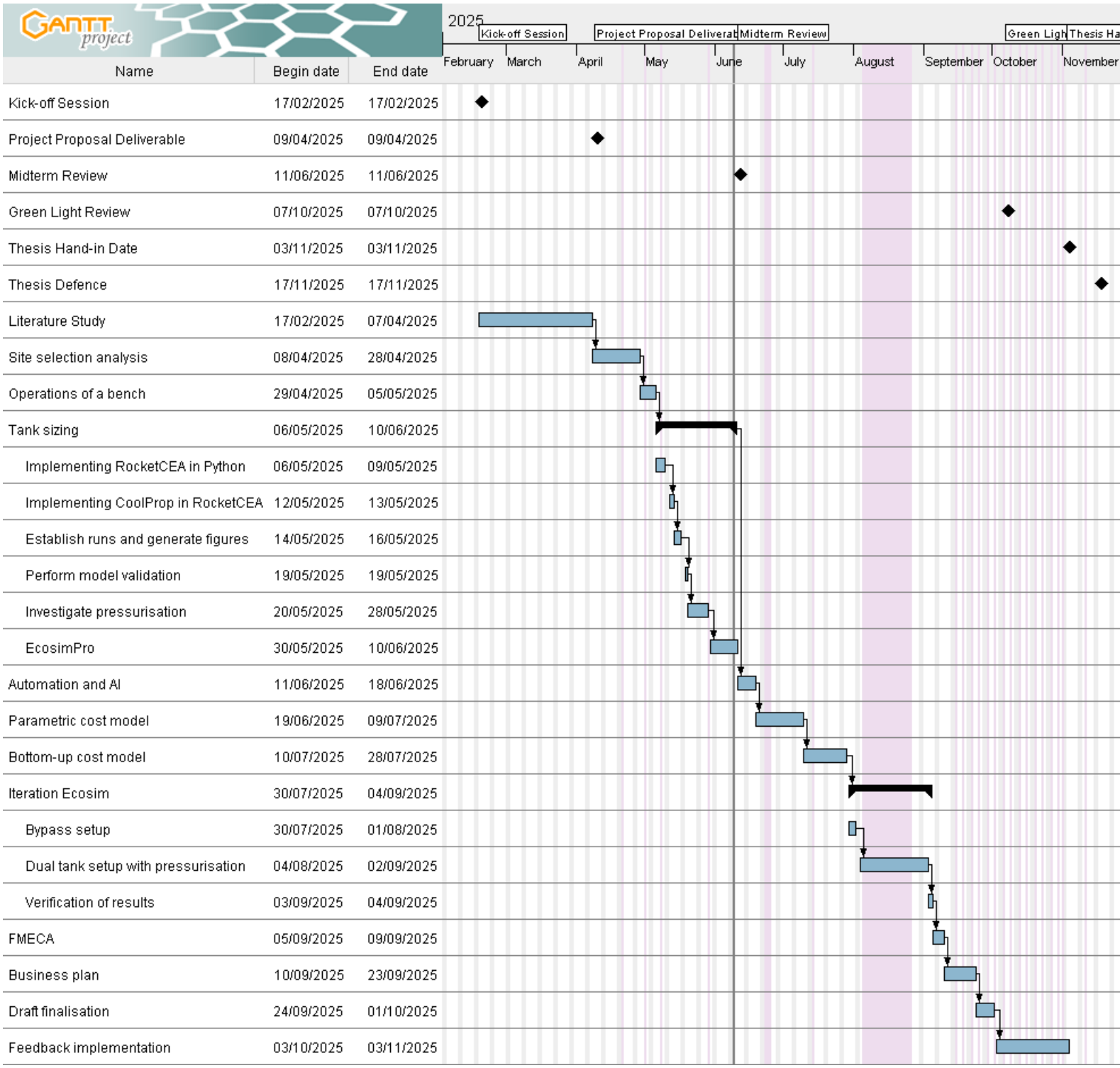

Name	Begin date	End date
Kick-off Session	17/02/2025	17/02/2025
Project Proposal Deliverable	09/04/2025	09/04/2025
Midterm Review	11/06/2025	11/06/2025
Green Light Review	07/10/2025	07/10/2025
Thesis Hand-in Date	03/11/2025	03/11/2025
Thesis Defence	17/11/2025	17/11/2025
Literature Study	17/02/2025	07/04/2025
Site selection analysis	08/04/2025	28/04/2025
Operations of a bench	29/04/2025	05/05/2025
Tank sizing	06/05/2025	10/06/2025
Implementing RocketCEA in Python	06/05/2025	09/05/2025
Implementing CoolProp in RocketCEA	12/05/2025	13/05/2025
Establish runs and generate figures	14/05/2025	16/05/2025
Perform model validation	19/05/2025	19/05/2025
Investigate pressurisation	20/05/2025	28/05/2025
EcosimPro	30/05/2025	10/06/2025
Automation and AI	11/06/2025	18/06/2025
Parametric cost model	19/06/2025	09/07/2025
Bottom-up cost model	10/07/2025	28/07/2025
Iteration Ecosim	30/07/2025	04/09/2025
Bypass setup	30/07/2025	01/08/2025
Dual tank setup with pressurisation	04/08/2025	02/09/2025
Verification of results	03/09/2025	04/09/2025
FMECA	05/09/2025	09/09/2025
Business plan	10/09/2025	23/09/2025
Draft finalisation	24/09/2025	01/10/2025
Feedback implementation	03/10/2025	03/11/2025

Figure A.1: Gantt Chart

B

EcosimPro Background

This appendix provides the design iterations performed before arriving at the full system, shown in Figure B.5.

B.1. Design Iterations

A run tank is typically pressurized in more than 30 minutes, to avoid unnecessary risks of pressure spikes. The first iteration considered an approach with a dedicated bypass loop. The intuition was straightforward: lines sized to pressurise a run tank over ∼30 minutes are, by definition, too small to support the much higher mass flows demanded once the engine is drawing propellant. A bypass offers an additional flow path, avoiding over-sizing the pressurisation line. The layout can be seen in Figure B.1 and Figure B.2. This solution is historically common and operationally robust, but it comes with tangible drawbacks: more piping in different sizes and extra fittings increase CAPEX and points of failure, and complicate maintenance and hazard analysis. Moreover, the cost-reliability balance has, in recent time, shifted: modern instrumentation and electrically actuated control valves are cheap, fast, and proven, so the extra path the bypass used to provide can be replaced by closed-loop control. By keeping a single pressurisation line and letting the control system handle pressure drop and mass flow, less hardware is necessary, as well as fewer interfaces. This simplifies the layout, and moves complexity into software where it is easier to test, monitor, and update.

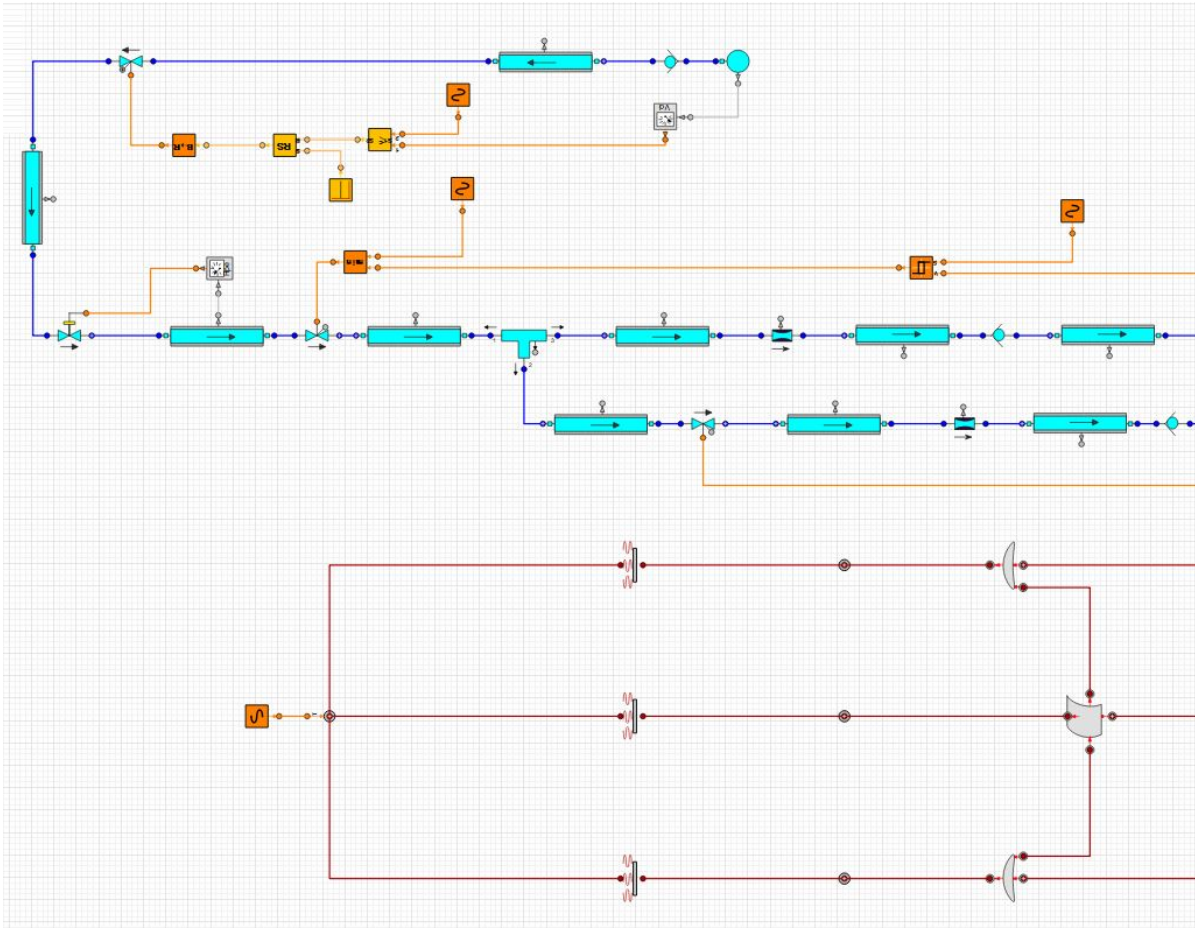

Figure B.1: Simplified model architecture for a single-tank pressurization using a bypass, and engine feed system (1 of 2).

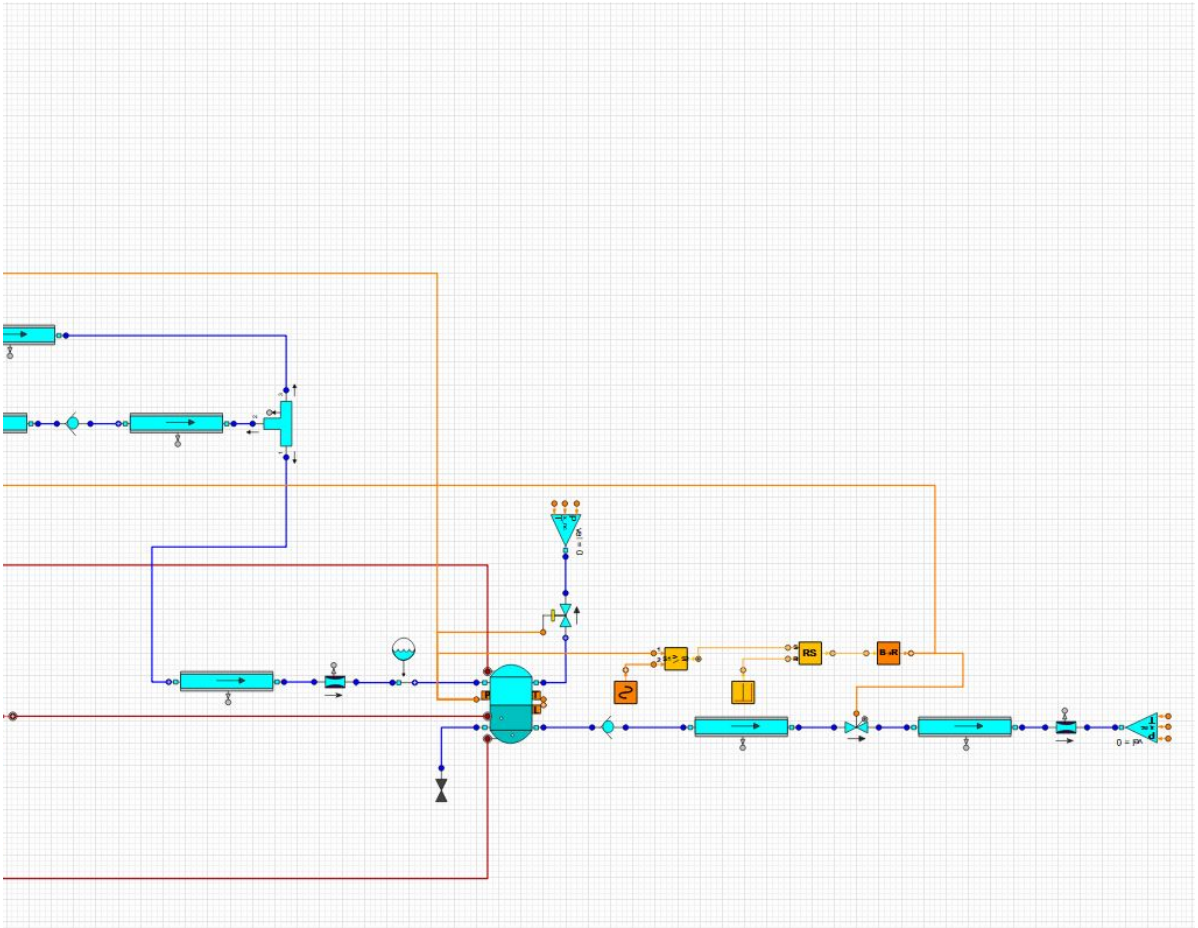

Figure B.2: Simplified model architecture for a single-tank pressurization using a bypass, and engine feed system (2 of 2).

In the refined concept Figure B.3 and Figure B.4, the bypass is eliminated. Instead, a single pressurisation line feeds the tank, and an electrically actuated control valve manages both the pressure drop and the delivered mass flow. If the system is scaled and adjusted accordingly, this system can be used for all different propellants. However, it is not yet the final design form. Creating a working design for one tank is a setup to the design where a multi-tank setup is realised. This design can be seen in Figure B.5. The only difference here is the added tank, and junctions and extra piping to merge the flows. This image is in A3 format for readability

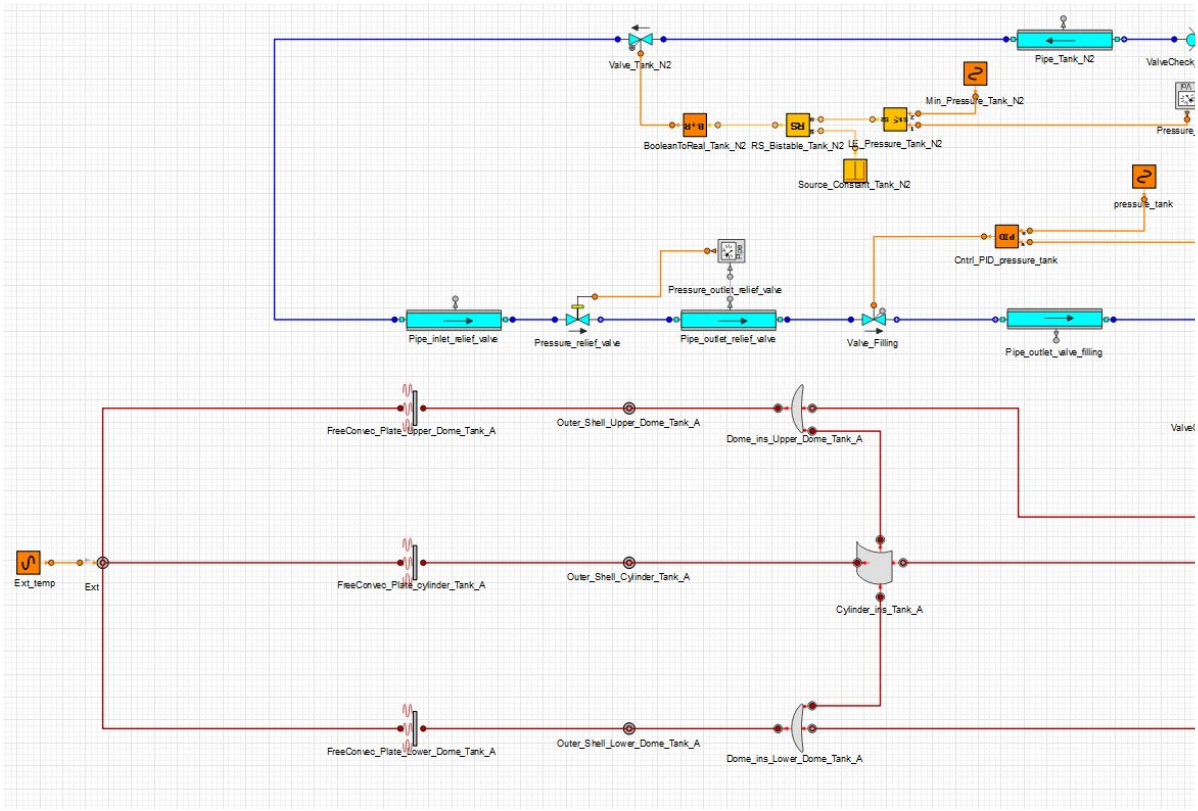

Figure B.3: Simplified model architecture for a single-tank pressurisation and engine feed system (1 of 2).

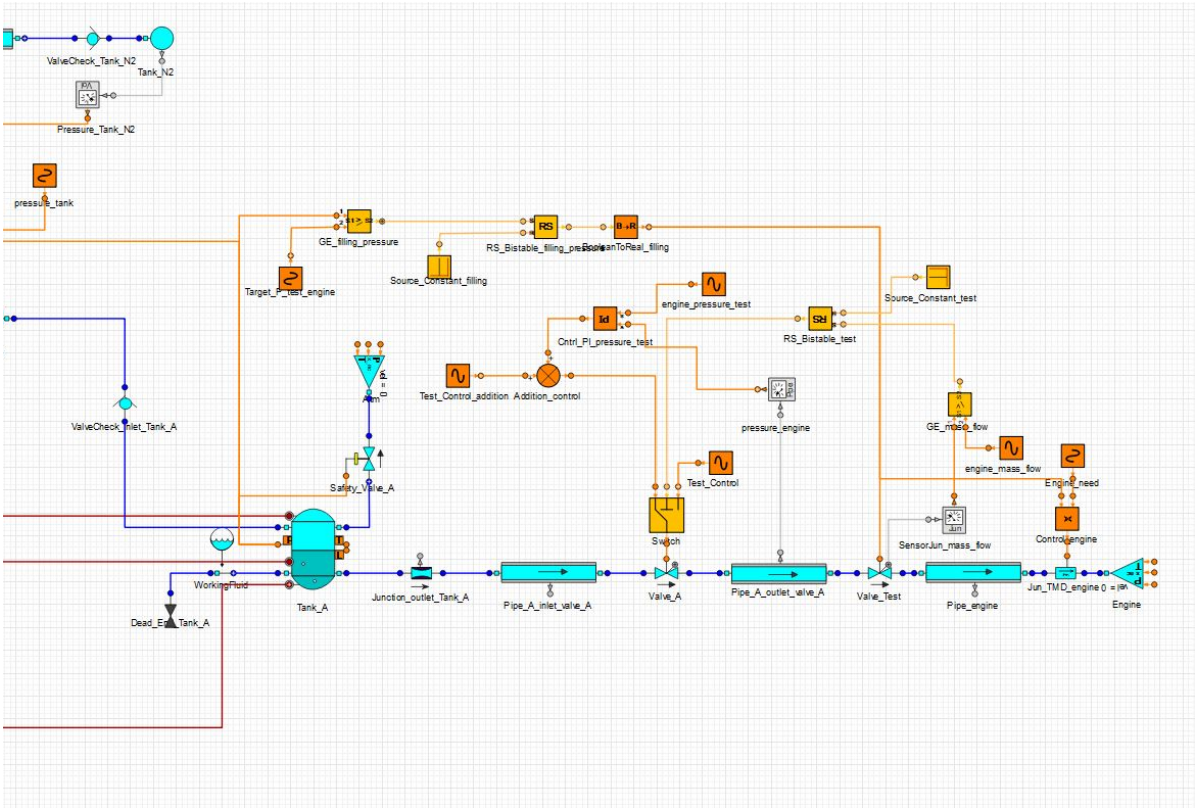

Figure B.4: Simplified model architecture for a single-tank pressurisation and engine feed system (2 of 2).

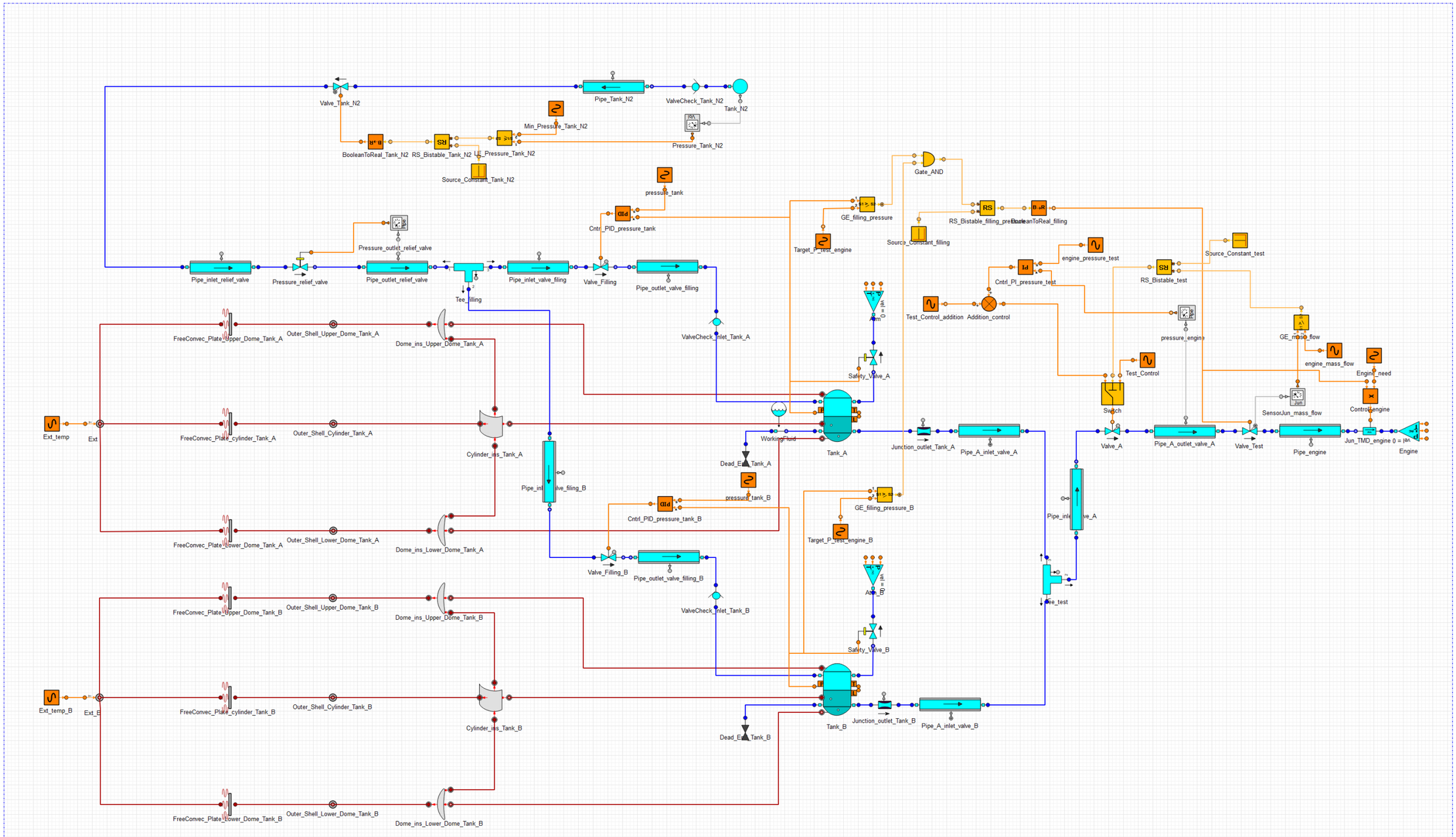

Figure B.5: Simplified model architecture for a multi-tank pressurisation and engine feed system.

C

Adjustment Factors for Rocket Test Stands

The adjustment factors in Table 7.2 are supported by (a) a *performance factor* based on functional capability and (b) a *construction factor* based on scope of works inferred from public records, news reports, and agency documentation. These are shown in Table C.1 and Table C.2.

Criteria

Table C.1: Performance factor criteria by type of bench.

Performance factor	Type of bench
2.00	Altitude simulation hot-fire
1.66	Sea-level; simultaneous multi-engine in different configurations
1.33	Sea-level; multiple positions/configurations (e.g., vertical/horizontal)
1.00	Sea-level; single position

Table C.2: Construction factor criteria by scope of works.

Construction factor	Scope definition
1.00	New build: full (re)build of infrastructure and systems
0.75	Modernization: major upgrades; civil work, usually major, focused on expanding the capabilities of the bench, but reusing the core stand.
0.50	Refurbishment: upgrades; limited civil work, typical of a legacy stand reactivation.
0.25	Maintenance: overhauls/minor works only, similar to Repex.

The criteria mentioned in the previous tables are used in the following sections to assess each test bench mentioned in chapter 7. The sources used for this assessment are stated per bench in Table 7.1. For each bench, rationales are provided for the construction factor, and the performance factor is inferred from the aforementioned sources. If additional sources were necessary, these are stated in the respective analyses.

C.1. NASA A-3 (SSC)

Table C.3: Assessment for NASA A-3 (SSC). Performance factor chosen per Table C.1; construction factor per Table C.2.

Criterion	Assessment
Altitude simulation capability	✓
Simultaneous multi-engine (no altitude simulation)	✗
Multiple positions (no altitude simulation)	✗
Sea-level single position	✗
Performance factor	**2.00** (Altitude simulation)
Scope of works	Built from the ground up. Enables both atmospheric and sea level testing.
Construction factor	**1.00** (New build)
Rationale	The facility has been fully built using the budget mentioned.

C.2. NASA B-2 (SSC)

Table C.4: Assessment for NASA B-2 (SSC). Performance factor chosen per Table C.1; construction factor per Table C.2.

Criterion	Assessment
Altitude simulation capability	✗
Simultaneous multi-engine (no altitude simulation)	✗
Multiple positions (no altitude simulation)	✗
Sea-level single position	✓
Performance factor	**1.00** (Sea-level, can only test SLS in one position)
Scope of works	Extensive upgrades on legacy structure (SLS era)
Construction factor	**0.75** (Modernization)
Rationale	Large sea-level, vertical stand that was modified and upgraded for SLS. It included major civil work on the height of the stand, as well as the flame trench.

C.3. NASA A-2 (SSC)

Table C.5: Assessment for NASA A-2 (SSC). Performance factor chosen per Table C.1; construction factor per Table C.2.

Criterion	Assessment
Altitude simulation capability	✗
Simultaneous multi-engine (no altitude simulation)	✗
Multiple positions (no altitude simulation)	✗
Sea-level single position	✓
Performance factor	**1.00**
Scope of works	Turning a system built for sea-level and altitude testing into a sea-level, single position stage test facility
Construction factor	**0.75** (Modernization)
Rationale	Relativity Space is modernizing an underutilized legacy test stand with modifications to existing A-2 infrastructure. They are performing upgrades to the thrust capabilities of the bench, and removing the altitude simulation capabilities. The foundations stay intact, but the bench is stripped of a lot of original infrastructure (it was used for altitude simulations as well as sea-level testing) to allow stage testing. As most of the work is stripping the bench, it could be argued that the construction factor is too high, but it fits the definition as presented at the beginning of this appendix. When it is considered that a new flame trench capable of withstanding 14 MN needs to be built, the construction factor is not a topic of discussion anymore. [35, 108, 109, 119]

C.4. Stand 4670 (MSFC)

Table C.6: Assessment for Stand 4670 (MSFC). Performance factor chosen per Table C.1; construction factor per Table C.2.

Criterion	Assessment
Altitude simulation capability	✗
Simultaneous multi-engine (no altitude simulation)	✗
Multiple positions (no altitude simulation)	✓
Sea-level single position	✗
Performance factor	**1.33** (Multiple positions)
Scope of works	Limited works relative to legacy structure
Construction factor	**0.50** (Refurbishment)
Rationale	The bench was originally designed for Saturn V engines. Blue Origin refurbished the bench, to fit its engines and improve the steel infrastructure, as they found corroded steel. The civil works done on the bench are non-negligible, but they are purely focused on the existing infrastructure, and not on building new infrastructure.

C.5. USAF 2-A (Edwards)

Table C.7: Assessment for USAF 2-A (Edwards). Performance factor chosen per Table C.1; construction factor per Table C.2.

Criterion	Assessment
Altitude simulation capability	✗
Simultaneous multi-engine (no altitude simulation)	✗
Multiple positions (no altitude simulation)	✗
Sea-level single position	✓
Performance factor	**1.00** (Sea-level; single position)
Scope of works	Minor upgrades, would be called extraordinary maintenance in Europe.
Construction factor	**0.50** (Refurbishment)
Rationale	Work performed on the bench was no civil work. It rather included the exchange of old elements (the bench was built in the 60's) to more modern components.

C.6. DLR P5.2 (Lampoldshausen)

Table C.8: Assessment for DLR P5.2 (Lampoldshausen). Performance factor chosen per Table C.1; construction factor per Table C.2.

Criterion	Assessment
Altitude simulation capability	✓
Simultaneous multi-engine (no altitude simulation)	✗
Multiple positions (no altitude simulation)	✗
Sea-level single position	✗
Performance factor	**2.00** (Altitude simulation)
Scope of works	New facility build with dedicated systems
Construction factor	**1.00** (New build)
Rationale	Dedicated altitude simulation engine stand; new construction, but for relatively low thrust (180 kN), especially considering the other benches.

C.7. SIET (India)

Table C.9: Assessment for SIET (India). Performance factor chosen per Table C.1; construction factor per Table C.2.

Criterion	Assessment
Altitude simulation capability	✗
Simultaneous multi-engine (no altitude simulation)	✓
Multiple positions (no altitude simulation)	✗
Sea-level single position	✗
Performance factor	**1.66** (Simultaneous multiple positions)
Scope of works	New construction
Construction factor	**1.00** (New build)
Rationale	Parallel testing in different configurations is possible [98].

D

Valuation spreadsheet: structure and formulas

This appendix enables exact reproduction of the business-case figures, Figure 7.2 and Figure 7.3, from the provided workbook. All flows are nominal (inflated by π) and discounted at a nominal rate r. There is no hidden stochastic element; results are deterministic given inputs. Monetary units are kEUR. Depreciation/amortisation is not included in cash flows and therefore not in NPV.

Project inputs are specified on Table 7.6. Year index t starts at $t = 0$, the total investment done over the previous years (building the bench) aggregated in one value, and $t = 1$ for operating years. The nominal discount factor is entered as $(1 + r)$ and used as $d_t = (1 + r)^{-t}$. Price per test day P_t is generated from a base P_1 using the following escalation rule: bi-yearly steps, where the price is raised following an inflation of 2.5% per year. The reasoning behind this is that fixing the price for two years allows for customers to make long-term plannings, knowing what to expect. Utilisation D_t follows an operational ramp, capping at 110 days. This is done because engines usually follow test campaigns where they are tested a maximum of three times per week, but during start-up and at the end of the campaign, this frequency is less. Therefore, it was argued that half of the work days in a year can be the maximum test cadence. This assumption is valid, until a SpaceX like testing campaign is possible in Europe (testing every day with multiple different engines on the same bench). There is a ramp-up from 60 to 110, because a new bench first has to establish itself in the market before it will be fully booked.

Cost components (inelastic OPEX, elastic OPEX, Repex) inflate annually and start as a percentage of CAPEX, with the inelastic OPEX being fixed at 2%, the elastic OPEX a function of utilisation, with maximum utilisation being 2% of CAPEX, and the Repex fixed at 1%. The inelastic and elastic OPEX are both 50% of the total OPEX, set at 4% of the CAPEX. While this percentage can lower once operations have been streamlined, and the goal is usually to have an OPEX around 2%, for this analysis 4% is used. If the OPEX ends up being lower, either the prices should be adjusted, or this is extra margin. Annual revenue is $R_t = P_t D_t$, cash flow is $\mathrm{NCF}_t = R_t - \mathrm{Inel}_t - \mathrm{Elas}_t - \mathrm{Repex}_t$, and the per-year present value is $d_t \mathrm{NCF}_t$ with $t = 0$ set to $-\mathrm{CAPEX}_0$. Cumulative NPV is the running sum of per-year PVs.

D.1. Core equations.

The most important equations, some of which were briefly mentioned in the previous paragraph, are shown below.

$$I_t = (1+\pi)^{t-1}, \qquad d_t = (1+r)^{-t}, \tag{D.1}$$

$$R_t = P_t D_t, \qquad \mathrm{NCF}_t = R_t - \mathrm{Inel}_t - \mathrm{Elas}_t - \mathrm{Repex}_t, \tag{D.2}$$

$$\mathrm{NPV} = -\mathrm{CAPEX}_0 + \sum_{t=1}^{T} d_t \,\mathrm{NCF}_t, \tag{D.3}$$

$$\mathrm{PV}_R(K) = \sum_{t=1}^{K} d_t R_t, \qquad \mathrm{PV}_C(K) = \sum_{t=1}^{K} d_t(\mathrm{Inel}_t + \mathrm{Elas}_t + \mathrm{Repex}_t), \tag{D.4}$$

$$u^{(K)} = \frac{\mathrm{CAPEX}_0 + \mathrm{PV}_C(K)}{\mathrm{PV}_R(K)} - 1, \tag{D.5}$$

$$P_1^{(K)} = \frac{\mathrm{CAPEX}_0 + \mathrm{PV}_C(K)}{\sum_{t=1}^{K} d_t\, \alpha_t D_t}, \quad \alpha_t = \frac{P_t}{P_1}. \tag{D.6}$$

D.2. Excel sheet layout

To be able to reproduce the results as discussed in section 7.1, the sheet layout is discussed in detail, and pictures are provided. With the abovementioned equations, it should be possible to recreate these results.

C: Year t	D: CAPEX_0
E,F,G: Inelastic OPEX, Elastic OPEX, Repex	I,J: P_t (kEUR/day), D_t (days)
K: $R_t = I \cdot J$	L: $\mathrm{NCF}_t = K - E - F - G$
N: per-year PV $d_t\mathrm{NCF}_t$ with $N_{t=0} = -\mathrm{CAPEX}_0$	O: cumulative NPV $\sum N$
Q: $\mathrm{PV\_Rev}_t := R_t\, N_t/\mathrm{NCF}_t$ (if $\mathrm{NCF}_t \neq 0$)	R: $\mathrm{PV\_Cost}_t := (\mathrm{Inel}_t + \mathrm{Elas}_t + \mathrm{Repex}_t)\, N_t/\mathrm{NCF}_t$

Breakeven calculations.

$$\mathrm{PV}_R(K) = \sum_{t \le K} \mathrm{PV\_Rev}_t, \qquad \mathrm{PV}_C(K) = \sum_{t \le K} \mathrm{PV\_Cost}_t,$$

are inserted into $u^{(K)}$ and $P_1^{(K)}$ to generate the heatmaps and the required P_1 curves. These are shown below in Excel format. In the chapter, Python was used for the visualisation.

D.3. Model verification

The valuation workbook was verified with four deterministic checks:

(1) Row identities. For selected years $t \in \{1, 5, 10, 20, 30\}$ the revenue, cash-flow, and present-value identities evaluate to zero: $R_t - P_t D_t = 0$, $\mathrm{NCF}_t - (R_t - \mathrm{Inel}_t - \mathrm{Elas}_t - \mathrm{Repex}_t) = 0$, and $d_t\mathrm{NCF}_t - \mathrm{NCF}_t/(1+r)^t = 0$.

(2) NPV closure. The final cumulative NPV equals $\sum_{t=1}^{T} d_t\mathrm{NCF}_t - \mathrm{CAPEX}_0$ and the $t = 0$ check $d_0\mathrm{NCF}_0 + \mathrm{CAPEX}_0 = 0$ holds.

(3) Discounted payback. The first year where the *discounted* cumulative NPV crosses zero is found by linear interpolation between the last negative and first non-negative years.

(4) Heatmap NPV frontier consistency. Using $\mathrm{PV}_R(K) = \sum_{t \le K} d_t R_t$ and $\mathrm{PV}_C(K) = \sum_{t \le K} d_t(\mathrm{Inel}_t + \mathrm{Elas}_t + \mathrm{Repex}_t)$, the analytic zero-NPV frontier $u^{(C)} = \frac{C + \mathrm{PV}_C(K)}{\mathrm{PV}_R(K)} - 1$ is compared against grid cells;

	Year	Capex	Inelastic Opex	Elastic Opex	Repex	Amortization	Cost of Test Day	Days in Use	Revenue	Net Cash Flow	Running total	NPV	Cum. NPV	Acc inf.	PV_Rev_t	PV_Cost_t	CumPV_Rev	CumPV_Cost
	0	100000									-100000	-100000	-100000					
inflation	1	0	2.000	1.091	1.000	2.857	85	60	5.100	1.009	-98.991	970	-99.030	1,00	4903,85	3933,57	4903,85	3933,57
1,025	2	0	2.050	1.491	1.025	2.857	85	80	6.800	2.234	-96.757	2.066	-96.964	1,03	6286,98	4221,44	11190,83	8155,01
	3	0	2.101	1.719	1.051	2.857	89	90	8.037	3.166	-93.591	2.815	-94.149	1,05	7145,11	4330,37	18335,94	12485,38
Discount r	4	0	2.154	1.958	1.077	2.857	89	100	8.930	3.742	-89.849	3.198	-90.951	1,08	7633,67	4435,28	25969,61	16920,66
1,04	5	0	2.208	2.007	1.104	2.857	94	100	9.382	4.064	-85.785	3.340	-87.611	1,10	7711,66	4371,31	33681,27	21291,98
	6	0	2.263	2.263	1.131	2.857	94	110	10.321	4.664	-81.121	3.686	-83.925	1,13	8156,56	4470,84	41837,83	25762,82
	7	0	2.319	2.319	1.160	2.857	99	110	10.843	5.045	-76.077	3.834	-80.091	1,16	8239,89	4406,36	50077,72	30169,18
	8	0	2.377	2.377	1.189	2.857	99	110	10.843	4.900	-71.177	3.580	-76.511	1,19	7922,97	4342,81	58000,69	34511,98
	9	0	2.437	2.437	1.218	2.857	104	110	11.392	5.300	-65.877	3.724	-72.788	1,22	8003,92	4280,17	66004,60	38792,15
	10	0	2.498	2.498	1.249	2.857	104	110	11.392	5.148	-60.729	3.478	-69.310	1,25	7696,07	4218,44	73700,68	43010,58
	11	0	2.560	2.560	1.280	2.857	109	110	11.969	5.568	-55.161	3.617	-65.693	1,28	7774,70	4157,59	81475,37	47168,18
	12	0	2.624	2.624	1.312	2.857	109	110	11.969	5.408	-49.752	3.378	-62.315	1,31	7475,67	4097,63	88951,05	51265,80
	13	0	2.690	2.690	1.345	2.857	114	110	12.575	5.850	-43.902	3.514	-58.801	1,34	7552,05	4038,53	96503,09	55304,33
	14	0	2.757	2.757	1.379	2.857	114	110	12.575	5.682	-38.220	3.281	-55.520	1,38	7261,58	3980,28	103764,67	59284,61
	15	0	2.826	2.826	1.413	2.857	120	110	13.211	6.146	-32.074	3.413	-52.107	1,41	7335,77	3922,87	111100,44	63207,48
	16	0	2.897	2.897	1.448	2.857	120	110	13.211	5.970	-26.104	3.187	-48.920	1,45	7053,62	3866,29	118154,07	67073,77
	17	0	2.969	2.969	1.485	2.857	126	110	13.880	6.458	-19.646	3.315	-45.605	1,48	7125,69	3810,53	125279,75	70884,30
	18	0	3.043	3.043	1.522	2.857	126	110	13.880	6.272	-13.374	3.096	-42.508	1,52	6851,62	3755,57	132131,37	74639,87
	19	0	3.119	3.119	1.560	2.857	133	110	14.583	6.785	-6.590	3.220	-39.288	1,56	6921,62	3701,40	139052,99	78341,27
	20	0	3.197	3.197	1.599	2.857	133	110	14.583	6.590	0	3.007	-36.281	1,60	6655,40	3648,02	145708,40	81989,28
	21	0	3.277	3.277	1.639	2.857	139	110	15.321	7.128	7.128	3.128	-33.153	1,64	6723,40	3595,40	152431,79	85584,68
	22	0	3.359	3.359	1.680	2.857	139	110	15.321	6.923	14.051	2.921	-30.232	1,68	6464,81	3543,54	158896,60	89128,23
	23	0	3.443	3.443	1.722	2.857	146	110	16.097	7.489	21.540	3.038	-27.193	1,72	6530,85	3492,43	165427,45	92620,66
	24	0	3.529	3.529	1.765	2.857	146	110	16.097	7.274	28.814	2.838	-24.356	1,76	6279,67	3442,06	171707,12	96062,72
	25	0	3.617	3.617	1.809	2.857	154	110	16.912	7.868	36.682	2.951	-21.404	1,81	6343,82	3392,42	178050,94	99455,14
	26	0	3.708	3.708	1.854	2.857	154	110	16.912	7.642	44.323	2.756	-18.648	1,85	6099,83	3343,49	184150,77	102798,63
	27	0	3.801	3.801	1.900	2.857	162	110	17.768	8.266	52.590	2.867	-15.781	1,90	6162,15	3295,26	190312,91	106093,89
	28	0	3.896	3.896	1.948	2.857	162	110	17.768	8.029	60.618	2.677	-13.104	1,95	5925,14	3247,74	196238,05	109341,63
	29	0	3.993	3.993	1.996	2.857	170	110	18.667	8.685	69.303	2.785	-10.319	2,00	5985,67	3200,89	202223,72	112542,53
	30	0	4.093	4.093	2.046	2.857	170	110	18.667	8.435	77.738	2.601	-7.718	2,05	5755,46	3154,73	207979,18	115697,25
	31	0	4.195	4.195	2.098	2.857	178	110	19.612	9.124	86.863	2.705	-5.013	2,10	5814,25	3109,23	213793,43	118806,48
	32	0	4.300	4.300	2.150	2.857	178	110	19.612	8.862	95.725	2.526	-2.487	2,15	5590,63	3064,38	219384,06	121870,86
	33	0	4.408	4.408	2.204	2.857	187	110	20.605	9.586	105.311	2.628	141	2,20	5647,75	3020,18	225031,81	124891,05
	34	0	4.518	4.518	2.259	2.857	187	110	20.605	9.311	114.622	2.454	2.595	2,26	5430,52	2976,62	230462,33	127867,67
	35	0	4.631	4.631	2.315	2.857	197	110	21.648	10.072	124.694	2.552	5.147	2,32	5486,00	2933,69	235948,34	130801,37
												5.147						

Figure D.1: Valuation spreadsheet: base-case inputs and year-by-year nominal cash flows with discounted series ($\mathrm{PV\_Rev}_t$, $\mathrm{PV\_Cost}_t$) and cumulative NPV (CAPEX 100 M, $P_1 = 85$k/day, $\pi = 2.5\%$, $r = 4\%$). CAPEX and cumulative NPV are marked in red.

at $u^{(C)}$ the grid returns NPV ≈ 0.

All residuals are within ± 1 kEUR tolerance due to rounding; therefore the implementation is consistent with the economics and discounting used. Table D.1 and Table D.2 show the residuals of the analyses. After that, the full sheet is shown in Figure D.1, and an Excel heatmap is added as background to the Python heatmaps, visible in Figure D.2.

Table D.1: Verification checks and outcomes

Check	**Expression / Years**	**Result**	**Verdict**
Revenue identity	$R_t - P_t D_t$; $t = 1, 5, 10, 20, 30$	0	Pass
Cash–flow identity	$\mathrm{NCF}_t - (R_t - \mathrm{Inel}_t - \mathrm{Elas}_t - \mathrm{Repex}_t)$	0	Pass
PV identity	$d_t \mathrm{NCF}_t - \mathrm{NCF}_t/(1+r)^t$	0	Pass
$t = 0$ closure	$d_0 \mathrm{NCF}_0 + \mathrm{CAPEX}_0$	0	Pass
Final NPV closure	$\sum_{t \geq 1} d_t \mathrm{NCF}_t - \mathrm{CAPEX}_0 - \mathrm{CumNPV}_T$	-2.4×10^{-11}	Pass
Discounted payback	Interpolated zero crossing (yr)	32.63	Pass

Table D.2: Zero-NPV frontier $u^{(C)}$ at sample CAPEX values.

CAPEX (kEUR)	$u^{(20)}$ **(%)**	$u^{(30)}$ **(%)**	**NPV at** $u^{(C)}$
80,000	11.11	-5.91	≈ 0
100,000	24.84	3.71	≈ 0
120,000	38.56	13.33	≈ 0

	Target year K	PV_R_≤K	PV_C_≤K										
	30	207979,2	115697,3										
CAPEX ↓ / Uplift →	-30,0%	-25,0%	-20,0%	-15,0%	-10,0%	-5,0%	0,0%	5,0%	10,0%	15,0%	20,0%	25,0%	30,0%
80000	-50111,8	-39712,9	-29313,9	-18915	-8515,99	1882,966	12281,92	22680,88	33079,84	43478,8	53877,76	64276,72	74675,68
85000	-55111,8	-44712,9	-34313,9	-23915	-13516	-3117,03	7281,925	17680,88	28079,84	38478,8	48877,76	59276,72	69675,68
90000	-60111,8	-49712,9	-39313,9	-28915	-18516	-8117,03	2281,925	12680,88	23079,84	33478,8	43877,76	54276,72	64675,68
95000	-65111,8	-54712,9	-44313,9	-33915	-23516	-13117	-2718,08	7680,884	18079,84	28478,8	38877,76	49276,72	59675,68
100000	-70111,8	-59712,9	-49313,9	-38915	-28516	-18117	-7718,08	2680,884	13079,84	23478,8	33877,76	44276,72	54675,68
105000	-75111,8	-64712,9	-54313,9	-43915	-33516	-23117	-12718,1	-2319,12	8079,843	18478,8	28877,76	39276,72	49675,68
110000	-80111,8	-69712,9	-59313,9	-48915	-38516	-28117	-17718,1	-7319,12	3079,843	13478,8	23877,76	34276,72	44675,68
115000	-85111,8	-74712,9	-64313,9	-53915	-43516	-33117	-22718,1	-12319,1	-1920,16	8478,802	18877,76	29276,72	39675,68
120000	-90111,8	-79712,9	-69313,9	-58915	-48516	-38117	-27718,1	-17319,1	-6920,16	3478,802	13877,76	24276,72	34675,68

Figure D.2: Heatmap showing cumulative NPV values for different CAPEX and P_1. $P_1 = 85$k/day

Lastly, as mentioned in the chapter, the discount rate is fixed at 4%. This is not a typical discount rate for a project where private investors are present (7% according to [40]), which is why it is relevant to show the sensitivity of the analysis to changes in discount rate. This is shown in Figure D.3 and Figure D.4.

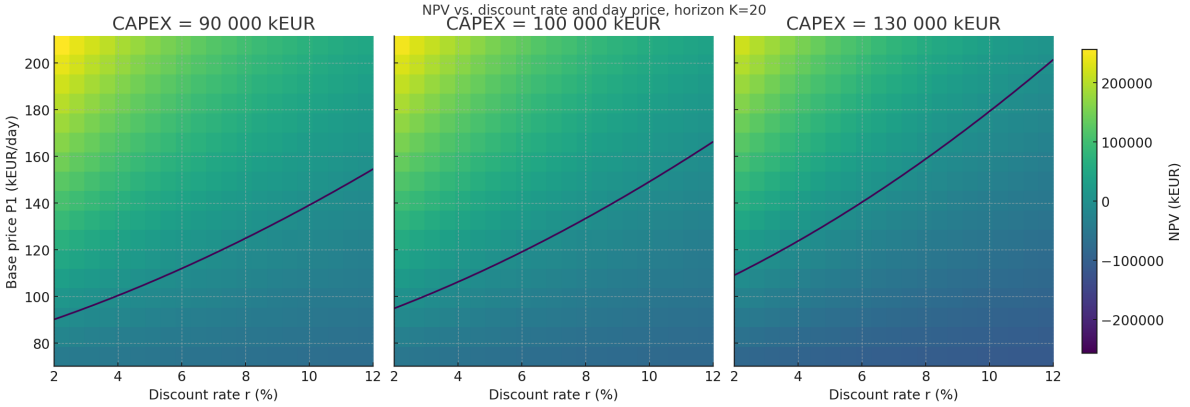

Figure D.3: NPV as a function of discount rate r and base price P_1 for three CAPEX cases (90, 100, 130 M); horizon $K = 20$.

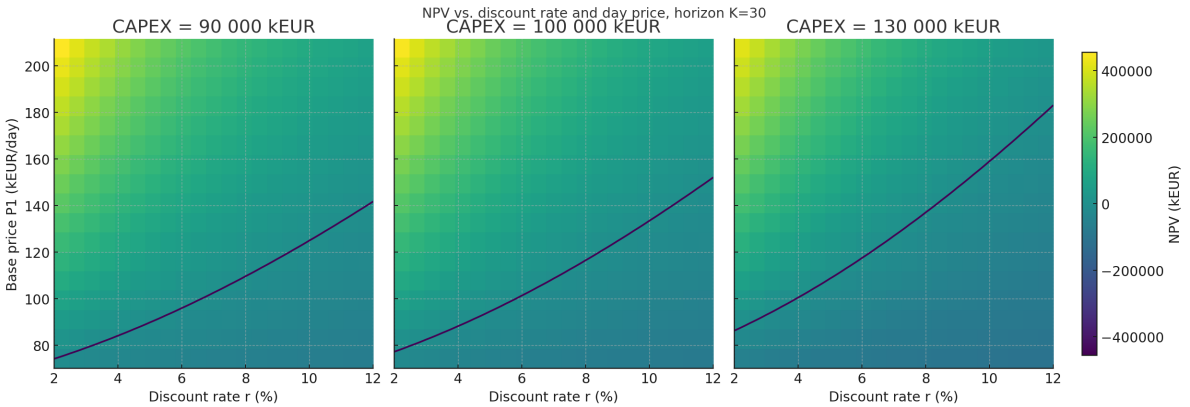

Figure D.4: NPV as a function of discount rate r and base price P_1 for three CAPEX cases (90, 100, 130 M); horizon $K = 30$.

As can be expected, and can be seen in the graphs, changing the discount rate has a bigger effect on higher CAPEX projects. With more money tied up upfront, a larger share of value comes from late cash flows; raising the discount rate discounts those cash flows more aggressively, so the zero-NPV frontier shifts up faster for 130 M than for 90 M. Practically, each 1 pp increase in r requires a larger increase in the day rate P_1 (or utilisation) at high-CAPEX builds to hold breakeven. Extending the horizon

from $K = 20$ to $K = 30$ partly offsets this because the longer window restores present value, but the CAPEX-driven sensitivity remains.